KERNFORSCHUNGSZENTRUM

KARLSRUHE

Oktober 1977 KFK 2504

Institut für Angewandte Kernphysik

ANNUAL REPORT
Teilinstitut Kernphysik
(July 1, 1976 - June 30, 1977)

Editors: V. Bechtold, H. Ottmar

GESELLSCHAFT
FÜR
KERNFORSCHUNG M.B.H.

KARLSRUHE

Als Manuskript vervielfältigt

Für diesen Bericht behalten wir uns alle Rechte vor

GESELLSCHAFT FÜR KERNFORSCHUNG M. B. H.

KARLSRUHE

KERNFORSCHUNGSZENTRUM KARLSRUHE

KFK 2504

Institut für Angewandte Kernphysik

A N N U A L R E P O R T

Teilinstitut Kernphysik

(July 1, 1976 - June 30, 1977)

Editors: V. Bechtold and H. Ottmar

Gesellschaft für Kernforschung mbH, Karlsruhe

Abstract

The activities of the Nuclear Physics Section of the Institute of Applied Nuclear Physics from mid 1976 to mid 1977 are surveyed. The research program comprises both contributions to fundamental and applied nuclear research. The activities on the application of nuclear methods mainly concentrate on the measurements of cross sections of neutron-induced nuclear reactions for the fast breeder project, the application of gamma-ray spectrometry to nuclear fuel assay problems, the development of a proton microbeam for elemental analysis, and the production of ^{123}J for medical application. The study of nuclear reactions induced by α particles, ^{6}Li ions and fast neutrons, and the measurement of optical hyperfine structure using high-resolution laser spectroscopy form the major part of the fundamental research work. In addition, the operation of the two accelerators of the institute, an isochronous cyclotron and a 3 MV Van de Graaff accelerator, are briefly reviewed.

Zusammenfassung

Es wird über die Tätigkeit des Teilinstituts Kernphysik des Instituts für Angewandte Kernphysik von Mitte 1976 bis Mitte 1977 berichtet. Das Forschungsprogramm beinhaltet sowohl Anwendungen der Kernphysik auf Probleme der Kernenergie als auch grundlagenphysikalische Arbeiten. Schwerpunkte der angewandten Arbeiten bilden die Messungen von Neutronenwirkungsquerschnitten für das Projekt Schneller Brüter, die Anwendung gammaspektrometrischer Meßverfahren zur Spaltstoffbestimmung, die Entwicklung einer Protonenmikrosonde für die Elementanalyse sowie die Erzeugung von ^{123}J für medizinische Anwendungen. Zu den grundlagenphysikalischen Arbeiten gehören Untersuchungen von Kernreaktionen mit α-Teilchen, ^{6}Li-Ionen und schnellen Neutronen sowie die Messung der optischen Hyperfeinstruktur mittels hochauflösender Laserspektroskopie. Ferner wird der Betrieb der beiden Beschleuniger des Instituts, eines Isochronzyklotrons und eines 3 MV-Van-de-Graaff-Beschleunigers, kurz geschildert.

The Institute of Applied Nuclear Physics of the Karlsruhe Nuclear Research Centre is engaged in research work on the application of nuclear physics to problems of nuclear energy, solid state physics, medicine, and analysis. These investigations are supported by some fundamental research. This report, the third one in a series of annual reports, gives a survey of the work of the Nuclear Physics Section from mid 1976 to mid 1977. Progress of the Nuclear Solid State Physics Section is reported separately.

Measurements of cross sections of neutron-induced nuclear reactions are among the main activities of the institute. The major part of this work is to provide nuclear data that are required for the design of fast breeder reactors. Here a new method to measure neutron capture cross sections of radioactive materials has been developed and applied to two isotopes of plutonium. This shows that, with refined methods of measurement, an old-fashioned accelerator such as our 3 MV Van de Graaff can successfully compete with larger (and more expensive) installations.

Methods of gamma-ray spectrometry are applied to problems of the nuclear fuel cycle such as the determination of plutonium in waste and of the isotopic composition of nuclear fuel. This also includes such practical work as installation and testing of a portal monitor to prevent diversion of fissile material.
In the field of materials analysis, a proton microbeam installation is nearing completion which is to be used for analysis by proton induced x-rays and/or nuclear reactions.

In addition to this applied research, a number of experiments in fundamental nuclear physics are carried out, most of them in close cooperation with visiting groups from German universities. A close connection between applied and fundamental work is one of the characteristics of the institute and has led to a stimulating exchange of ideas in either way. Work at the cyclotron has taken advantage of the ^{6}Li ion beam of 156 MeV and has demonstrated that these are the ideal projectiles to study higher giant resonances by inelastic scattering. Another group that investigates nuclear moments and radii by high resolution laser spectroscopy

has achieved the first results on radioactive barium isotopes.

The institute operates two accelerators. A 3MV single stage Van de Graaff accelerator is primarily used for neutron time-of-flight experiments and solid state physics. The Karlsruhe Isochronous Cyclotron, a fixed frequency machine, provides beams of 52 MeV deuterons, 104 MeV alpha particles, 26 MeV protons, and 156 MeV ^{6}Li ions. The cyclotron group has been able to increase intensity and reliability of the ^{6}Li beam considerably during the last year,and some exciting results have been obtained with this beam. Another new development at the cyclotron is the routine production of ^{123}J for medical application. For the major part of its beam time the cyclotron is used by a large number of groups from other institutes of the research centre, from universities and several other institutes for research in a variety of fields. This report covers only that part of the work at the cyclotron in which staff of the Institute of Applied Nuclear Physics has participated. A separate report on the operation of the cyclotron is available.

G. Schatz

(G. Schatz)

Das Institut für Angewandte Kernphysik des Kernforschungszentrums Karlsruhe beschäftigt sich mit Anwendungen der Kernphysik auf Probleme der Kernenergie, Festkörperphysik und Analyse. Diese Untersuchungen werden durch grundlagenphysikalische Arbeiten begleitet. Der vorliegende Bericht, der dritte in der Reihe der Jahresberichte, gibt einen Überblick über die Arbeiten des Teilinstituts Kernphysik von Mitte 1976 bis Mitte 1977. Über die Tätigkeit des Teilinstitutes Nukleare Festkörperphysik wird getrennt berichtet.

Die Messung von Wirkungsquerschnitten neutroneninduzierter Kernreaktionen stellt eines der Hauptarbeitsgebiete des Teilinstituts dar. Der größte Teil dieser Untersuchungen dient der Bereitstellung von Kerndaten, die für den Entwurf Schneller Brutreaktoren benötigt werden. Auf diesem Arbeitsgebiet ist eine neu entwickelte Methode zur Messung von Einfangquerschnitten radioaktiver Proben hervorzuheben, die auf zwei Plutonium-Isotope angewendet wurde. Diese Arbeiten zeigen, daß man bei entsprechend verfeinerter Meßtechnik auch mit altmodischen Beschleunigern wie unserem 3 MV-Van-de-Graaff erfolgreich mit größeren (und teureren) Anlagen konkurrieren kann.

Methoden der Gamma-Spektroskopie werden auf Probleme des Kernbrennstoff-Zyklus angewandt. Beispiele dafür sind die Bestimmung von Plutonium in radioaktivem Abfall und die Messung der Isotopenzusammensetzung in Kernbrennstoffen. Dazu gehören auch so praktische Arbeiten wie die Installation und Erprobung einer Personenschleuse zur Verhinderung der Abzweigung spaltbaren Materials.

Auf dem Gebiet der Material-Analyse ist eine Protonenmikrosonde im Aufbau, die für Untersuchungen mit protonen-induzierter Röntgenstrahlung und/oder Kernreaktionen bestimmt ist.

Außer diesen angewandten Forschungsvorhaben wird eine Reihe von Experimenten auf dem Gebiet der Grundlagenphysik durchgeführt, die meisten davon in enger Zusammenarbeit mit Gastgruppen deutscher Universitäten. Eine enge Verbindung zwischen angewandter grundlagenorientierter Forschung ist für das Institut charakte-

ristisch und hat zu einem fruchtbaren Gedankenaustausch zwischen beiden Gebieten geführt. Die Arbeiten am Zyklotron nutzen in erster Linie den Strahl von ^{6}Li-Ionen von 156 MeV. Sie haben gezeigt, daß diese Projektile zum Studium höherer Riesenresonanzen mit inelastischer Streuung geradezu ideal sind. Eine andere Gruppe, die Kernmomente und Kernradien mit hochauflösender Laserspektroskopie bestimmt, hat erste Ergebnisse an radioaktiven Barium-Isotopen erhalten.

Das Institut betreibt zwei Beschleuniger. Ein einstufiger Van-de-Graaff-Beschleuniger von 3 MV wird hauptsächlich für Neutronenflugzeitexperimente und für die Festkörperphysik benutzt. Das Isochronzyklotron Karlsruhe, ein Festfrequenz-Zyklotron, liefert Strahlen von 52 MeV-Deuteronen, 104 MeV-Alphateilchen, 26 MeV-Protonen und 156 MeV-^{6}Li-Ionen. Der Zyklotron-Betriebsgruppe gelang es im letzten Jahr, Intensität und Zuverlässigkeit des ^{6}Li-Strahls wesentlich zu verbessern. Mit diesen Teilchen wurden bereits einige sehr interessante Ergebnisse erzielt. Eine weitere Neuentwicklung am Zyklotron ist die routinemäßige Herstellung von ^{123}J für medizinische Anwendungen. Trotzdem wird das Zyklotron weiterhin von Gruppen aus anderen Instituten des Kernforschungszentrums und von Universitäten sowie anderen externen Forschungs-Instituten für Arbeiten auf den verschiedensten Forschungsgebieten genutzt. In diesem Bericht wurden nur diejenigen Arbeiten am Zyklotron aufgenommen, an denen Mitarbeiter des Instituts für Angewandte Kernphysik beteiligt waren. Ein getrenner Bericht über den Betrieb des Zyklotrons liegt vor und wird auf Anfrage gern versandt.

G. Schatz

(G. Schatz)

CONTENTS

Page

1. NEUTRON PHYSICS

1.1 FUNDAMENTAL RESEARCH

1.1.1 Investigation of the Level Structure of ^{17}O and ^{29}Si

I. Schouky and S. Cierjacks

Although investigated previously by several groups, the level structure of ^{17}O and particularly that of ^{29}Si was not yet well known. Therefore, a new investigation for these nuclei was made by analyzing high-resolution total and differential elastic neutron scattering cross sections in the range between 0.5 and 6 MeV. Unambiguous spin and parity assignments were obtained by shape analyses of the highly resolved data. In our analyses the experimental resonance shapes were visually compared with the shapes of standard resonances calculated with a single channel, multilevel R-matrix code /1/. In the range below E_n = 6 MeV only a few partial waves contribute to neutron scattering, but resonances are already closely spaced, so that the general features of the resonance pattern are partly modified by resonance-resonance interference. Such effects were also considered by a calculation of the characteristic resonance behaviour in cases of level-level coherence. With this method, J and π values for 31 levels in ^{17}O between 0.5 and 6 MeV and for 51 levels in ^{29}Si between 0.5 and 3 MeV were determined. A list of the observed ^{29}Si resonances is given in table 1.

Using the improved information about the level structure of ^{17}O, we tried to interprete the experimental results with the predictions of the generalized shell model /2,3/. A description including only the 1 p 1/2, 2 s 1/2 and the 1 d 5/2 orbits generated most of the observed states below $\sim$9.5 MeV excitation energy. From the almost one-to-one correspondence with the observed levels it can be concluded that most of the levels, except the ground and first excited state and the broad level at E_x = 5.08 MeV, have a complicated multiparticle-multihole (up to 5p-4h) configuration.

Table 1. Spin and parity assignments for neutron resonances of ^{28}Si+n

	$E_{lab.}$ (MeV)	$E_{exc.}$ (MeV)	J^{π}		$E_{lab.}$ (MeV)	$E_{exc.}$ (MeV)	J^{π}
1	0.5321	8.988	$5/2^+$	27	1.804	10.216	$3/2^+$
2	0.562	9.017	$3/2^-$	28	1.850	10.260	$3/2^-$
3	0.5867	9.041	$1/2^-$	29	1.860	10.270	$5/2^+$
4	0.5904	9.044	$1/2^-$	30	1.918	10.326	$3/2^-$
5	0.7711	9.219	>1/2	31	1.926	10.334	>1/2
6	0.812	9.258	$3/2^-$	32	1.971	10.377	$3/2^+$
7	0.8441	9.289	$1/2^-$	33	2.038	10.442	$1/2^+$
8	0.9096	9.352	$3/2^-$	34	2.059	10.462	$1/2^-$
9	0.974	9.415	$1/2^-$	35	2.084	10.486	$3/2^-$
10	1.016	9.455	>1/2	36	2.115	10.516	$3/2^+$
11	1.042	9.480	$3/2^+$	37	2.171	10.570	$1/2^+$
12	1.163	9.597	$1/2^+$	38	2.226	10.623	$3/2^+$
13	1.186	9.619	$1/2^+$	39	2.288	10.683	3/2
14	1.203	9.636	1/2	40	2.300	10.695	$5/2^+$
15	1.255	9.686	$1/2^+$	41	2.373	10.765	$3/2^+$
16	1.263	9.694	$1/2^-$	42	2.439	10.829	$1/2^+$
17	1.408	9.834	$3/2^-$	43	2.456	10.845	$3/2^-$
18	1.478	9.901	$3/2^+$	44	2.490	10.878	$1/2^-$
19	1.5104	9.933	>1/2	45	2.495	10.883	$5/2^-$
20	1.527	9.949	$3/2^+$	46	2.657	11.040	$5/2^+$
21	1.579	9.999	$3/2^+$	47	2.696	11.077	$3/2^-$
22	1.595	10.014	$3/2^-$	48	2.778	11.156	$1/2^-$
23	1.628	10.046	$1/2^-$	49	2.854	11.230	$3/2^+$
24	1.636	10.054	$5/2^+$	50	2.937	11.310	$5/2^+$
25	1.650	10.067	$5/2^+$	51	2.971	11.343	$1/2^+$
26	1.783	10.196	>1/2				

For ^{29}Si single-particle strengths of fragmented single-particle levels were derived for nuclear states above the neutron binding energy. The observed percentages of the Wigner limits for s-, p- and d-wave resonances are consistent with experimentally determined spectroscopic factors from charged particle work. Analyzed data in the energy range between 1.05 and 1.40 MeV formed the basis for a study of isospin mixing in isobaric analog states of this nucleus (compare also section 1.1.4 of this report).

References

/1/ G.J. Kirouac, J. Nebe, Report KFK 1069 (1969).

1.1.2 Isospin Mixing of Low-Lying T = 3/2 Resonances in Light T_Z = 1/2 Nuclei

S. Cierjacks, D. Erbe, F. Hinterberger[+], B. Leugers, P. v. Rossen[+], and G. Schmalz

The neutron decay of T = 3/2 states in light T_Z = 1/2 nuclei is isospin-forbidden and can only proceed via isospin impurities in either the initial or the final states. Thus, ignoring the certainly small T = 1 admixture in the T = 0 ground states of the target nuclei, the investigation of neutron widths of T = 3/2 resonances provides a good means to obtain information about the isospin purity of such states. Furthermore, isospin admixtures are related to charge-dependent effects in the nuclear states, arising from a small charge-dependent contribution to the nuclear interaction produced by the Coulomb interaction and from a charge-dependent part of the nucleon-nucleon interaction. Thus, additional information with respect to the charge dependence of the nuclear force may also be expected from the above mentioned studies.

In continuation of the programme on the study of narrow T = 3/2 resonances, ultra high-resolution transmission measurements were performed for oxygen. For this nucleus only little information about low-lying T = 3/2 states exists from previous work. Information about four T = 3/2

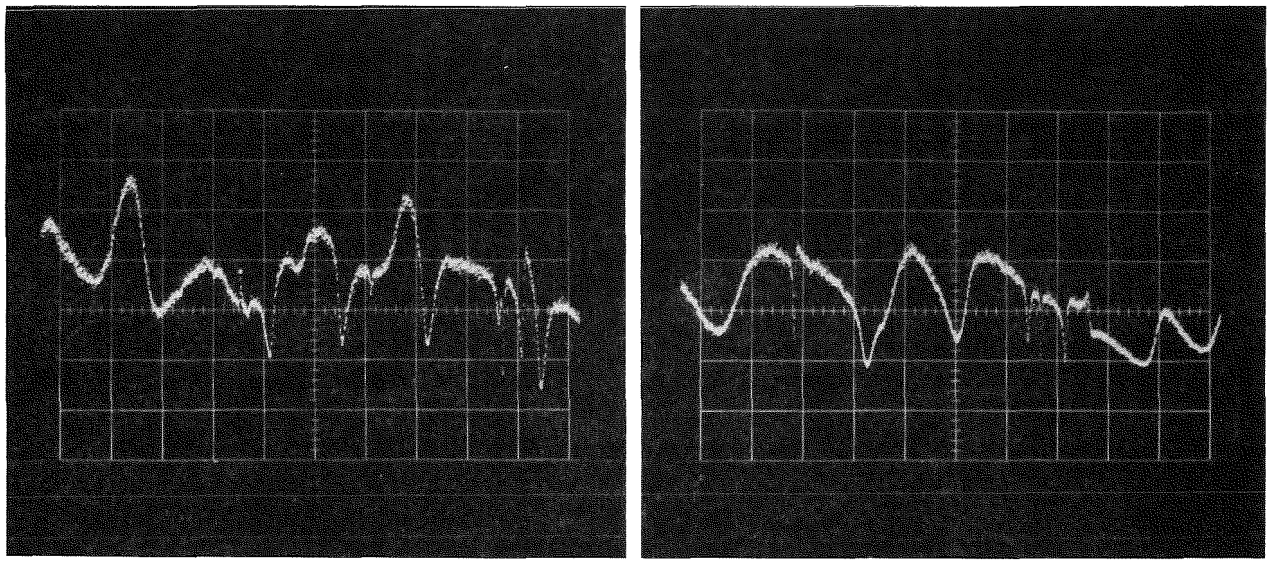

$8.579 \geq E_n \geq 5.715$ MeV

$5.715 \geq E_n \geq 4.138$ MeV

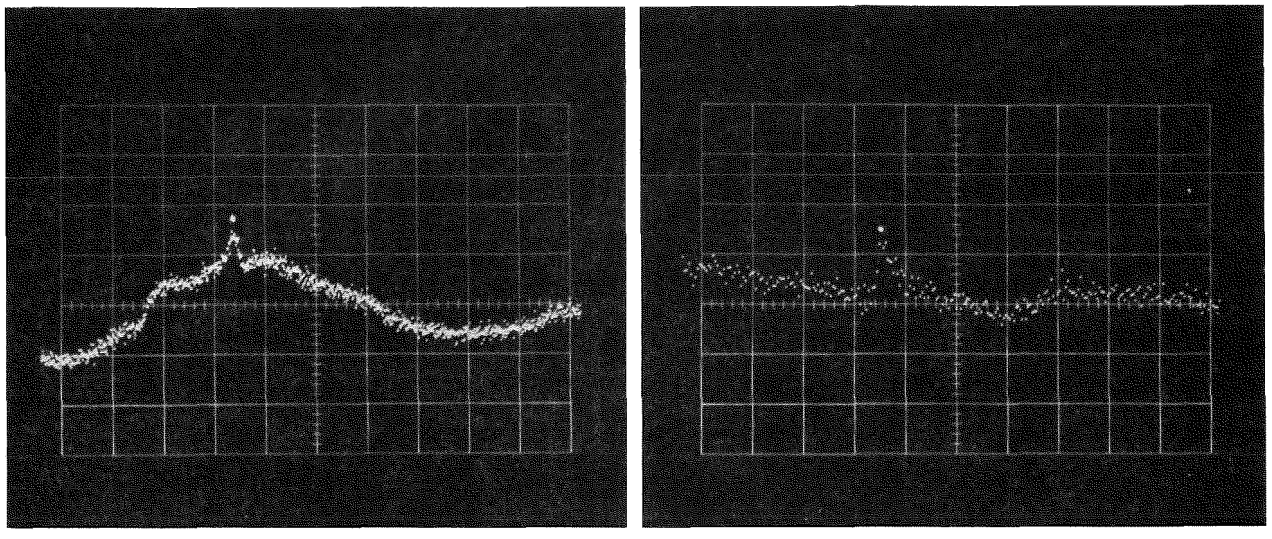

$11.208 \geq E_n \geq 9.9273$ MeV

$7.4483 \geq E_n \geq 7.2606$ MeV

Fig. 1. Top: Transmission time-of-flight spectrum from oxygen between ∿4-8 MeV. The pronounced broad structure in both photographs is mostly due to well-known broad ^{17}O resonances. The overintensified point in the photograph on the left side marks the position of the narrow first T=3/2 resonance at E_n = 7.3716 MeV.
Bottom: Details of resonance patterns from two of the five measured candidates for T=3/2 resonances. Both resonances are of the inverse type, i.e. they exhibit destructive interference with potential scattering indicated by the maxima in the transmission spectra.

resonances was obtained from a study of the ^{13}C (α,n) reaction carried out by McDonald et al. /1/. These authors placed the resonance energies at E_x = 11.077, 12.466, 12.946 and 12.994 MeV and determined total widths ranging between 3 and 8 keV. Five additional T = 3/2 resonances are predicated from studies of isobaric analog states in the mirror nucleus ^{17}F /2,3/.

In the ultra high-resolution transmission measurements with the Karlsruhe isochronous cyclotron fast neutron spectrometer five extremely narrow resonances were observed at exactly the energies predicted for the T = 3/2 analog states. Typical results for a part of the measured energy region are shown in fig. 1. In this illustration the upper two photographs show the transmission time-of-flight spectrum in the energy range from 4.1 to 8 MeV. The pronounced structure in these curves is mainly due to the transmission dips of well-known broad ^{17}O resonances. The overintensified point in the photograph on the left side marks the position of the very narrow first T = 3/2 resonance at E_n = 7.3729 MeV. The two bottom curves show in more detail the resonance pattern of two out of the five candidates for T = 3/2 resonances. In particular, these are the candidates for the first T = 3/2 resonance suggested by McDonald et al. /1/ and the fifth T=3/2 state predicted by Skwiersky et al. /2/.Both resonances are of the inverse type, i.e.,they exhibit destructive interference with potential scattering as can be seen by the maxima in the transmission spectra.

+Institut für Strahlen- und Kernphysik, Universität Bonn ,Germany

References

/1/ A.B. McDonald, T.K. Alexander and O. Häusser, Nucl. Phys.A273 (1976) 464.

/2/ B.M. Skwiersky, C.M. Baglin and P.P. Parker, Phys. Rev. C9 (1974) 910.

/3/ F. Ajzenberg-Selove, Nucl. Phys. A 281 (1977) 1.

1.1.3 Investigations on the Isospin-Dependence of the Electromagnetic Interaction

S. Cierjacks, D. Erbe, F. Hinterberger[+], B. Leugers, P. v. Rossen[+], and G. Schmalz

To test the existence of a possible isotensor component in the electromagnetic interaction there are mainly three methods in the field of low-energy nuclear physics. The first is to look for deviations from the quadratic mass formula $M = M_o\ (1 + a\ T_Z + b\ T_Z^2)$ which should hold for the members of an isospin multiplet assuming only isoscalar and isovector, but no isotensor currents in the electromagnetic interaction. The second is to search for isospin-forbidden $\Delta T = 2$ gamma transitions induced by nuclear reactions. The third method, suggested by Blin-Stoyle /1/, is to compare the decay widths for $T = 3/2 \rightarrow T = 1/2$ transitions in mirror nuclei. An isotensor component would reveal itself by a different decay width for both nuclei, the difference of the widths being predicted to be of the order of 10 % /1/.

While the first two methods are scarcely used, mainly due to the lack of many candidates of well established isospin states with either $\Delta T = 2$ or the lack of completely known sets of all $2\ T + 1$ members of an isospin multiplet , most recent work has concentrated on the application of the third method, and here mainly on the study of the ^{13}C - ^{13}N mirror pair. Despite of various investigations, no decisive conclusions about the existence of an isotensor current could be drawn. Presently, sufficiently precise values exist only for $\Gamma_{\gamma o}$ of ^{13}N and for the ratio $\Gamma_{\gamma o}/\Gamma$ of ^{13}C. Therefore, an accurate measurement of the total width of ^{13}C in a neutron scattering experiment would be a valuable contribution to the problem of charge-asymmetry effects from isotensor currents. Of course, the decay widths $\Gamma_{\gamma o}$ of ^{13}C can also be directly determined from a very precise electron scattering experiment. But there the problem of the extrapolation to the real photon point exists, so that a different independent determination seemed to be highly desirable.

In order to search for the 15.11 MeV $T = 3/2$ resonance in ^{13}C, an ultra-high-resolution transmission measurement on carbon was performed with the cyclotron fast neutron time-of-flight spectrometer. The experimental study of this resonance required a very high resolution, since previous work indicated a width ranging between 5-8 keV. The necessary energy resolution of

better than 4×10^{-4} at the above excitation energy was achieved by a substantial improvement of the spectrometer employing a neutron detector with a largely improved time characteristic and a considerably decreased neutron pulse length. The latter improvement was achieved by optimizing the phase conditions in the centre of the machine. Under the improved conditions, a statistically significant resonance excursion was discovered for the first time in a transmission spectrum. A preliminary estimate of the resonance height indicated that the earlier predicted value for the ratio Γ_n/Γ of 0.07 is much too large. The analysis of the data is in progress.

+ Institut für Strahlen- und Kernphysik, Universität Bonn, Germany

References

/1/ R.J. Blin-Stoyle, Phys. Rev. Lett. 23 (1969) 535.

1.1.4 Isobaric Analog Impurity from Total and Differential Neutron Scattering Cross Sections of Silicon*

S.K. Gupta+, S. Cierjacks, and I. Schouky

Resonance parameters of four resonances in silicon have been obtained by analyzing the recently measured differential neutron scattering cross section on Si combined with the total neutron cross section in the neutron energy range from 1.05 to 1.40 MeV with the R-matrix single-channel multilevel theory. The resonance at 1254 keV has been identified as the s-wave analog resonance in ^{29}Si. The identification also takes into account the experimental radiative neutron capture data as well as the shell model calculation of the radiative width. Some estimates of the isospin mixing matrix element have been made and compared with similar data of Weigmann et al. for the ^{24}Mg+n system.

* Submitted to Phys. Rev.

+ Guest scientist from Nuclear Physics Division, Bhabha Atomic Research Centre, Bombay 400-085, India

1.1.5 The Total Cross Section of ^{45}Sc in the Neutron Energy Range from 10 to 100 keV

M.A. Kazerouni, F. Fröhner[+], and G. Rohr[++]

The total cross section of ^{45}Sc was determined by a transmission experiment between 10 and 300 keV using the time-of-flight technique. A resolution of 0.13 nsec m^{-1} was obtained at a flight path of 22 m. This was sufficient to largely resolve the s-wave resonance structure in ^{45}Sc below 110 keV. For the 50 observed resonances the energies, widths and spins were determined by shape analysis of the total cross section using an R-matrix multilevel formalism /1/. The distributions of level widths and spacings for individual spins were compared both with Porter-Thomas and Wigner distributions and the number of missed levels were determined from these comparisons. Good agreement was found between experimental and theoretical distributions. The strength function was found to be spin dependent:

$$S_- = (7.7 \pm 1.4) \times 10^{-4} \quad \text{for spin 3}$$

and

$$S_+ = (3.4 \pm 0.7) \times 10^{-4} \quad \text{for spin 4.}$$

This result can hardly be explained by statistical fluctuations in view of the large number of resonances included in the present studies.

[+] Institut für Neutronenphysik und Reaktortechnik

[++] CBNM Euratom, Geel, Belgium

References

/1/ A.M. Lane, R.G. Thomas, Rev. Mod. Phys. 30 (1968) 257.

1.1.6 A Measurement of the Neutron Capture Cross Section of ^{58}Fe

Ly Di Hong, H. Beer, and F. Käppeler

The neutron capture cross section of ^{58}Fe is of particular interest for the astrophysical nucleosynthesis. Near the mass number 56 the solar

system abundances of the chemical elements are determined by two different synthezising processes: an equilibrium process (e-process) at very high temperature and density forming preferably isotopes with high binding energy per nucleon up to A $\sim$ 65, and a slow neutron capture process (s-process) which builds up the isotopes with A > 56, starting from the most abundant nuclide ^{56}Fe as a seed nuclide /1/.

For a quantitative understanding of the solar abundance distribution in the mass range A = 56 to 65, the observed total abundances have to be decomposed in their s- and e-process contributions. The s-process is characterized by the smooth behaviour of the product N $\langle\sigma\rangle$ as a function of mass number A, where N represents the solar elemental abundance and $\langle\sigma\rangle$ the Maxwellian averaged neutron capture cross section. This implies that for theoretical calculations of abundances generated along the s-process path the sequence of Maxwellian averaged capture cross sections has to be known. These data have been measured previously for a series of nuclides /2,3/.

For the normalization of the N $\langle\sigma\rangle$curve the abundances and averaged neutron capture cross sections for at least two nuclides originating from a pure s-process are required. Above A $\sim$ 65 there exist several such nuclides. However, in the vicinity of A = 56, only ^{58}Fe can be considered as a pure s-nuclide because its small binding energy would not have allowed to synthesize it in an e-process environment. Thus, the averaged neutron capture cross section of ^{58}Fe represents a crucial link for the calculations of s-process abundances in the mass range A = 56 to 65. For this reason, the previously not known cross section for capture of keV neutrons in ^{58}Fe has been measured at the Karlsruhe 3 MV pulsed Van de Graaff accelerator. Neutrons were produced from the ^{7}Li (p,n) reaction with a pulsed proton beam (repetition rate 500 kHz, pulse width $\lesssim$1 nsec) providing an average beam current of 0.4 µA. Neutron energies were determined by the time-of-flight technique covering the energy interval between 10 and 200 keV. Capture γ rays were detected by an 800 ℓ liquid scintillator tank and the events were stored in a matrix of 16 pulse height channels versus 1024 time-of-flight channels. Details about the experimental technique are described in ref. /4/. The measurement was complicated by the small available sample mass (16.4 g Fe_2O_3 enriched to 65 % in ^{58}Fe). Therefore, only a poor signal-to-background ratio could be achieved resulting in rather large uncertainties of the measured

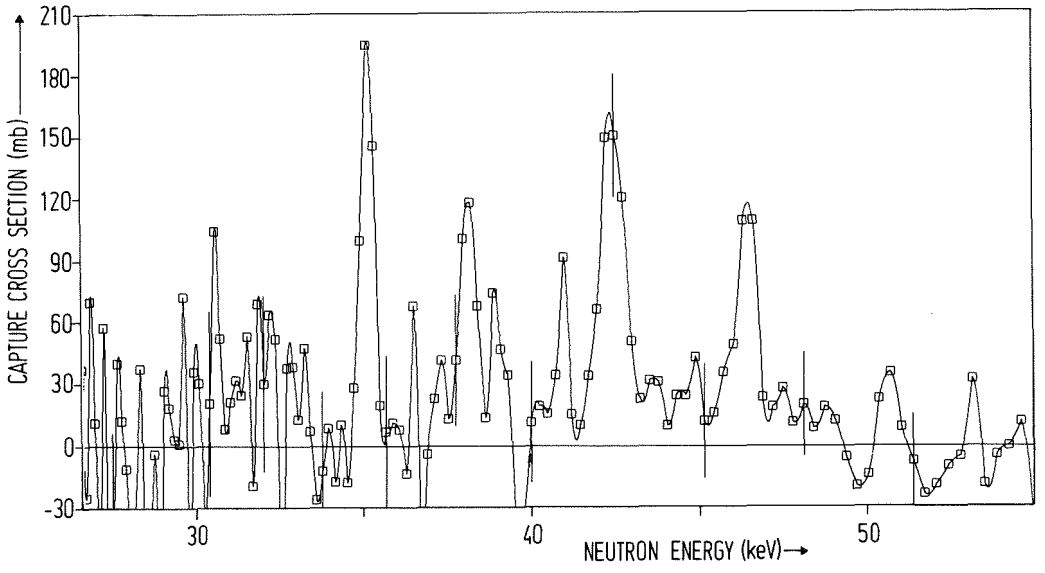

Fig. 1. The capture cross section of ^{58}Fe between 25 and 55 keV (not corrected for multiple scattering and self-screening).

cross section. Fig. 1 shows the cross section as it was calculated from the count rates (without multiple scattering and self-screening corrections) between 25 and 55 keV. The statistical uncertainty is greatly reduced by averaging over a Maxwellian energy distribution, but a systematic uncertainty of 25 % still remains. Since the data analysis is not yet completed, no final results can be given at present. However, the preliminary data evaluation clearly indicates that the experimental average capture cross section of ^{58}Fe is considerably larger than it was estimated previously /5,6/.

References

/1/ D.D. Clayton, "Principles of Stellar Evaluation and Nucleosynthesis", McGraw Hill, New York (1968).

/2/ H. Beer, R.R. Spencer, A. Ernst, Astron. & Astrophys. 37 (1974) 197.

/3/ R.R. Spencer, H. Beer, Nucl. Sci. and Eng. 60 (1976) 390.

/4/ H. Beer, R.R. Spencer, Nucl. Phys. A 240 (1975) 29.

/5/ B.J. Allen, J.H. Gibbons, R.L. Macklin, Adv. Nucl. Phys. 4 (1971) 202.

/6/ J. Holmes, S.J. Woosley, in preparation.

1.1.7 Neutron Capture Cross Section Measurements on Krypton

F. Hensley

Measurements of the neutron capture cross section of natural krypton in the neutron energy region 5 keV $\leq E_n \leq$ 200 keV are presently being performed at the Karlsruhe pulsed Van de Graaff accelerator. This data is important for theoretical calculations of solar isotopic abundances in the vicinity of the iron peak produced by the astrophysical s-process /1/. It allows the normalization of the $N_A \langle\sigma_A\rangle$ curve (N_A = natural isotopic abundance, $\langle\sigma_A\rangle$ = Maxwellian averaged neutron capture cross section) which fairly well describes the isotopic abundances built up in the s-process. Furthermore, the data is needed for the determination of capture cross sections of enriched krypton isotopes which are planned later on.

The sample preparation for the cross section measurements starts with one litre of krypton gas at normal conditions. This gas volume is condensed into a canning of 1.91 cm^3 volume initially cooled to the temperature of liquid nitrogen. To assure that the krypton is located in the probe volume irradiated by the neutron beam, the canning is heated to a temperature where the krypton is liquid. The heater is regulated with a temperature control circuit, keeping the average temperature constant within $\pm$ 0.05°. This temperature variation gives rise to a variation of $\pm$ 30 Torr in the vapour pressure of the liquid providing a constancy of the amount of irradiated material within 0.2 %. Under best conditions, 95 % of the gas sample material has been liquified into the probe volume. From the known density and geometrical size of the sample one can determine the sample mass with an accuracy of <0.6 % as given by the uncertainty in the temperature-density relation.

Neutrons are produced via the $^7Li(p,n)^7Be$ reaction at the Karlsruhe Van de Graaff accelerator which provides a pulsed proton beam with an average beam current of 2-3 μA, a pulse length of $\leq$ 1 nsec and a repetition rate of 1 MHz. The neutron beam is collimated in a double tapered guide tube of $^6Li_2CO_3$ (pressed to 86 % crystal density) so that only a small amount of the structural materials surrounding the sample is directly irradiated. The neutron energy is determined by time-of-flight at a distance of 70 cm from the ^7Li target with a time resolution of 1.5 ns.

The neutron flux is measured by the detection of neutron capture events from a gold sample which is interchanged with the krypton sample by means of a sample changer. The measuring intervals are defined by integrating the beam current to a preselected charge. Capture events are detected by measuring the prompt γ rays with two C_6D_6 liquid scintillators using the Maier-Leibnitz pulse height weighting technique /2/. The background from neutron capture in structural materials is corrected by subtracting capture events from an empty sample canning which is also mounted on the sample changer.

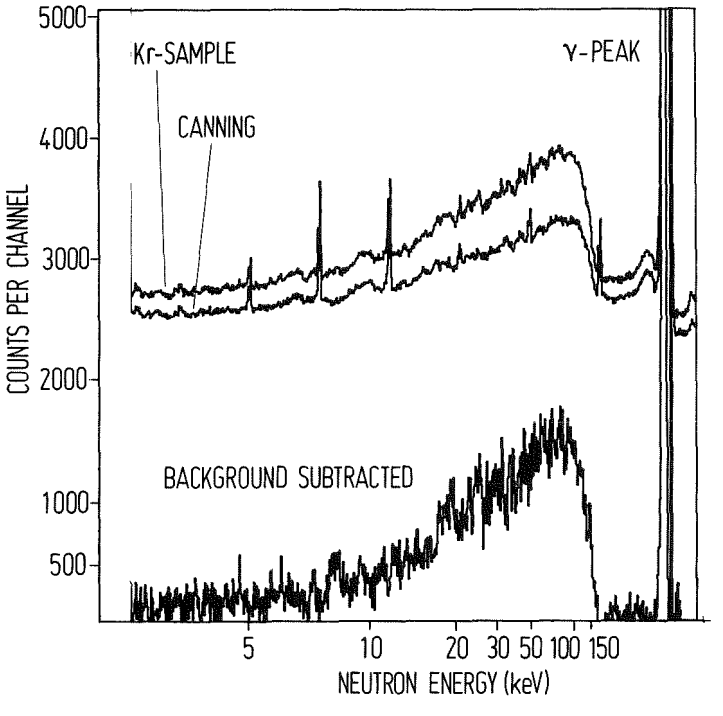

Fig. 1. Time-of-flight spectra from neutron capture cross section measurements on natural krypton.

Fig. 1 shows time-of-flight spectra obtained from a natural krypton sample and an empty canning and the net krypton spectrum after subtracting the background. Further measurements on separated krypton isotopes will be carried out this year.

References

/1/ F. Hensley, Report KFK 2379 (1976) p. 16.

/2/ R.L. Macklin, J.H. Gibbons, Phys. Rev. 190 (1967) 1007.

1.1.8 A Measurement of Correlated Fission Fragments From Fission of ^{235}U with 550 keV Neutrons

R. Müller[+], A. Naqvi, and F. Käppeler

The 4-parameter experiment for the determination of kinetic energies and velocities of correlated fragments in fast neutron induced fission of ^{235}U was described in detail in the preceding annual report /1/. At the Karlsruhe 3 MV pulsed Van de Graaff accelerator the $^{7}Li(p,n)$ reaction was used as a neutron source. The fissile sample was located very close to the neutron target and the fragments were detected by large area solid state detectors at flight paths of up to 860 mm. The fragment velocity was measured by the time of their arrival at the detector with reference to the pulse pick-up signal from the accelerator. Thus, no time-zero detector was required.

The analysis of the data obtained from the first runs at 550 $\pm$ 50 keV neutron energy showed that significant long term drifts in the electronics occurred during the 4 weeks of the experimental runs. Corrections for these drifts were possible by normalizing the data to accurate values of average fragment kinetic energies and average velocities. Therefore, in a second run it was tried to carefully measure these quantities. In these measurements the overall time resolution could be improved to less than 1 nsec by an accurate adjustment of the electronics and by the automatic control of the 500 psec pulse width of the accelerator.

The prompt fragment mass yields are calculated from the fragment velocities. For the neutron energy interval of 550 $\pm$ 50 keV no significant deviations from the thermal fission mass distribution was found. Even the same peak-to-valley ratio of about 600 was achieved, indicating that an increase of 0.5 MeV in excitation energy is not sufficient to deteriorate the shell effects between the saddle and scission point in ^{235}U.

The initial total kinetic energy is also determined from the fragment velocities only. The calculation of the final masses and energies uses the energy calibration of Schmitt /2/ for semiconductor detectors. In order to obtain good agreement with radiochemical mean final masses /3/, the energies determined in this way must be reduced by about 2 MeV. The number of emitted neutrons results from the difference of the initial and final mass. The

measured mean values of initial and final quantities are summarized in table 1.

Table 1. Mean values of initial (*) and final quantities

V_L^*, $\sigma_{V_L}^*$	1.415 cm/ns	0.058 cm/ns
V_H^*, $\sigma_{V_H}^*$	0.983 cm/ns	0.068 cm/ns
A_L^*, $\sigma_{A_L}^*$	96.6 amu	5.5 amu
A_H^*, $\sigma_{A_H}^*$	139.3 amu	5.5 amu
E_T^*, $\sigma_{E_T}^*$	170.0 MeV	10.3 MeV
A_L, σ_{A_L}	95.2[+)] amu	5.5[+)] amu
A_H, σ_{A_H}	138.5[+)] amu	5.4[+)] amu
ν_L, $d\nu_L/dA^*$	1.4 amu	0.04
ν_H, $d\nu_H/dA^*$	0.8 amu	0.12

[+)] Values taken from Ref. /3/

The experiment will be further improved with respect to resolution by using a low mass neutron target and thin fissile samples, and by a flight path adjustment which accounts for the deviation of the fragment directions from collinearity due to momentum transfer by the fission inducing neutron. This adjustment is important at higher neutron energies where further measurements will be carried out.

[+] Physikalisches Institut der Universität Tübingen, Germany

References

/1/ R. Müller, F. Käppeler, A. Naqvi, F. Gönnenwein, and A. Ernst, Report KFK 2379 (1976) p. 6.

/2/ H.W. Schmitt, W.E. Kiker, C.W. Williams, Phys. Rev. 137, B 837 (1965).

/3/ K.F. Flynn, L.E. Glendenin, Rep. ANL-7749 Argonne Nat. Lab. (1970).

1.2 NUCLEAR DATA FOR REACTORS

1.2.1 Gamma-Ray Production Cross Sections from Inelastic Neutron Scattering in Nickel and Chromium

F. Voß

Inelastic scattering cross sections of structural materials are important quantities for the lay-out of fission and future fusion reactors. One possible approach to obtain these data is to measure the gamma rays from the excited nuclear states. This method has been chosen at the Karlsruhe fast neutron time-of-flight spectrometer.

Cross sections for the production of gamma rays following inelastic neutron scattering on Cr and Ni have been measured. The overall experimental set-up is described in ref. /1/. Details of the actual experiment are given in table 1. Neutrons are scattered from a ring-shaped sample at a flight path of 58 m. The gamma rays are detected in a Ge(Li) detector located at 125^{o}. The neutron flux is measured with a NE 102 plastic scintillator detector.

Table 1. Specifications of the experimental set-up

	Cr	Ni
Scattering sample:		
Inner diameter	120 mm	122 mm
Outer diameter	254 mm	257 mm
Height	6.7 mm	9.4 mm
Flight path length	57.918 m	57.917 m
Gamma detector:		
Size	42 cm^3 Ge(Li)	
ΔE(FWHM)	2.1 keV for E_γ = 1333 keV (^{60}Co)	
Mean scattering angle	125^{o}	

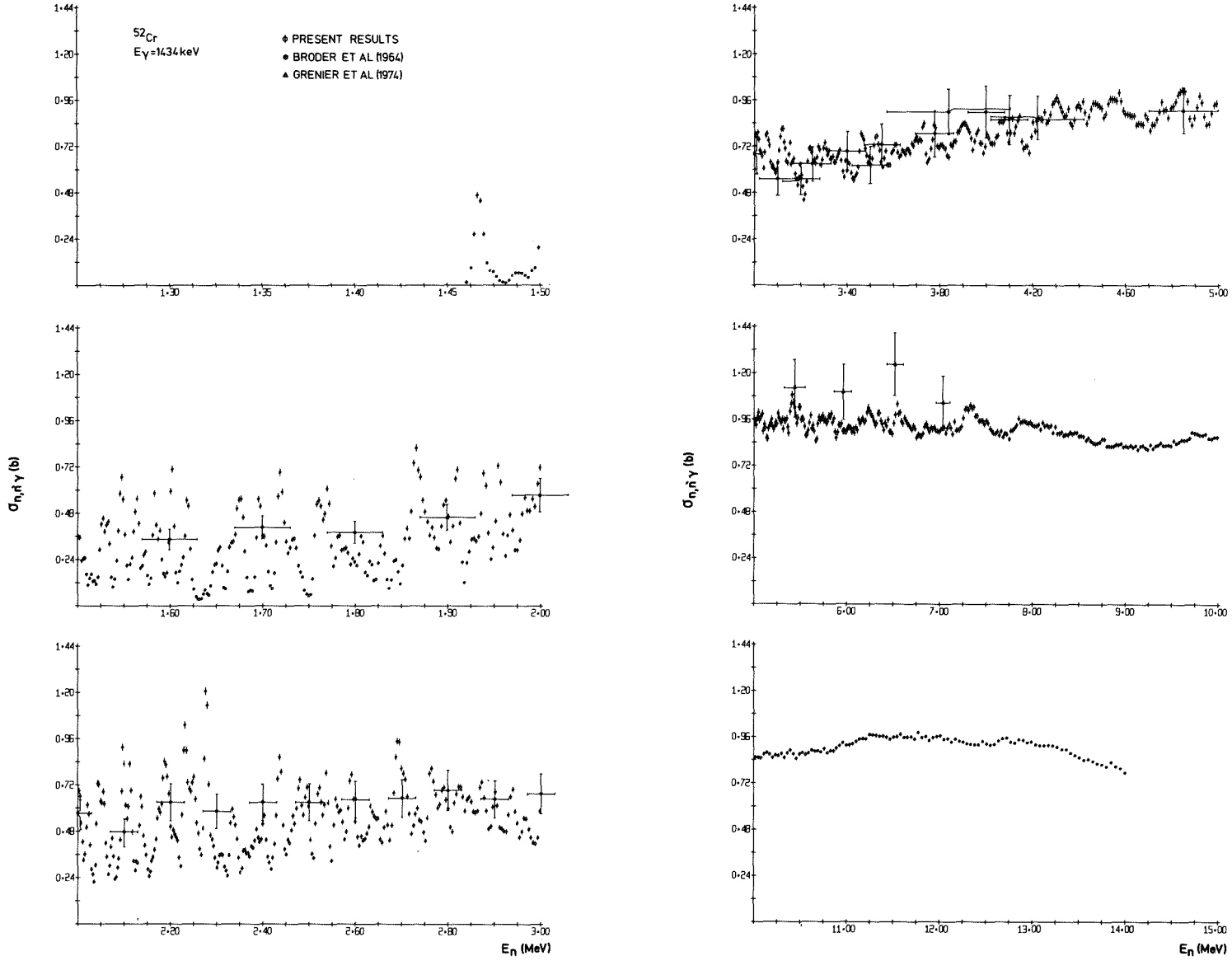

Fig. 1. $\sigma(n,n'\gamma)$ of ^{52}Cr for E_γ = 1434 keV

Excitation functions for ten gamma rays from Cr isotopes and for eight gamma rays from Ni isotopes have been measured in the neutron energy range from the threshold energy for the individual excited levels up to 14 MeV. The gamma-ray energies are summarized in tab. 2 together with the corresponding isotopes and the excited level energy E_x. Gamma-ray production cross sections have been obtained by multiplying the measured differential cross sections with 4 π. The gamma-ray production cross sections can be uniquely assigned to indiviual isotopes except that for the 1172 keV gamma rays which result from two different isotopes (^{60}Ni and ^{62}Ni).

Table 2. Summary of gamma rays and their isotopic assignments

Cr			Ni		
Isotope	E_x(keV)	E_γ(keV)	Isotope	E_x(keV)	E_γ(keV)
^{50}Cr	783	783	^{58}Ni	2459	1005
				2775	1321
^{52}Cr	3414	648		1454	1454
	3114	744		3038	1584
	2369	934	^{60}Ni	2626	467
	2766	1332		2159	826
	1434	1434		1333	1333
	2965	1531			
	3162	1728	^{60}Ni	2506	1173
	3472	2038	^{62}Ni	1172	1172
^{53}Cr	1289	1289			

The following corrections have been applied to the data:

a) The corrections for gamma-ray self absorption in the sample range from 17-25 % in Cr and from 30-44 % in Ni.

b) The average correction for the neutron flux attenuation is approximately 10 %, but reaches values up to 20 % in the maxima of the

total neutron cross section.

c) The corrections for multiple scattering have been calculated with a Monte-Carlo programme. They are normally less than 20 %, but they can be considerably higher in the partial cross section minima at low neutron energies.

As an example for the results, the excitation function for E_γ = 1434 keV in ^{52}Cr is given in fig. 1. The error bars represent the statistical errors. The combined error from the Ge(Li) detector efficiency and the neutron flux determination is estimated to be less than 11 %. Data from two other laboratories are shown for comparison. The overall agreement is satisfying.

References

/1/ F. Voß, Report KFK 1611 (1972).

/2/ D.L. Broder, V.E. Kolesov, A.I. Lashuk, I.P. Sadokhin, A.G. Dovbenko, Atom. Energy. 16 (1964) 103.

/3/ G. Grenier, B. Duchemin, D. Parisot, Report CEA-R-4634 (1974).

1.2.2 An Accurate Determination of the ^{235}U Capture-to-Fission Ratio in the Energy Range from 10 to 500 keV

H. Beer and F. Käppeler

The capture-to-fission cross section ratio σ_c/σ_f of ^{235}U has been measured in the neutron energy range between 10 and 500 keV at the Karlsruhe pulsed 3 MV Van de Graaff accelerator /1/. An 800 ℓ liquid scintillator tank served to detect capture and fission events by means of their gamma rays. A fission neutron counter in coincidence with the scintillator tank was used to discriminate between capture and fission events. The whole energy range of the measurement was covered in five different runs with overlapping energy regions.

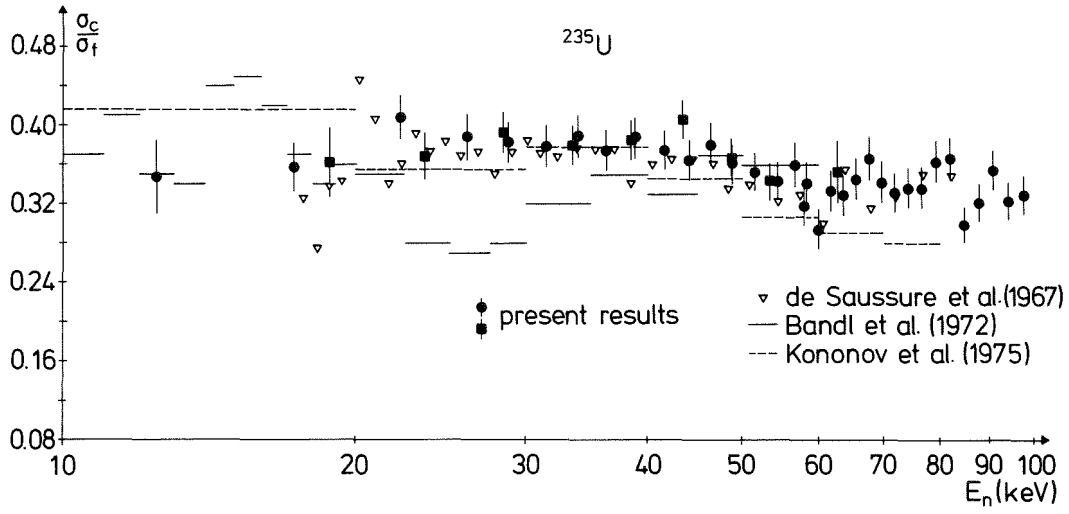

Fig. 1. The capture-to-fission cross section ratio σ_c/σ_f of ^{235}U in the energy region 10-100 keV. Black dots and squares represent different runs of the present data. For comparison, the results from previous measurements are also given. At 30 keV the following total uncertainties are quoted by the various authors:

de Saussure et al. /2/	:	*8.6 %*
Bandl et al. /3/	:	*12.5 %*
Kononov et al. /4/	:	*10.3 %*
This work	:	*5.5 %* .

The results obtained represent an accurate determination of the capture-to-fission ratio. The uncertainty of the data values from the present measurement is composed of a statistical uncertainty of typically 6 % and a systematic uncertainty of 3 to 4 % , which results from the calculation of the respective spectrum fractions for capture and fission events. In fig. 1 the measured data in the energy range between 10 and 100 keV are plotted together with results from other authors. Excellent agreement was obtained between the present values and the data of de Saussure et al. /2/. All measurement results shown in the figure are consistent within the quoted error bars except the results of Bandl et al. /3/ in the energy range between 20 and 30 keV.

References

/1/ H. Beer, F. Käppeler, Report KFK 2223 (1975) p. 22;
Report KFK 2379 (1976) p. 12.

/2/ G. de Saussure, L.W. Weston, R. Gwin, R.W. Ingle, J.H. Todd, A. Lottin, Proc. of the Conf. on Nucl. Data for Reactors, Paris 1966, Vol. II (IAEA, Vienna 1967) p. 233.

/3/ R.E. Bandl, H. Miessner, F.H. Fröhner, Nucl. Sci. and Eng. 48 (1972) 324.

/4/ V.N. Kononov, E.D. Poletaev, B.D. Yurlov, Sov. Atomic Energy, 38, (1975) 105.

1.2.3 Precision Measurements of Fission Cross Section Ratios for ^{239}Pu and ^{240}Pu Relative to ^{235}U

S. Cierjacks, K. Kari, D. Erbe, B. Leugers, and G. Schmalz

The fission cross sections of ^{239}Pu and ^{240}Pu are fundamental data in reactor technology. Precise values are important for optimizing the design of fast breeder reactors. Although a large number of measurements have been performed, the cross sections for these nuclei are still unsufficiently known. Individual measurements still show deviations ranging between 10 and 15 %. These discrepancies are mainly due to the fact that both nuclei have small alpha half-lives and thus are highly radioactive, which complicates precise cross section measurements. A new measurement aiming at high precision was carried out for both Pu isotopes between 0.5 and 20 MeV employing time-of-flight techniques /1/. The measurements were conducted using gas scintillation counters of a special design, capable to measure fission events in the presence of a very high alpha background. Since flux measurements in fast neutron spectra are difficult to perform, fission cross sections were measured in a first step relative to the fission cross section of ^{235}U, which is the internationally recommended fission standard. As a typical result, fig. 1 shows the fission cross section ratio for ^{240}Pu in the energy region from 0.1 to 20 MeV on a semilogarithmic scale. In this diagram, our data are compared with the values of a recent evaluation performed by Hunter et al. from the Los Alamos Laboratory /2/. It can be seen that rather good agreement exists between

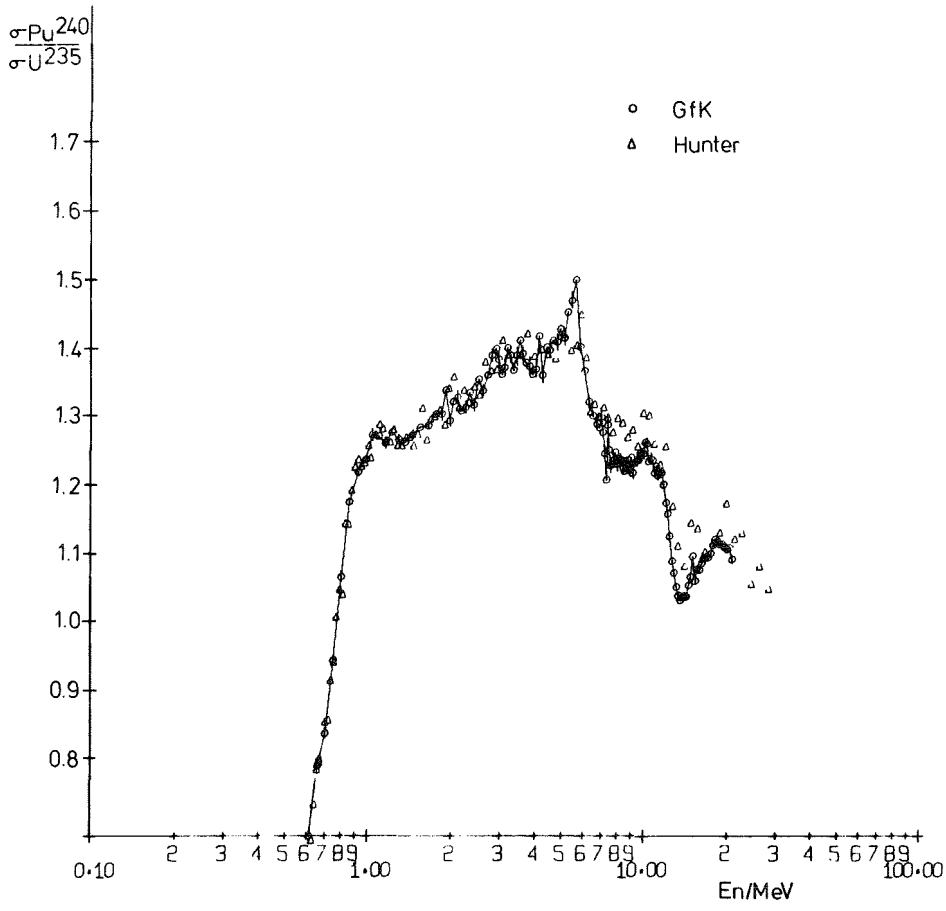

Fig. 1. Fission cross section ratio $^{240}Pu/^{235}U$. Present results are compared with evaluated data from the Los Alamos Scientific Laboratory (ref. 2).

the two data sets, except in the range above about 10 MeV, which is, however unimportant for a fast reactor spectrum. In the energy regions around 12 and 20 MeV there also seems to exist a discrepancy between the energy scales of the two data sets.

References

/1/ S.W. Cierjacks, B. Leugers, K. Kari, P. Brotz, D. Erbe, D. Gröschel, G. Schmalz, F. Voß, Proc. NEA-Specialists Meeting on Fast-Neutron Fission Cross Sections, Argonne, June 1976, Report ANL-76-90, p. 96.

/2/ R.E. Hunter, L. Steward, T.Y. Hirous, Report LA-5172 (1973).

1.2.4 Absolute Fast Neutron Fission Cross Sections of ^{239}Pu and ^{240}Pu

K. Kari, S. Cierjacks, B. Leugers, D. Erbe, and G. Schmalz

Absolute fission cross sections of ^{239}Pu and ^{240}Pu were determined from the same experiment described in the preceding section 1.2.3. This determination was possible since the neutron flux was determined simultaneously during the cross section measurements using a novel

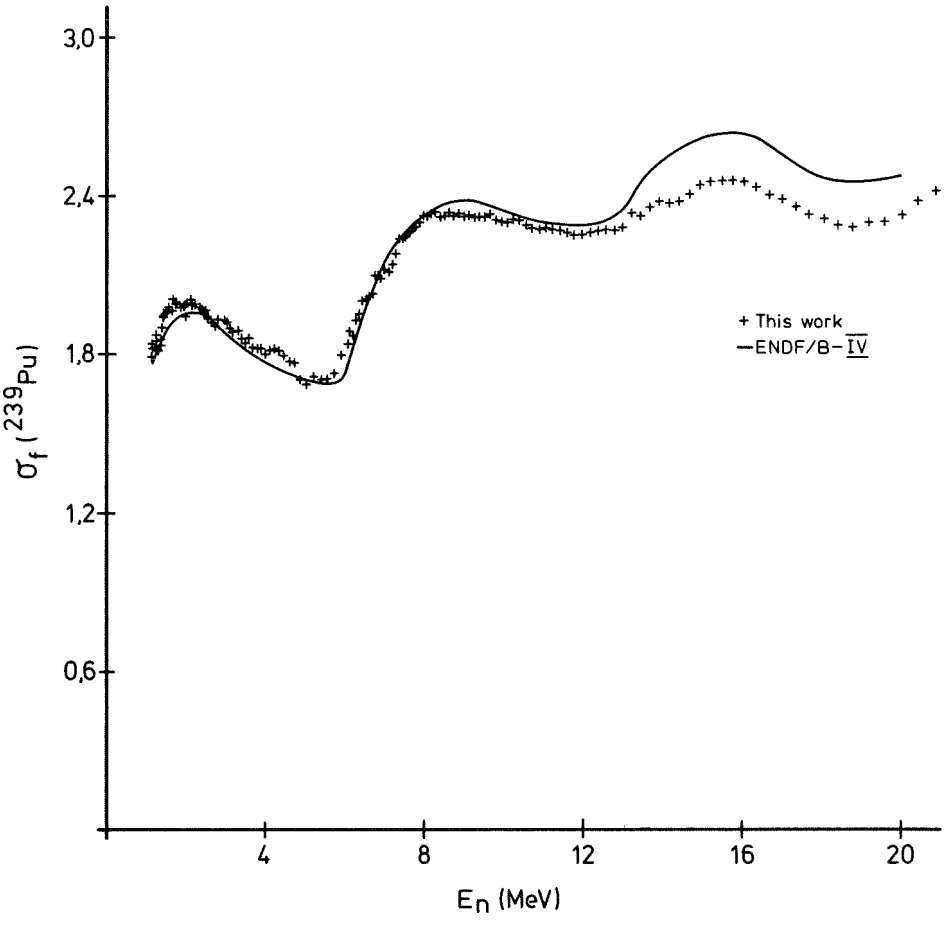

Fig. 1 Fission Cross Section of ^{239}Pu between 1 and 20 MeV. For the determination of absolute values, the H(n,p) standard reaction was employed. For comparison, the evaluated data from ENDF/B-IV are also shown (solid line).

fast neutron transmission flux detector described elsewhere /1/. The flux determination was accomplished separately for energy regions ranging from 0.5 to 6 MeV and from 5 to 20 MeV, both having a small interval of overlap. Since the transmission of the flux detector is higher than 99 %, flux measurements could be performed directly in the irradiating neutron beam. The ultimately achieved accuracy of the flux determination was better than 3 % in the range from 1 to 20 MeV. A new result for the fission cross section of ^{239}Pu is shown in Fig. 1. For comparison, the evaluated data from ENDF/B IV are also included in the figure (solid line).

References

/1/ I. Schouky, S. Cierjacks, P. Brotz, D. Gröschel, B. Leugers, Proc. of the Conf. on Nuclear Cross Sections and Technology, Washington, D.C., March 1975, NBS Special Publication 425, Vol. I, p. 277.

1.2.5 Neutron Capture Cross Section Ratios of ^{240}Pu, ^{242}Pu, ^{238}U and ^{197}Au in the Energy Range from 10 to 90 keV*

K. Wisshak and F. Käppeler

The neutron capture cross sections of ^{240}Pu and ^{242}Pu were measured in the energy range from 10 to 90 keV. The capture cross sections of both ^{197}Au and ^{238}U were chosen as standards. Neutrons were produced via the ^{7}Li (p,n) reaction with the Karlsruhe 3 MV pulsed Van de Graaff accelerator. Capture events were detected by a Moxon-Rae detector. The high neutron flux available at flight paths as short as ∿10 cm offers a signal-to-background ratio one order of magnitude better than obtained in previous experiments. The cross section ratios could therefore be determined with a total statistical and systematic uncertainty of 4-10 % for ^{240}Pu and 6-10 % for ^{242}Pu. The

results agree with previous data while discrepancies to the evaluated files ENDF/B-IV and KEDAK 3 were found (up to 30 % for ^{240}Pu and up to 50 % for ^{242}Pu).

* Accepted for publication in Nucl. Sci. Eng.

1.2.6 Neutron Capture Cross Section Measurements on ^{240}Pu and ^{242}Pu in the Energy Range from 70 to 250 keV

K. Wisshak and F. Käppeler

To improve the information on neutron capture cross sections of Pu isotopes for fast reactor calculations, it was desirable to extend the energy range of our first measurement (see contribution 1.2.5) to higher energies. This was possible by using the T(p,n) reaction for the production of kinematically collimated neutrons. With this reaction and a slightly modified experimental set-up, a maximum neutron energy of about 250 keV was achieved.

The measurement has been performed at a flight path of 67 mm and using ^{197}Au as a reference sample. The target consisted of tritium-loaded titanium (0.8 Curie/cm^2) evaporated onto a tungsten backing. To minimize contamination, the target was coated with a thin aluminium layer. Since the neutron flux obtained from the T(p,n) reaction is one order of magnitude lower than that

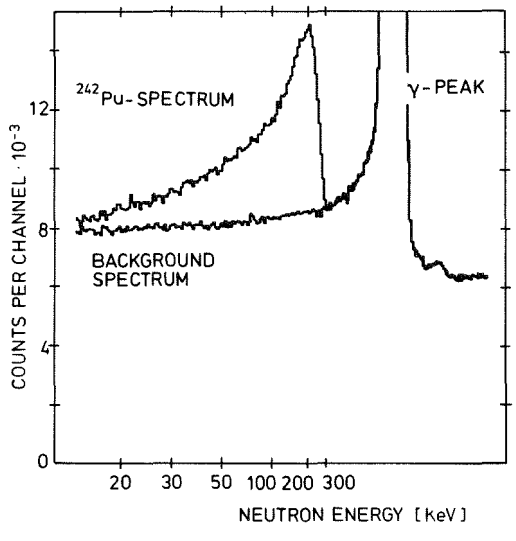

Fig. 1. Time-of-flight spectrum of capture events from a ^{242}Pu sample and background spectrum taken with a dummy sample.

from the $^{7}Li(p,n)$ reaction used in the previous measurements at lower neutron energies, the signal-to-background ratio was accordingly reduced in the present measurement. This reduction, however, is partly compensated by the fact that the capture events are recorded in increasingly shorter time intervals at the higher neutron energies; thus, the time-of-flight distribution gets narrower and higher with increasing neutron energy. Fig. 1 shows the time-of-flight spectrum obtained with the ^{242}Pu sample along with the respective background spectrum. The figure demonstrates that the signal-to-background ratio achieved is sufficient for a proper analysis.

The experiments with both plutonium isotopes have been finished and the data evaluation is in progress.

1.2.7 The Subthreshold Fission Cross Section of ^{240}Pu Between 10 and 250 keV

F. Käppeler and K. Wisshak

Each measurement of neutron capture cross sections of fissile isotopes with a gamma detector has to be corrected for the simultaneously observed fission gamma rays. In our experiments with Pu isotopes (see contributions 1.2.5 and 1.2.6), a fission neutron detector and a ^{235}U reference sample were used to determine this correction. On the other hand, this technique offers also the possibility to measure the fission cross section of the respective Pu isotope relative to ^{235}U. Unfortunately this holds only for the ^{240}Pu sample where the contamination with $^{239,241}Pu$ is small enough (0.74 % and 0.68 %, respectively). In this case about 70 % of the fission events observed are due to the subtreshold fission in ^{240}Pu, whereas in the case of ^{242}Pu the fission rate is completely dominated by the isotopic impurities in the sample.

The experimental set-up and the data analysis are described in contribution 1.2.5. The correction for fission events in ^{239}Pu and ^{241}Pu was calculated from evaluated cross sections taken from KEDAK 3 and normalized by the spectrum from the reference sample. The $\bar{\nu}$ values were taken from ref. /1/.

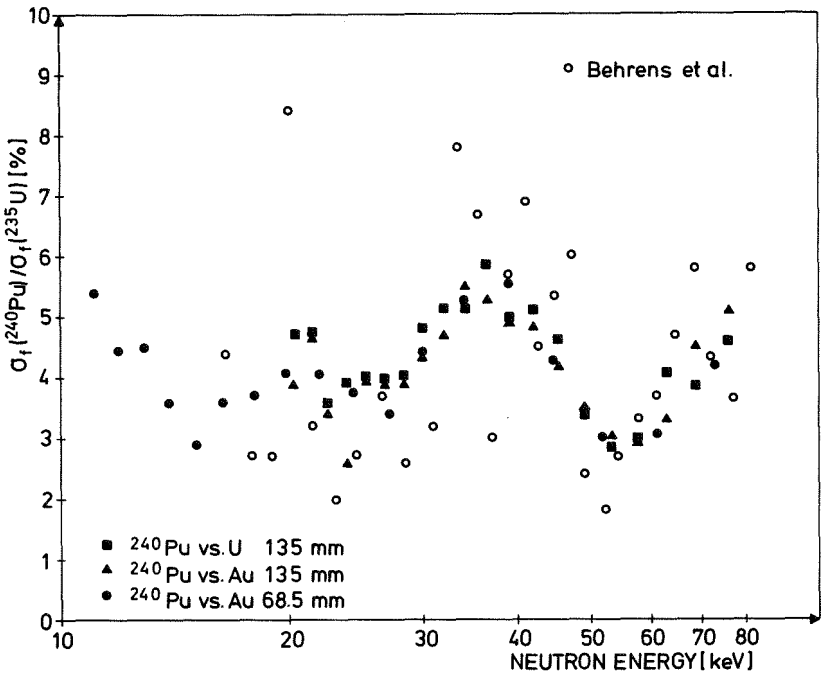

Fig. 1. The fission cross section of ^{240}Pu relative to ^{235}U (the different symbols identify the respective runs of the capture cross section measurement).

In fig. 1 the experimental values for the fission cross section ratio of ^{240}Pu relative to ^{235}U are shown for the neutron energy range from 10 to 90 keV. A total of three data sets can be given, corresponding to different runs of the ^{240}Pu capture cross section measurement (relative to ^{197}Au and ^{238}U at 135 mm flight path and relative to ^{197}Au at 68.5 mm flight path). The error analysis has not yet been completed, but a statistical uncertainty of less than 4 % and a total uncertainty of less than 10 % are expected for most of the data points given. For comparison, recent data of Behrens et al. /2/ are also shown in the figure. The statistical uncertainty of these values amounts to 10-30 %, whereas the systematic uncertainties in the energy range given are not discussed in detail in the preliminary publication of ref. /2/.

Each data point of fig. 1 represents the sum of four time-of-flight channels corresponding to the time resolution of the experiment. Therefore, in the measurements performed at 135 mm flight path where the energy resolu-

tion is completely determined by the time resolution, the energy resolution is given by half of the distance between the data points.

In the energy range from 70 to 250 keV the experiments have been finished and the data evaluation is in progress (see contribution 1.2.6).

References

/1/ F. Manero and V.A. Konshin, Atomic Energy Review 10 (1972) 637.

/2/ J.W. Behrens, J.C. Browne and G.W. Carlson, Report UCID-17047, Lawrence Livermore Laboratory (1976).

1.2.8 Preliminary Results from a Fission Cross Section Measurement on ^{241}Am in the Subthreshold Energy Region

W. Hage[+], H. Hettinger[+], F. Käppeler, and K. Wisshak

A systematic study of the ^{241}Am fission cross section between 20 and 1500 keV was started with a measurement of the cross section shape below 1 MeV. In view of the very small subthreshold cross section and the severe background problems caused by the high α activity, fission events were recorded detecting fission neutrons instead of fission fragments. Doing so, the sensitivity was improved considerably so that very distinct peaks for fission events could be observed in the time-of-flight spectra even for the lowest investigated energies. However, since the experimental information about the fission neutron spectrum of ^{241}Am is rather poor, the absolute accuracy of the fission cross sections obtained is limited. Very accurate information, however, was obtained on the energy dependence of the cross section relative to ^{235}U, which was used as a standard. Fig. 1 shows preliminary results for part of the energy range. The new results are plotted as black points. In all cases, the statistical uncertainty is less than the size of the dots; it is about 6 % at 130 keV and 1 % at 900 keV. For the evaluation, the energy dependence of $\bar{\nu}$ and the fission neutron spectrum of ^{241}Am has been assumed to be the same as that of ^{235}U. This, of course, is an approximation, although the agreement with the measurement of Behrens and Browne /1/ is remarkably good. In any case,

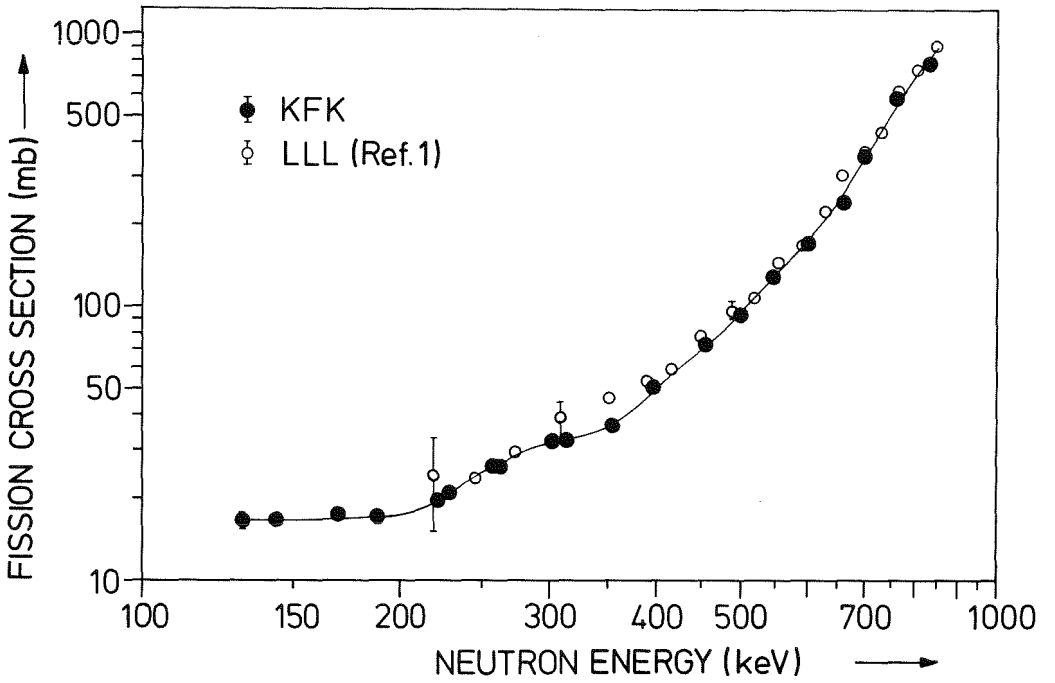

Fig. 1 Preliminary results from the ^{241}Am fission cross section measurement (black points). The values of ref. /1/ are shown for comparison (open points).

at the present stage of the measurements we would not like to stress the absolute figures for the fission cross section, as the main purpose of the investigations was an accurate shape measurement of the fission cross section down to low neutron energies. A second measurement using fragment detection will serve for normalization purposes.

Table 1. Parameters for the inner fission barrier of ^{241}Am

	Barrier Height E_A(MeV)	Barrier Curvature $\hbar\omega_A$ (MeV)
This work	6.44	0.80 ± 0.07
Back et al. /3/	6.35	0.60 ± 0.15

From the fission cross section of fig.1, the penetrability of the fission barrier of ^{241}Am was calculated assuming a 1/v-dependence for the compound formation and normalizing to 1.0 at a neutron energy of 1.4 MeV. A fit to this penetrability curve was carried out with the code of Wong and Bang /2/. In this way, improved parameters for the double-humped fission barrier could be determined as compared to the literature/3/.

+JRC Euratom, Ispra, Italy

References

/1/ J.W. Behrens and J.C. Browne, Report UCID-17324, Lawrence Livermore Laboratory (1976).

/2/ C.Y. Wong and J. Bang, Phys. Lett. 29 B (1969) 143.

/3/ B.B. Back, J.P. Bondorf, G.A. Otroschenko, J. Pedersen and B. Rasmussen, Nucl. Phys. A 165 (1971) 449.

1.2.9 A Method to Determine the Population of the Ground and Isomeric State in ^{242}Am Following keV Neutron Capture in ^{241}Am

K. Wisshak and F. Käppeler

Neutron capture in ^{241}Am populates not only the ground state of ^{242}Am ($T_{1/2}$ = 16 h), but also an isomeric state with a half-life of 152 years. In nuclear reactors ^{242g}Am will decay predominantly to ^{242}Cm which is a strong neutron emitter, whereas ^{242m}Am may be transformed to ^{243}Am via a second capture event. The isomeric ratio is therefore an important parameter in transuranium build-up calculations for reactors.

To determine the isomeric ratio, not only the total capture cross section but also the partial cross section for capture in either the ground or isomeric state of ^{242}Am has to be measured. This represents a rather difficult task because of the strong radiation from the ^{241}Am decay.

In our measurements the total capture cross section will be measured in the same way as for the Pu isotopes (time-of-flight technique with a Moxon-Rae detector, see contribution 1.2.5). The partial cross section for the population of the ground state will be measured by activating a thin ^{241}Am sample in a neutron flux of about 10^9 n/sec at the Van de Graaff accelerator. The ^{242g}Am nuclei thus produced will then be detected via the electrons emitted in the β^- decay to ^{242}Cm. The separation of the electrons from the intense γ and α radiation from ^{241}Am is accomplished with a "Mini-Orange-Spectrometer" /1/ together with a Si(Li) detector for energy analysis. The measurement will be performed relative to ^{197}Au where a nucleus with a similiar β^- spectrum is produced in neutron capture. The partial cross section can then be evaluated from the measured intensities of equivalent parts in the electron spectra near the endpoint energies.

References

/1/ J. van Klinken and K. Wisshak, Nucl. Instr. Meth. 98 (1972) 1;
J. van Klinken, S.J. Feenstra, K. Wisshak and H. Faust,
Nucl. Instr. Meth. 130 (1975) 427.

1.2.10 Experimental Techniques for Neutron Cross Section Measurements on Short-Lived Actinide Isotopes with a Van de Graaff Accelerator*

F. Käppeler and K. Wisshak

The difficulties of neutron cross section measurements on short lived actinide isotopes ($T_{1/2} < 10^4$ y) in the keV neutron energy range are reviewed. The experimental possibilities with comparably small Van de Graaff accelerators are discussed and examples for current measurements and for further developments are given.

* Proc. of the First Technical Meeting on the Nuclear Transmutation of Actinides (JCR Ispra), to be published.

1.2.11 ^{237}Np and ^{235}U as Possible Standards for the MeV Region*

S. Cierjacks

The aspects of using the fission cross sections of ^{237}Np and ^{238}U as possible standards in the MeV region are considered. In comparison to other neutron standards their application is particularly advantageous for experiments involving white-source techniques. Major distortions in fast neutron measurements due to frame-overlap problems and contributions from slow neutrons events can be avoided by spectrum cut-off at threshold energies. The present data basis for both nuclei is discussed and critically examined. Some suggestions are made of how to achieve an ultimate accuracy of 2 % with measurements employing ^{237}Np or ^{238}U as secondary standards.

* Proc. of the Int. Specialists Symposium on Neutron Standards and Applications, Gaithersburg (Maryland, USA), March 1976, to be published.

2. CHARGED-PARTICLE REACTIONS

2.1 POLARIZED AND UNPOLARIZED DEUTERONS

2.1.1 Recent Measurements of the Vector Analyzing Power in the $\vec{d} + p \rightarrow p + p + n$ reaction at $E_d = 52$ MeV

M.S. Abdel-Wahab[+], V. Bechtold, J. Bialy[+], L. Friedrich, and F.K. Schmidt[+]

The vector analyzing power of the final state interaction (n,p)-pair with relative energy $E_{np} \leq 1$ MeV is measured with complete kinematics in a coincidence experiment, using the 52 MeV purely vector polarized deuteron beam of the cyclotron.

The recent experimental results from Karlsruhe are given in fig. 1 together with the data obtained by Rad et al. /1/ in Berkeley by another method (interpretation of the continuous proton spectrum from symmetrical detectors).

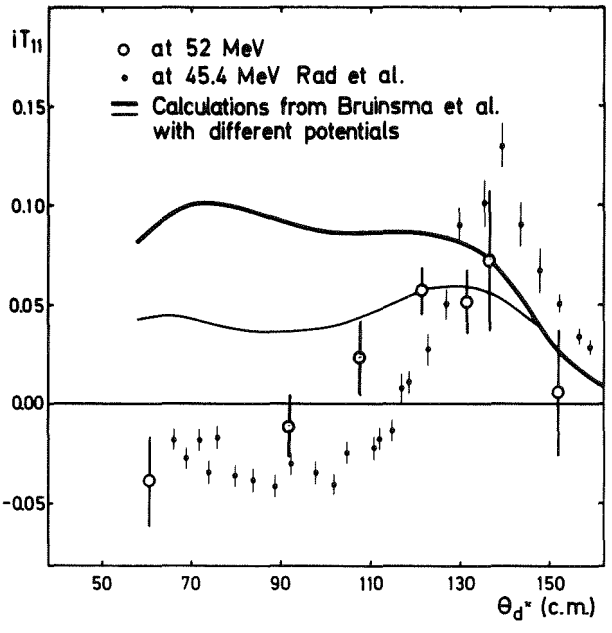

Fig. 1. The vector analyzing power in the $\vec{d} + p \rightarrow p + p + n$ reaction at 52 MeV (open circles). The other points are data from Rad et al. /1/. The two curves are calculations from Bruinsma et al. /2/.

Our results show discrepancies with theoretical calculations from Bruinsma and van Wageningen /2/ too, at least at small scattering angles. So it is an obvious need for further theoretical and experimental investigations. In particular, the measurement of the vector analyzing power as a function of the arc length of the kinematical curve could be very helpful in studying

the remaining discrepancies of the experimental results and provide additional information for the theoretical discussion. Hence, a much more rigorous effort in this direction is highly desirable.

+ Institut für Experimentelle Kernphysik der Universität Karlsruhe

References

/1/ F.N. Rad, H.E. Conzett, R. Roy, F. Seiler; Fourth Int. Symp. on Polarization Phenomena in Nuclear Reactions, Zürich (Switzerland) August 1975, p. 487.
F.N. Rad, H.E. Conzett, R. Roy and F. Seiler; Phys. Rev. Lett. 35 (1975) 1134.

/2/ J. Bruinsma, R. van Wageningen; Phys. Lett. 63 B (1976) 19.

2.1.2 Measurement of the Vector Analyzing Power in $\vec{d}$-^{4}He Elastic Scattering at 52 MeV

M.S. Abdel-Wahab+, V. Bechtold, J. Bialy+, L. Friedrich, and F.K. Schmidt+

The study of d-α elastic scattering is interesting for several reasons. Firstly, it is a source of information on the excited states of ^{6}Li. Secondly, it provides information on the deuteron spin-orbit interaction and finally, it has been demonstrated to be a useful analyzer for deuteron polarization /1-4/. In the present work the vector analyzing power iT_{11} for the d-α elastic scattering has been measured at 52 MeV deuteron energy, giving data at an energy greater than that obtained by König et al. /5/ and Conzett et al. /6/ at 42.8 and 44.9 MeV, respectively.

A purely vector polarized deuteron beam was delivered by the Lambshift source C-LASKA. A gas target with ^{4}He at 1 atm. pressure was used and a polarimeter consisting of a carbon foil target and a left-right pair of NaI counters at 47° was placed downstream. The vector analyzing power at 47° is known from a double scattering experiment /7/.

The scattered deuterons at energies greater than 10 MeV were detected with NaI counters whereas those at lower energies were detected with silicon surface-barrier detectors using the time-of-flight method /8/. The analyzing power iT_{11} was measured in alternating runs with polarization directions up and down as follows

$$iT_{11} = \frac{1}{2\sqrt{3}} \cdot \frac{A+1}{A-1} \cdot \frac{p^+ + p^-}{p^+ \cdot p^-} \cdot \left(1 - \sqrt{1-4\left(\frac{A-1}{A+1}\right)^2 \frac{p^+ \cdot p^-}{(p^+ + p^-)^2}}\right)$$

The quantity p^+ is the magnitude of the beam polarization p where the polarization direction is up (+), etc., and A is the geometric mean asymmetry factor

$$A = \frac{L^+ \cdot R^-}{R^+ \cdot L^-}$$

where L^+ is the number of counts in the left (L) detector when the polarization is up (+), etc.

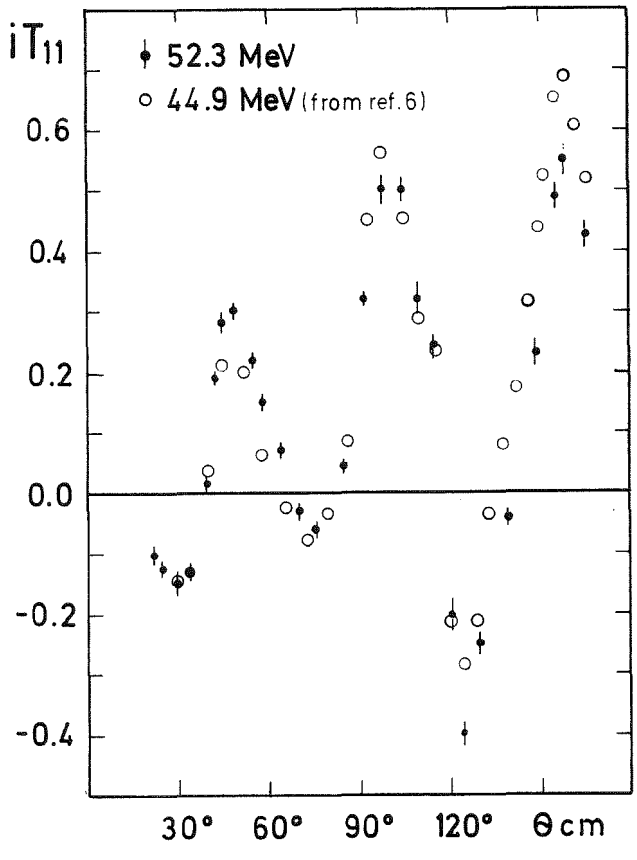

Fig. 1. The vector analyzing power in $\vec{d}$-^{4}He elastic scattering at 52 MeV. Open circles show the measured analyzing power at 44.9 MeV by Conzett et al. /6/.

The measured analyzing powers are shown in fig. 1 in comparison with those obtained by Cozett et al. at 44.9 MeV /6/.

+ Institut für Experimentelle Kernphysik der Universität Karlsruhe

References

/1/ L.C. McIntyre, W. Haeberli, Nucl. Phys. A 91 (1967) 361.
/2/ W. Grübler, V. König, P.A. Schmelzbach, P. Marmier, Nucl. Phys. A 134 (1969) 686.
/3/ V. König, W. Grübler, P.A. Schmelzbach, P. Marmier, Nucl. Phys. A 148 (1970) 388.
/4/ L.G. Keller, W. Haeberli, Nucl. Phys. A 150 (1970) 465.
/5/ V. König, W. Grübler, P.A. Schmelzbach, R. Risler, B. Jenny, H.R. Bürgi, G. Heidenreich, F. Seiler, H. Roser, W. Reichart, R.A. Hardekopf, J. Nurzinski, Jahresbericht 1976, ETH Zürich, 64
/6/ H.E. Conzett, W. Dahme, Ch. Leemann, J.A. Macdonald, J.P. Meulders, Proc. Fourth Int. Symp. on Pol. Phenomena in Nuclear Reactions Zürich 1975, p. 566.
/7/ E. Seibt, U. Weddigen, Nucl. Instr. Meth. 100 (1972) 253.
/8/ H. Brückmann, E.L. Haase, W. Kluge, L. Schänzler, Nucl. Instr. Meth. 67 (1969) 29.

2.1.3 Monitor Reaction for Tensor Analyzing Power Measurement at 52 MeV

V. Bechtold and L. Friedrich

Measurements of tensor analyzing powers at the energy range around 52 MeV are of increasing interest, especially in few nucleon studies. Whereas the vector polarization can be calibrated by d-^{12}C elastic scattering (the vector analyzing power has been obtained by a double scattering experiment /1/) tensor analyzing power measurements suffer from the lack of a well known polarization standard. To find out a suitable monitor reaction, a first attempt was started to determine the tensor analyzing power A_{yy} in $\vec{d}$-^{4}He elastic scatte-

ring at 52 MeV using a special property of the Lambshift source.

The cross section of deuteron scattering with spin direction fixed by the magnetic field of the cyclotron can be written:

$$\sigma(\theta) = \sigma_o(\theta) \cdot \{1 + \frac{3}{2} \cos \beta \cdot P_z A_z(\theta) + \frac{1}{2} \sin^2 \beta \cdot P_{zz} A_{xx}(\theta) + \frac{1}{2} \cos^2 \beta \cdot P_{zz} A_{yy}(\theta)\}$$

A_y and A_{yy} can be measured in the horizontal plane ($\beta = 0^o$). This experiment was done in the great scattering chamber of the Karlsruhe cyclotron with a deuteron intensity of typically 30 nA on the target. The determination of the analyzing power A_{yy} necessitates two experiments at the same scattering angle.

In a first step the vector polarization $\tilde{P}_z$ of the purely vector polarized beam was measured

$$(1) \quad \tilde{P}_z = \frac{2}{3A_y} \frac{\tilde{N}^+ - \tilde{N}^-}{\tilde{N}^+ + \tilde{N}^-}$$

$\tilde{N}^+$, $\tilde{N}^-$ are the counting rates with spin 'up' and 'down', respectively.

The vector analyzing power is known from the experiment described in contribution (2.1.2). Tuning up the field strength in the second quenching magnet of the Lambshift source, the vector polarization decreases by a known factor and a mixed polarized beam with $P_z = P_{zz}$ is achieved.

In a second step the counting rates N^+ and N^- with opposite spin direction were determined in a scattering experiment with mixed polarized deuteron beam. Then A_{yy} can be calculated by:

$$(2) \quad A_{yy} = \frac{2}{P_{zz}} \left(\frac{N^+ + N^-}{\tilde{N}^+ + \tilde{N}^-} - 1\right)$$

The recoil α particles were measured in the range of 11^o to 34^o θ_{Lab} corresponding to c.m. angles from 112^o to 158^o for the deuterons. The measured analyzing power A_{yy} at 52 MeV is compared with data from König et al. /3/ in fig. 1.

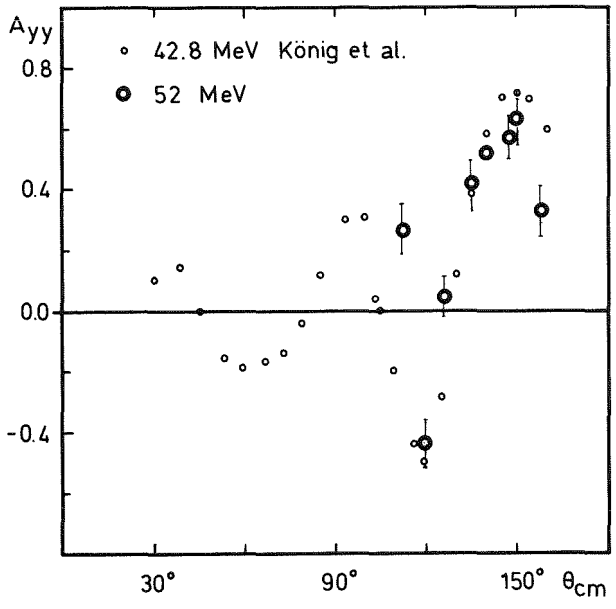

Fig. 1. The tensor analyzing power A_{yy} in the $\vec{d}$-^{4}He elastic scattering at 52 MeV. The small circles show the data from König et al. /3/.

These first experimental results show the d-^{4}He elastic scattering to be a suitable monitor reaction for tensor polarization. Further refinement of these data is planned by searching for scattering angles with $A_{yy} = 0$ and $A_y \neq 0$ using relation (2) and measuring P_z of the mixed polarized state at this angle.

References

/1/ E. Seibt, Ch. Weddigen, Nucl. Instr. Meth. 87 (1970) 155.

/2/ V. Bechtold, L. Friedrich, D. Finken, G. Strassner, P. Ziegler, Proc. of the Fourth Int. Symp. on Polarization Phen. in Nuclear Reactions, Zürich 1975, p. 849.

/3/ V. König, W. Grübler, P.A. Schmelzbach, R. Risler, B. Jenny, H.R. Bürgi, G. Heidenreich, F. Seiler, H. Roser, W. Reichert, R.A. Hardekopf, and J. Nurzynski, Jahresbericht 1976 der ETH Zürich, Laboratorium für Kernphysik, p. 64.

2.1.4 Study of Energy and Mass Distributions of Fission Fragments and Neutron Yields from the $^{233}U(d,pf)$ Reaction

S. Cierjacks, Y. Patin[+], J. Lachkar[+], J. Sigaud[+], C. Humeau[+], and J. Chardine[+]

During the last years the study of dynamical aspects of the fission process has gained increasing importance in fission physics. Of particular interest in this context are inertial and damping effects. Dynamical aspects play an important role in the last phase of fission during which the system crosses the fission barrier and descends from the saddle point to scission. During this phase the deformation of the system changes very rapidly. For a better theoretical description of this phase further experimental information is needed. Information of the required type can be obtained from the observation of the mass distributions, the distributions of kinetic energies and the yields of fission neutrons as a function of fragment masses and as a function of the excitation energies of the fissioning system.

Since many years the energy dependence of these quantities have been studied from fission reactions induced by charged particles and in particular by means of the (d,pf) reaction. In these experiments, however, the different distributions were mainly measured in kinematically incomplete experiments. The major method was to measure the kinetic energies of the fragments with two surface barrier detectors applying the Schmitt-method for calibration. The use of this method is connected with some approximations limiting the accuracy of the determined fragment masses and energies. In particular, a knowledge of the number of neutrons evaporated from the fission fragments is needed for a determination of the pre-neutron emisssion masses as a function of the fragment mass. This distribution is in fact often known for fissions induced by thermal neutrons but was never studied at other excitation energies.

To avoid such uncertainties,a double energy-double-time-of-flight experiment was designed allowing the determination of the energy and the velocity of both fission fragments simultaneously. In the experiments the Tandem accelerator of the Service de Physique Nucléaire of the Centre d'Etudes de Bruyères-le-Châtel was employed. The velocities of fission fragments were measured by

time-of-flight over a distance of 15.5 cm. The time-zero signal for a fission event was provided by a time signal from the proton telescope. The proton telescope provided also the analog information for a determination of the excitation energy of the fissioning system. After several corrections for rise times of electronic pulses, for proton time-of-flights, for the recoil energy of the fissioning nucleus and energy losses in the sample and the backing, the pre-neutron emission masses can be determined from the relation: $m_1^* = A \cdot \frac{V_2}{V_1+V_2}$.

In fig. 1 the fragment kinetic energy $E_K^*(m)$ before neutron emission is shown as a function of the pre-neutron emission mass. In this diagram our

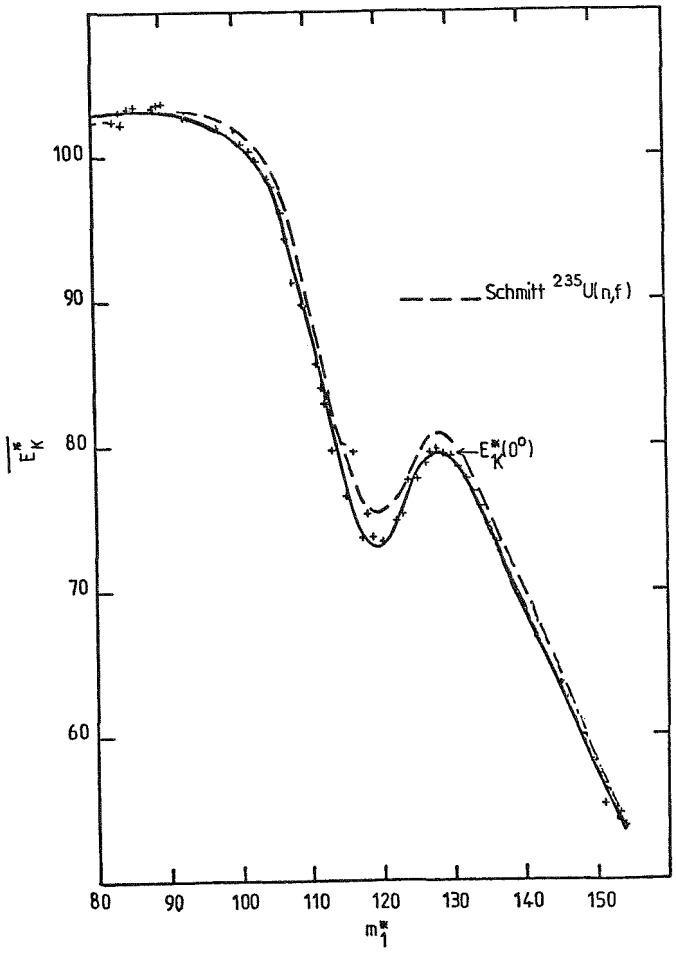

Fig. 1. Fragment kinetic energy E_K^* before neutron emission from the ^{235}U (d,pf) reaction. The preliminary results are shown in comparison with data of Schmitt et al. /1/ obtained for thermal neutron fission of ^{235}U.

preliminary data are shown in comparison with results from Schmitt et al. /1/ which were measured at thermal energy for ^{235}U. Such a comparison with the neighbour isotope seems to be reasonable due to a relative measurement of Milton and Fraser /2/ showing that the energy distributions for ^{233}U and ^{235}U are largely the same, except for a small peak displacement to lower masses due to the different compound-nucleus masses. Unfortunately the absolute energy values of Milton and Fraser are distorted by fragment scattering from the walls of the flight tubes in the double-velocity experiments and thus cannot be used for direct comparison. The agreement of the present results with those of Schmitt is well within the stated uncertainties.

+ Service de Physique Nucléaire, Centre d'Etudes de Bruyères-le-Châtel, France

References

/1/ H.W. Schmitt, J.H. Neiler, and F.J. Walter, Phys. Rev. 141 (1966) 1146.

/2/ J.C.D. Milton and J.S. Fraser, Can. J. Phys. 40 (1962) 1626.

2.2 ALPHA-PARTICLE REACTIONS

2.2.1 Nuclear Matter Sizes and Isoscalar Octupole Transition Rates of ^{204,206,208}Pb from 104 MeV α-Particle Scattering *

H.J. Gils, H. Rebel, J. Buschmann, H. Klewe-Nebenius+,
G.P. Nowicki, and W. Nowatzke

Differential cross sections for elastic and inelastic scattering of 104 MeV α particles from ^{204,206,208}Pb were measured with high angular accuracy. The experimental results were analysed on the basis of a semi-microscopic folding model in order to determine the matter distributions at the nuclear surface and the transition densities. Using phenomenological parametrizations of the densities the analyses of elastic scattering yield rms radii of $\langle r^2 \rangle^{1/2}$ = 5.55 ± 0.06 (^{204}Pb), 5.57 ± 0.06 (^{206}Pb), 5.63 ± 0.05 (^{208}Pb) fm. Various sensitivities affecting the results were studied. From the inelastic cross sections for the 3^-_1-states octupole transition probabilities and transition radii were derived by using different methods proposed in literature.

* Z. Physik A 279 (1976) 55.

+Institut für Radiochemie

2.2.2 Investigation of the Reaction ^{12}C(α, ^{6}Li)^{10}B at E_α = 104 MeV

R. Latz, H.J. Gils, H. Rebel, J. Buschmann, and S. Zagromski

In the course of studies of ^{6}Li-induced nuclear reactions at energies up to 156 MeV /1/ the reversed reaction ^{12}C(α, ^{6}Li)^{10}B has been investigated at the energy-analyzed 104 MeV α-particle beam (ΔE = 50 keV FWHM) of the Karlsruhe Isochronous Cyclotron. The ejected particles were detected by several ΔE-E surface barrier detector telescopes having thicknesses of 150 μm for the ΔE and 4000 μm for the E detectors. A preselection of reaction products between 4 < A < 9 amu was electronically performed in order to suppress

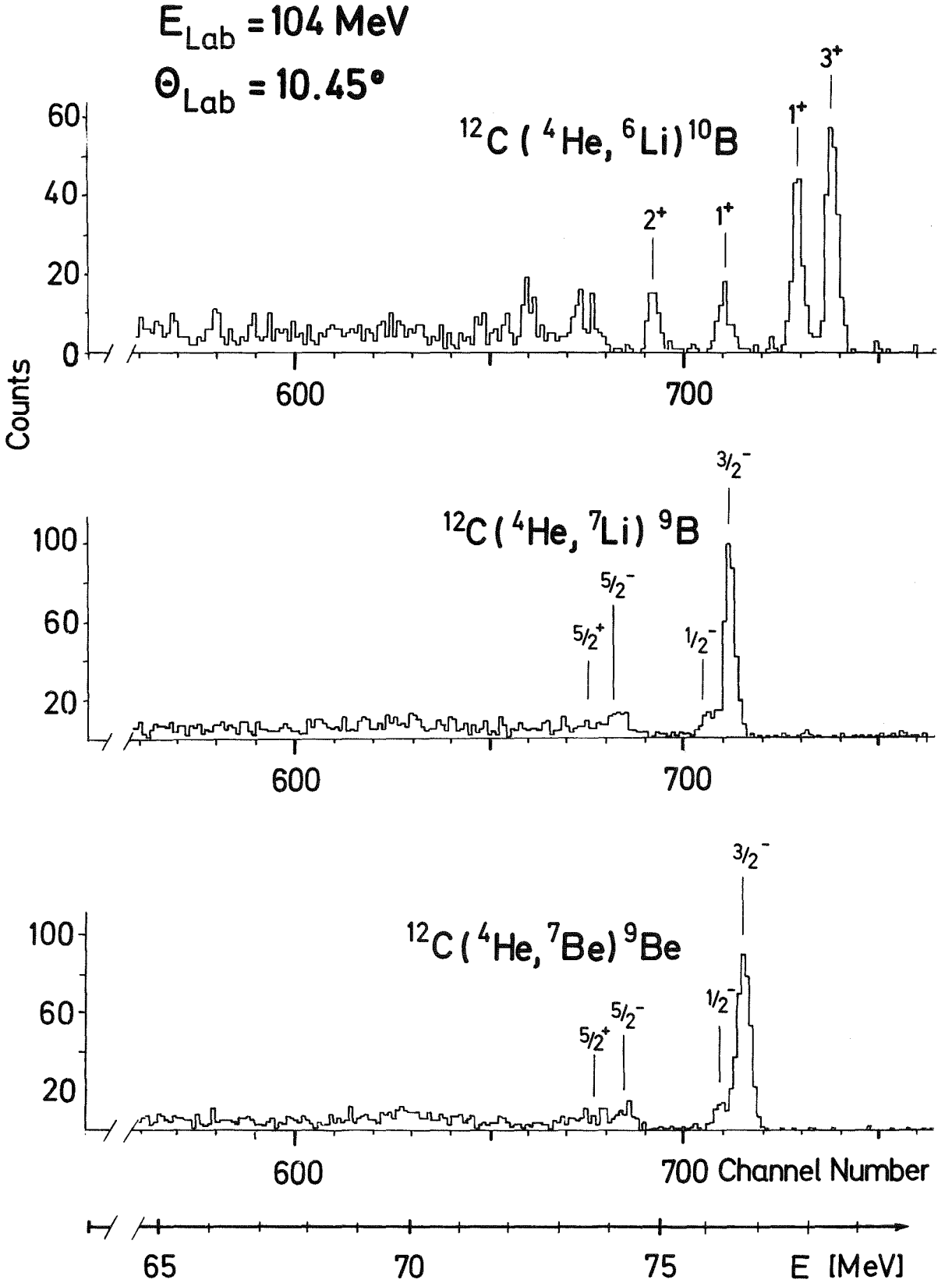

Fig. 1. Particle specific spectra of α-particle induced nuclear reactions on ^{12}C. Besides the excitation peaks of the residual nuclei, the lower two spectra also show peaks of ejectile excitation.

the large amount of scattered α particles. The final particle identification of the list-mode data using the method of Goulding et al. /2/ was able to distinguish ^{6}Li and ^{7}Li from each other and from all other ejectiles.

The targets used were polypropylene foils of 0.48 mg/cm^2 thickness and a 0.15 mg/cm^2 thick graphite target. These targets were thick enough to provide acceptable measuring times in view of the small reaction cross sections, but on the other hand they were thin enough to guarantee a sufficient energy resolution for separating the first excited state (1^+) at E_x = 0.717 MeV from the ^{10}B ground state (3^+). Typical particle specific spectra for ^{6}Li, ^{7}Li and ^{7}Be particles are displayed in fig. 1. The angular distribution for the reaction ^{12}C (α, ^{6}Li) ^{10}B has been measured

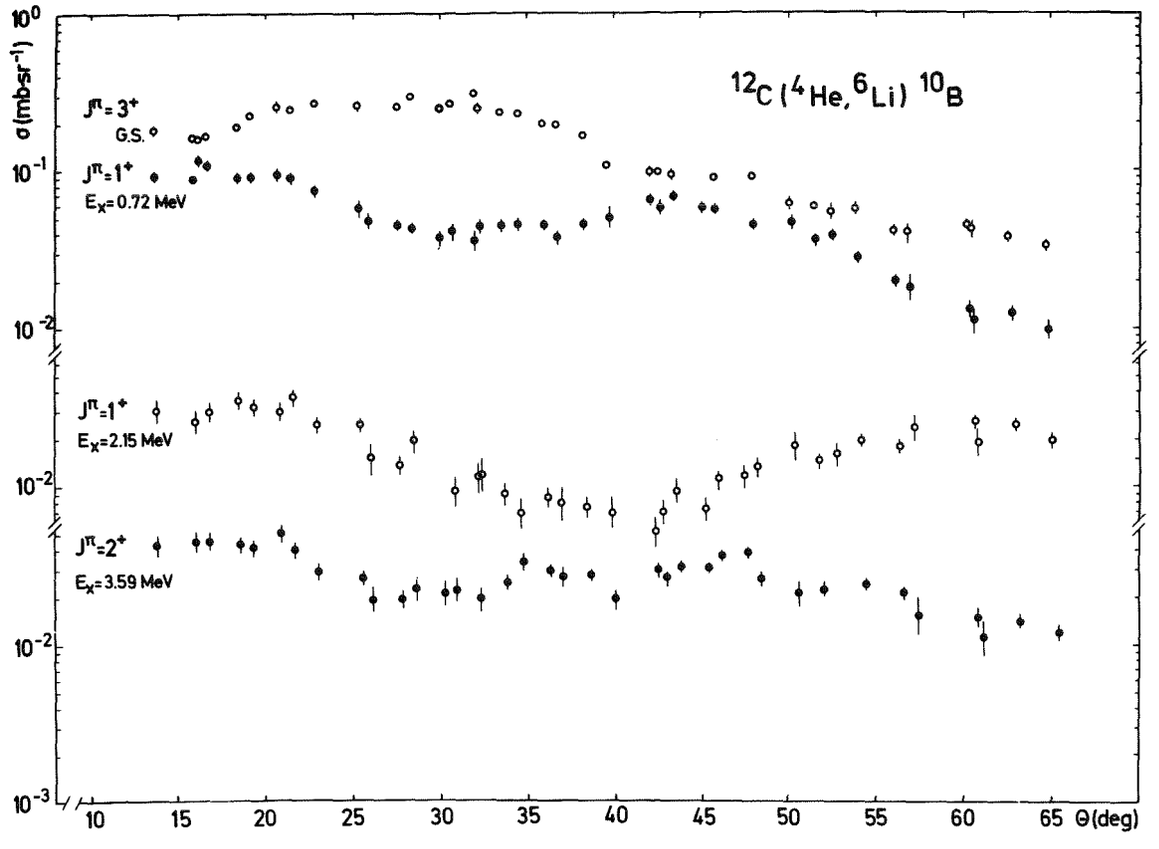

Fig. 2. Measured differential cross sections for the reaction $^{12}C(\alpha,^{6}Li)^{10}B$ at E_α = 104 MeV.

between $\Theta_{Lab} = 9^{o}$ and 50^{o}. The experimental cross sections are shown in fig. 2. The quoted error bars include only statistical errors. Errors due to the uncertainty of the absolute scattering angle ($\Delta\Theta \sim 0.2^{o}$) were not included because of the smooth behaviour of the angular distribution.

The not yet finished analysis of the data is performed with the finite range DWBA-code LOLA /3/. The main aim is to obtain information about the α-d cluster structure of the ^{6}Li particle.

References

/1/ J. Kropp, H. Klewe-Nebenius, H. Faust, J. Buschmann, H. Rebel, H.J. Gils, and K. Wisshak, Z. Physik A 280 (1977) 61; compare also contributions 2.3.1 and 2.3.2 of this report.

/2/ F.S. Goulding, D.A. Landis, J. Cerny, and R.H. Pehl, Nucl. Instr. Meth. 31 (1964) 1.

/3/ R.M. de Vries, Phys. Rev. C8 (1973) 951.

2.2.3 Alpha-Gamma Angular Correlation Measurements as a Sensitive Method Determining the Sign of the Nuclear Quadrupole Deformation *

W. Eyrich+, A. Hofmann+, U. Scheib+, S. Schneider+, F. Vogler+, and H. Rebel

In-plane ^{24}Mg $(\alpha,\alpha_1\gamma)$ angular correlations have been measured at $E_\alpha = 104$ MeV. The correlation parameters and the reaction amplitudes extracted from the data have been studied by a coupled-channel analysis. Drastic effects of the sign of the intrinsic quadrupole deformation are found.

* Phys. Lett. 63B (1976) 406.

+ Physikalisches Institut der Universität Erlangen-Nürnberg, Germany

2.2.4 Alpha-Gamma Angular Correlations in the Reaction ^{24}Mg $(\alpha,\alpha_1\gamma)$ at E_α = 104 MeV*

W. Eyrich+, A. Hofmann+, U. Scheib+, S. Schneider+,
F. Vogler+, and H. Rebel

The in-plane α_1-γ angular correlation of the reaction ^{24}Mg $(\alpha, \alpha_1\gamma)$ has been studied at a bombarding energy of 104 MeV. Double differential cross sections have been measured for 126 pairs of angles by use of a multidetector arrangement consisting of four Si(Li) particle detectors and two Ge(Li) γ detectors. The correlation data are described very well by coupled channel calculations on the basis of a symmetric rotator model. A strong sensitivity of the sign of the quadrupole deformation has been found. This sensitivity proves to be nearly independent of the remaining potential parameters. The main features of the observed prolate-oblate effects can be understood in the framework of a simple diffraction model.

* Report KFK 2455 (1977);
Nucl. Phys. (in press)

+ Physikalisches Institut der Universität Erlangen-Nürnberg, Germany

2.2.5 $(\alpha,\alpha_1\gamma)$ Angular Correlation Measurements on sd-Shell Nuclei

W. Eyrich+, A. Hofmann+, U. Scheib+, S. Schneider+,
F. Vogler+, and H. Rebel

Particle-γ angular correlations provide more detailed information about reaction mechanisms and nuclear structure than differential cross sections. In the special case of $(\alpha,\alpha_1\gamma)$ angular correlations on even-even nuclei it is possible to determine the individual reaction amplitudes, which describe the transitions to the various magnetic substates of the excited residual state. Therefore $(\alpha,\alpha_1\gamma)$ angular correlation measurements are especially suitable for the study of reaction- and structure-models and their parameters.

The "in-plane" angular correlation function for α-particle scattering and the spin sequence $0^+-2^+-0^+$ is given by

$$W(\Theta_\alpha=\frac{\pi}{2}\ ,\ \phi_\alpha;\ \Theta_\gamma=\frac{\pi}{2}\ ,\ \phi_\gamma) = A(\phi_\alpha) + C(\phi_\alpha) \cdot \sin^2 2\ (\phi_\gamma - \phi_2(\phi_\alpha)).$$

The quantities A, C and ϕ_2 which depend on the α-particle scattering angle ϕ_α are simply related to reaction amplitudes /1/.

For the reaction ^{24}Mg $(\alpha,\alpha_1\gamma)$ angular correlation it has been shown /2/ that coupled channels calculations based on the extended optical model (EOM) as well as on a semimicroscopic folding model /3/, which fit the differential cross sections, can also describe the individual reaction amplitudes. Moreover, it turned out that compared with the differential cross section the correlation amplitude C is very sensitive to the sign of the nuclear quadru-

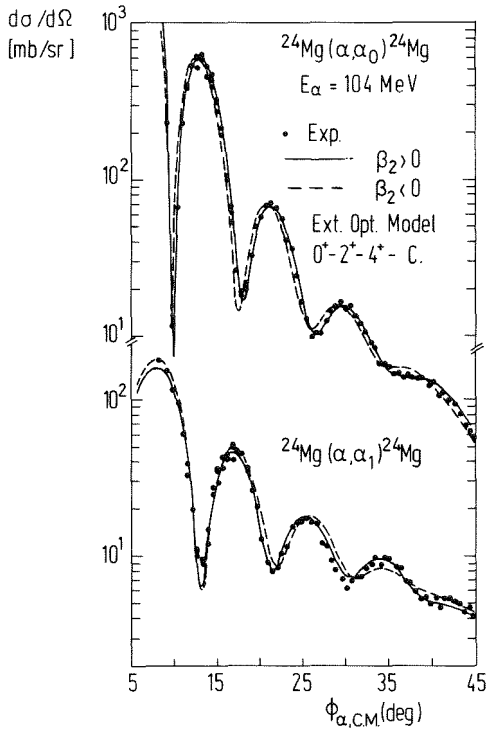

Fig. 1. Coupled channels analysis of the ^{24}Mg (α,α') differential cross section.

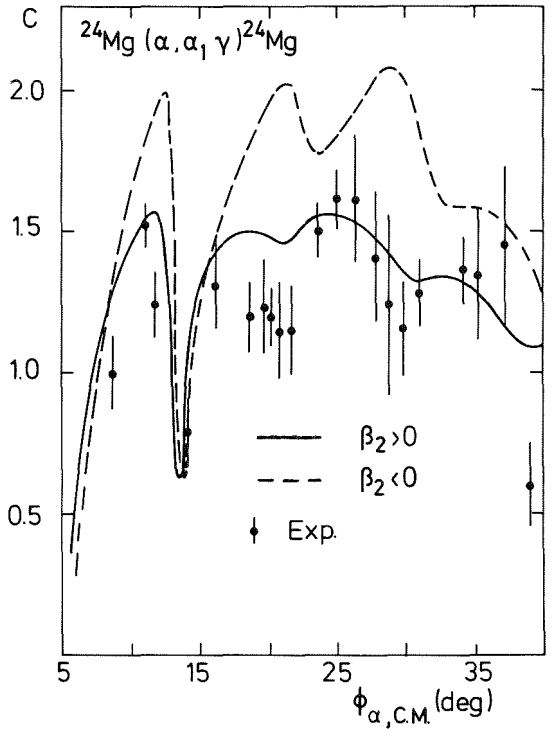

Fig. 2. The experimental correlation amplitude C of the reaction ^{24}Mg $(\alpha,\alpha_1\gamma)$ and coupled channels predictions for prolate and oblate deformation.

pole deformation. This is demonstrated for the EOM-analysis in figs. 1 and 2. In fig. 1 the experimental differential cross sections are shown together with the best fits for prolate ($\beta_2 > 0$) and oblate ($\beta_2 < 0$) deformation. Both fits can reproduce the data, favouring the positive sign of β_2. In fig. 2 the experimental values of the correlation amplitude C are compared with the calculations for $\beta_2 > 0$ and $\beta_2 < 0$ using the best fit parameters of the cross section analysis. There are large differences between both calculations and only the calculation with $\beta_2 > 0$ can reproduce the data.

We have continued these studies measuring the ^{28}Si $(\alpha,\alpha_1\gamma)$ angular correlation. The sign of the quadrupole deformation of ^{28}Si was not as clearly assigned /4/ as in the case of ^{24}Mg, although in most publications oblate deformation is favoured. Our experimental set-up was similar as in the case of the ^{24}Mg-correlation experiment, which is described in detail in /2/. In contrast to this measurement, however, the energy-analysed beam has been used and the data have been acquired two-dimensionally.

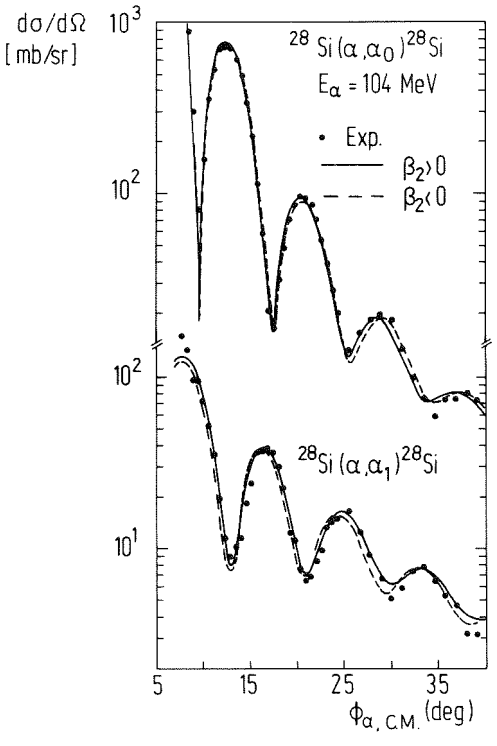

Fig. 3. Coupled channels analysis of the ^{28}Si (α,α') differential cross section.

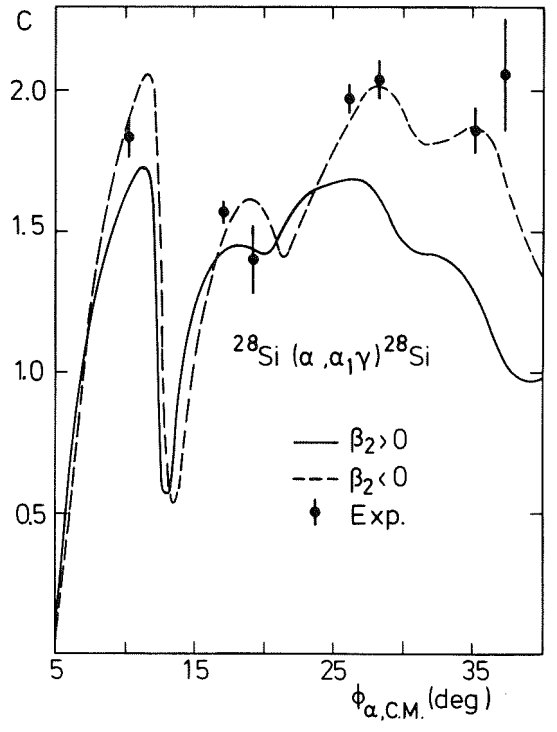

Fig. 4. The experimental correlation amplitude C of the reaction $^{28}Si(\alpha,\alpha_1\gamma)$ and coupled channels predictions for prolate and oblate deformation.

Again the analyses have been performed in terms of coupled channels on the basis of the symmetric rotator using the extended optical model (EOM) and the semimicroscopic folding model. The experimental cross sections are shown in fig. 3 together with the best fits for prolate and oblate deformation in the framework of the EOM. Both fits can reproduce the data favouring slightly the oblate deformation. In fig. 4 the correlation amplitude C is shown. Like in the case of ^{24}Mg, large differences between both calculations occur. The experimental data allow an unambiguous decision for oblate deformation of ^{28}Si. Similar results are obtained from the folding model analyses where at least in the diffraction region the correlation data can be well reproduced by the calculations assuming oblate deformation for ^{28}Si. In all analyses done so far the characteristic differences between prolate and oblate deformation prove to be independent of the potential parameters. They can be explained in the framework of Blair's diffraction model /5/ as shown in /2/. Therefore, α-γ angular correlations should provide a powerful tool to determine the sign of the quadrupole deformation of nuclei also in critical cases. Under this aspect work is in progress to study the α-γ angular correlation on ^{26}Mg.

+ Physikalisches Institut der Universität Erlangen-Nürnberg, Germany

References

/1/ H. Wagner et al., Phys. Lett. 47B (1973) 497.

/2/ W. Eyrich et al., Phys. Lett. 63B (1976) 406 and submitted to Nucl. Phys.

/3/ H. Rebel, Proceedings of the Intern. Summer School of Nucl. Phys. Predeal, Romania (1974), ed. by A. Ciocanel, Report KFK 2065 (1974), and further references therein.

/4/ A. Nakada and H. Torizuka, Phys. Soc. (Japan) 32 (1972) 1;
H. Rebel et al., Nucl. Phys. A 182 (1972) 145;
C.E. Ahlfeld et al., Nucl. Phys. A 191 (1972) 137.

/5/ N. Austern and J.S. Blair, Ann. Phys. 33 (1965) 15.

2.3 ^{6}Li-PARTICLE REACTIONS

2.3.1 Giant Resonance Excitation by Scattering of ^{6}Li Ions at E_{Li} = 156 MeV

H.J. Gils, H. Rebel, J. Buschmann, and H. Klewe-Nebenius[+]

Recent investigations of electron and hadron scattering have revealed a new type of giant resonance in nuclei which is ascribed to an isoscalar quadrupole oscillation. Generally the corresponding peak in the spectra of inelastically scattered particles occurs at 2 MeV lower in excitation energy than the well established giant dipole resonance. In (p,p'), (d,d'), (τ,τ') and (α,α') spectra it has been observed as a broad bump superimposed upon a considerable continuum background. This background arising from more complicated processes such as quasielastic reactions and preequilibrium decay is the reason for difficulties to interprete the measured spectra quantitatively.

As part of a general study of ^{6}Li-induced reactions at bombarding energies up to 156 MeV we report the observation of the giant quadrupole resonance (and possibly some components of different multipolarities hidden in the broad bump observed) excited by scattering of ^{6}Li projectiles on ^{90}Zr and ^{208}Pb. The excitation of highly excited states by inelastic scattering of more complex projectiles may be assumed to provide advantages concerning the reduction of the continuum background in the scattering spectra. ^{6}Li projectiles (T = 0) seem to be of particular interest since - in contrast to heavier projectiles - ejectile excitation is suppressed due to the low lying α-d break-up threshold. In this experiment we used the 156 MeV ^{6}Li beam of the Karlsruhe Isochronous Cyclotron. The inherent acceleration conditions require a charge to mass ratio e/m = 1/2 so that $^{6}Li^{3+}$ ions injected from an external penning ion source have been accelerated /1/. This implies severe restrictions to the beam current which was limited to about 30 nA in the present measurements. The measurements were performed in a scattering chamber (130 cm $\emptyset$) installed behind a deflecting magnet operated in the non-dispersive mode. Because of the restricted intensity, the ^{6}Li beam has not been energy-analyzed, but the magnet provides some advantages for preparing a clean beam. The energy width of the beam was approximately 500 keV (FWHM). The particles scattered from highly enriched (>99 %) targets of ^{90}Zr (4.8 mg/cm^2) and ^{208}Pb (8 mg/cm^2) were detected with several surface barrier detector telescopes which allowed to distinguish ^{7}Li and ^{6}Li particles

from each other and from all other reaction products. Despite of the limited beam intensity the giant resonance bump could be detected very quickly as a distinct peak at the supposed energy position /2/, clearly separated from peaks due to target impurities and with the correct kinematic behaviour when varying the scattering angle. Without any background subtraction, fig. 1 displays the interesting part of (^{6}Li, ^{6}Li') spectra revealing the giant resonance bumps as convincingly as in more tedious α particle-decay particle coincidence experiments /3/. Approximating the background linearly we extracted the giant resonance cross sections for several scattering angles. The values obtained are compared to theoretical predictions on the basis of the phenomenological collective model for the quadrupole giant resonance centered around E_x = 14.5 MeV (^{90}Zr) and E_x = 11 MeV (^{208}Pb), respectively (fig. 2). The coupled channel calculations which have been performed in a 0^+-2^+ (GQR)-coupling scheme utilized the op-

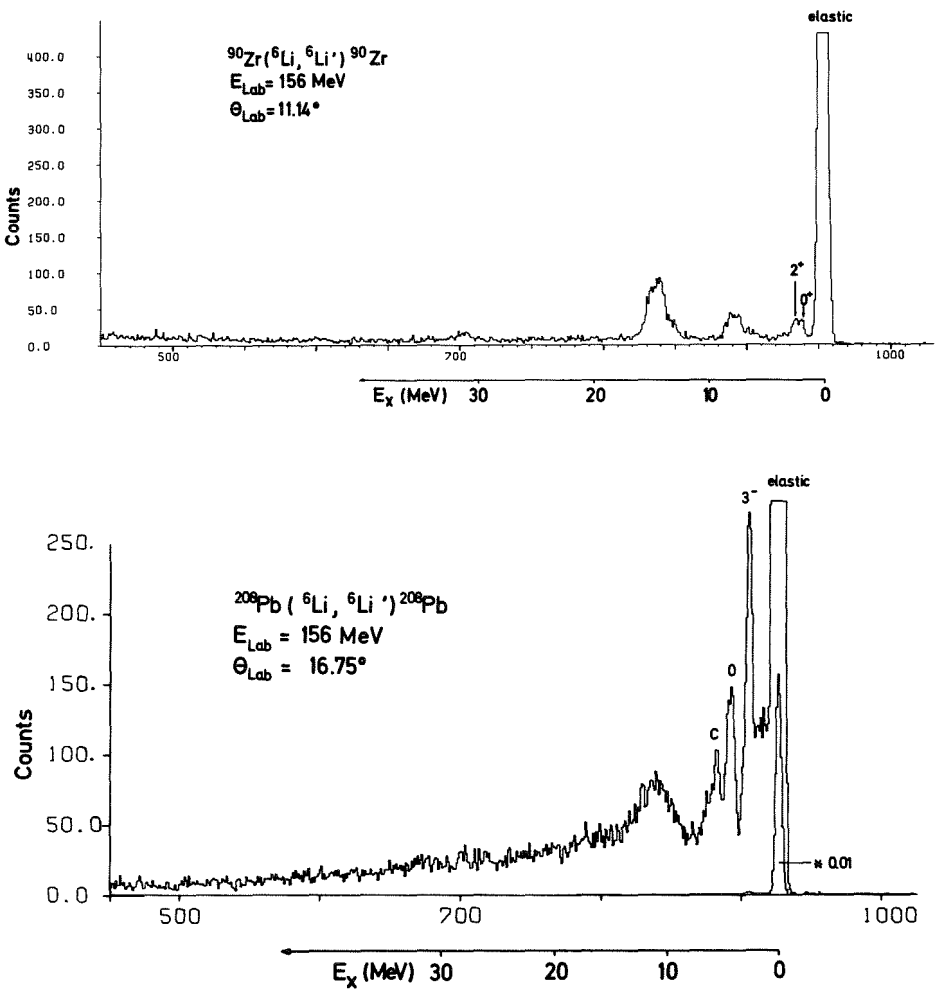

Fig. 1. Spectra of scattered ^{6}Li ions of 156 MeV from ^{90}Zr and ^{208}Pb showing the giant resonance region.

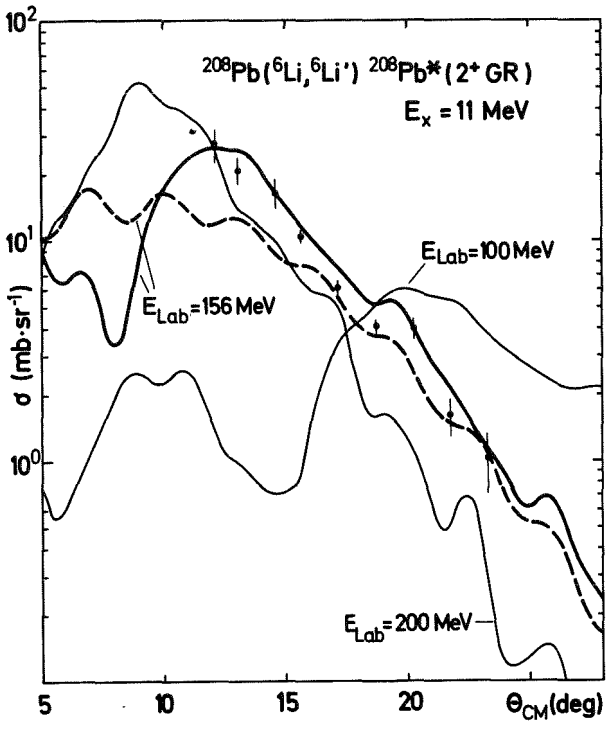

Fig. 2. Differential cross sections for the excitation of the observed giant resonance in ^{208}Pb ($7.5<E_x<16$ MeV) compared to the theoretical cross sections of quadrupole transitions for different projectile energies. The solid curves were obtained by complex coupling, the dashed curve corresponds to real coupling.

tical potentials derived from elastic scattering of 156 MeV ^{6}Li particles from ^{90}Zr and ^{208}Pb /4/. The $\beta_2 R$ values were adopted from α-particle scattering results /2/. In general, complex coupling has been used with equal coupling parameters for the real and imaginary part (the latter assumption $\beta^{Real} = \beta^{Imag}$ does not influence the results very strongly). For the purpose of our exploratory calculations a spin-orbit term of the optical potential has been ignored. The calculations indicate that the cross sections are strongly decreasing at energies $E_{Li} \lesssim 100$ MeV. The experiment demonstrates that ^{6}Li scattering at sufficiently high bombarding energy and with improved beam quality appears to be an excellent tool for more detailed studies of shape, components and multipolarities of giant resonance excitation peaks.

+ Institut für Radiochemie

References

/1/ F. Schulz and H. Schweickert, Report KFK 2298 (1976).

/2/ D.H. Youngblood, J.M. Moos, C.M. Rozsa, J.D. Bronson, A.D. Bacher, and D.R. Brown, Phys. Rev. C13 (1976) 934.

/3/ K.T. Knöpfle and G.J. Wagner, private communication.

/4/ H.J. Gils, H. Rebel, J. Buschmann, H. Faust, H. Klewe-Nebenius, and S. Zagromski, to be published; see also contr. 2.3.3.

2.3.2 Excitation Functions of $^{191+193}Ir$, ^{197}Au (^{6}Li, xn+yp) Compound Nuclear Reactions at E_{Li} = 48 - 156 MeV*

J. Kropp+, H. Klewe-Nebenius++, H. Faust+, J. Buschmann, H. Rebel, H.J. Gils, and K. Wisshak

Excitation functions of the compound nuclear reactions $^{191+193}Ir$, ^{197}Au (^{6}Li,xn + yp) for x = 3-13 and y = 0-2 have been investigated by means of in-beam γ-ray spectroscopy at the 156 MeV ^{6}Li beam of the Karlsruhe Isochronous Cyclotron. The beam energy has been varied in the range of 48 to 156 MeV in steps of about 10 MeV by Be-absorber foils in the external beam line. Absolute cross sections have been determined by normalizing the measured γ-ray intensities to the production cross sections of K-X rays in the target. The experimental excitation functions are discussed on the basis of predictions of the preequilibrium (hybrid) model. While in most cases the theoretical calculations fairly well reproduce energy position and shapes of the curves, strong discrepancies in the absolute scale of the cross sections are observed. The theoretical predictions overestimate the (^{6}Li,xn) cross sections by a factor of about 6. Conspicuous anomalies have been detected when comparing the (^{6}Li, xn+1(2)p) reactions with (^{6}Li,xn) reactions. The reactions with emission of one or two protons are considerably enhanced. The discrepancies and anomalies observed are tentatively explained by the influence of direct reaction channels as the ^{6}Li break-up, which experimentally proved to be the dominant contribution to the total reaction cross section. The enhancement of the reactions with emission of protons may be a consequence of transfer reactions into highly excited states combined with compound nucleus formation, thus implying a cluster effect in preequilibrium emission process.

* Z. Physik A 280 (1977) 61.

+ Physikalisches Institut der Universität Heidelberg, Germany
++ Institut für Radiochemie

2.3.3 Analyses of Elastic and Inelastic Scattering of 156 MeV ^{6}Li on ^{12}C, ^{40}Ca, ^{90}Zr, ^{208}Pb

H.J. Gils, J. Buschmann, H. Rebel, G. Bechtold, and S. Zagromski

Up to now information on phenomenological interaction parameters for high-energetic ^{6}Li procectiles is very scarce. In order to obtain realistic optical potentials for ^{6}Li interaction with nuclei, scattering experiments with the 156 MeV ^{6}Li beam have been performed at the Karlsruhe Isochronous Cyclotron. Details of the experiments have been described elsewhere /1/.

Angular distributions of elastic scattering were measured at Θ_{Lab} = 10-30° (^{12}C, ^{90}Zr, ^{208}Pb) and at Θ_{Lab} = 7 - 45° (^{40}Ca) in steps of 0.5°.

Fig. 1 shows the measured differential cross sections for ^{40}Ca and ^{90}Zr. The solid curves are the results of conventional optical model calculations using a 6-parameter Saxon-Woods potential fitted to the measured data. A spin-orbit term has not yet been included. The resulting parameter values of the optical potentials are compiled in tab. 1.

Table 1. Parameters of Saxon-Woods optical potential for elastic ^{6}Li scattering resulting from fit calculations. For ^{208}Pb the depth of the real potential was fixed.

Target	V (MeV)	r_v (fm)	a_v (fm)	W (MeV)	r_w (fm)	a_w (fm)
^{12}C	129.	1.21	0.89	28.	1.67	0.97
^{40}Ca	170.	1.22	0.89	29.	1.73	0.90
^{90}Zr	145.	1.19	0.93	19.	1.75	0.83
^{208}Pb	180.	1.22	0.78	20.	1.57	0.97

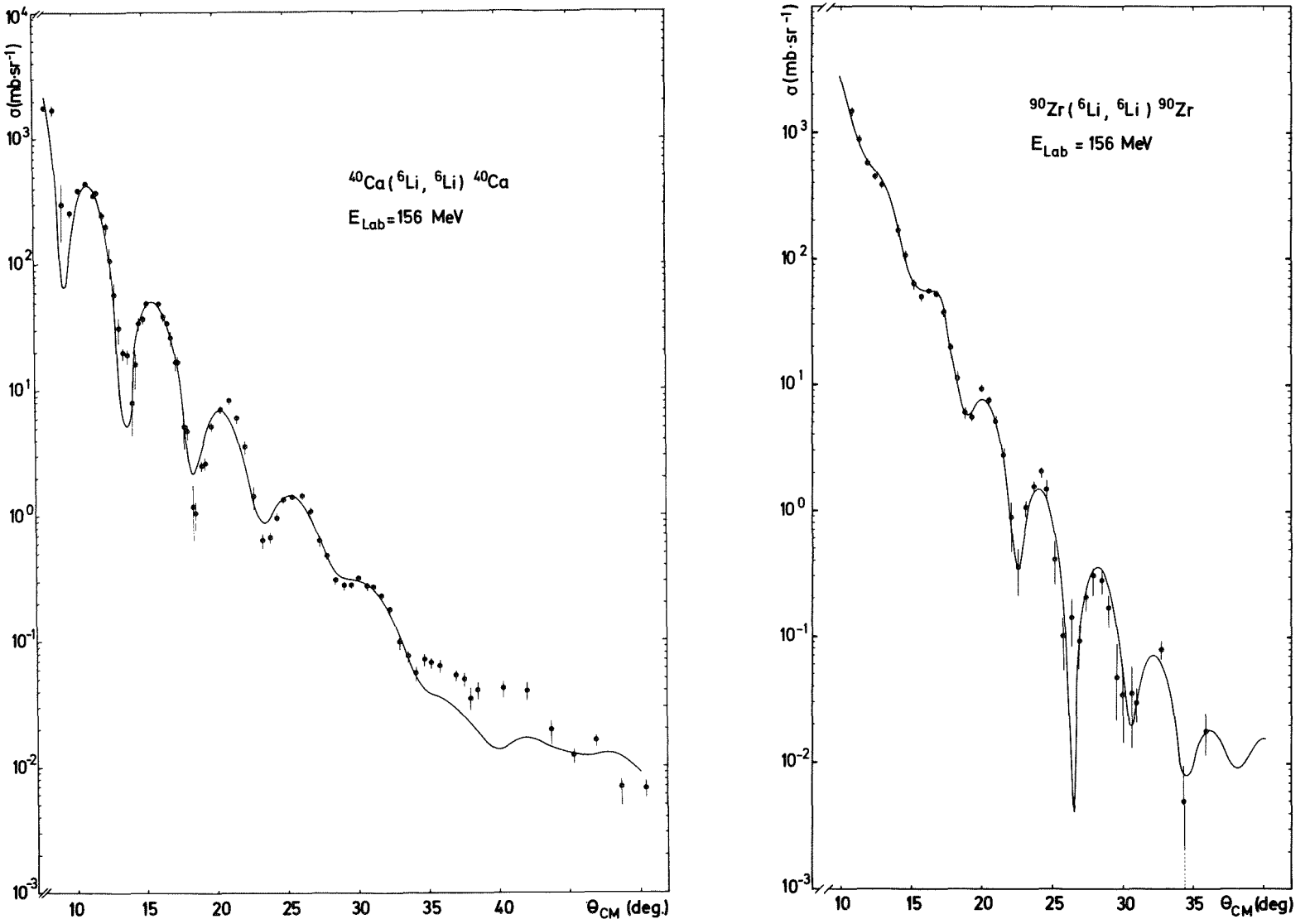

Fig. 1. Measured cross sections of elastic ^{6}Li scattering on ^{40}Ca and ^{90}Zr. The solid curves are the result of optical model fit calculations. The corresponding optical model parameters are given in table 1.

For the heavier nuclei ^{90}Zr and ^{208}Pb, the potential depth could not unambiguously be determined. The radius and diffuseness parameters of the real potential, however, are well determined and are nearly the same for all nuclei. One should note that the resulting diffuseness parameters of the imaginary part are rather large, which possibly can be ascribed to the influence of the strong ^{6}Li break-up channel.

References

/1/ J. Buschmann, H.J. Gils, H. Rebel, H. Klewe-Nebenius, H. Faust, J. Kropp, W. Nowatzke and S. Zagromski, Report KFK 2379 (1976) p. 43.

3. NUCLEAR SPECTROSCOPY

3.1 Spins and Magnetic Moments of Neutron-Deficient Rb Isotopes by In-Beam Optical Pumping

J. Collignon[+], F. Buchinger[+], R. Neugart[+], and H. Schweickert

The method of in-beam optical pumping /1/ has been applied to ^{80}Rb and ^{82}Rb. Fig. 1 shows the principle of the experimental set-up. Both isotopes are produced from enriched Kr targets by the respective (p,n) reactions. The target cell containing free Rb atoms in a Kr atmosphere is simultaneously used for the optical pumping experiment. Polarization achieved by irradiating the circularly polarized D_1 resonance line is detected by the asymmetry in the ß decay. RF resonances between the hfs levels of the atomic ground state yield the spins, hfs splittings and magnetic moments.

The following results have been obtained

^{80}Rb (30 s) : I = 1 μ_I = - 0.0836(6) nm
^{82}Rb (1.3 m) : I = 1 μ_I = - 0.554 (3) nm

(including diamagnetic correction)

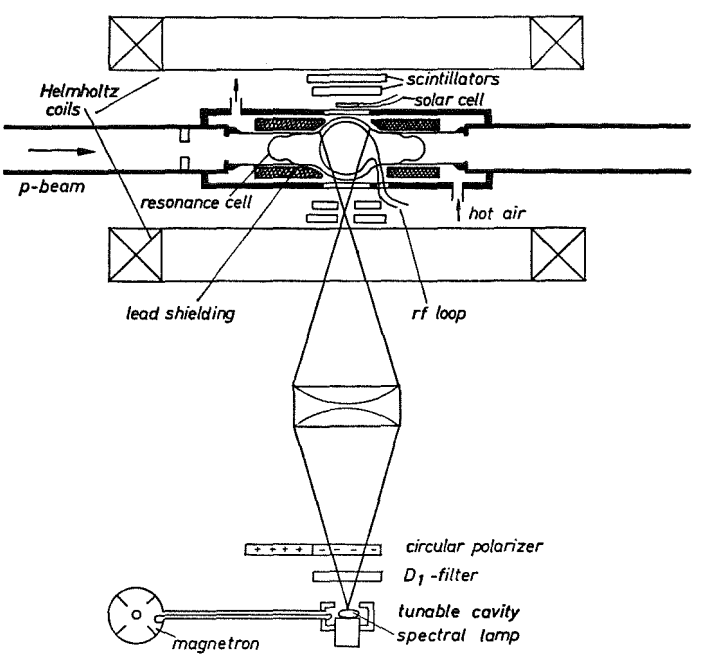

Fig. 1. Experimental set-up for on-line optical pumping.

In the case of ^{80}Rb a precision measurement of the hfs splitting has been performed, yielding $\Delta\nu$ = 233.936 (2) MHz. This result combined with the direct measurement of the nuclear moment gives an upper limit of 1 % for the hfs anomaly between ^{80}Rb and the stable ^{87}Rb.

Both isotopes considered here lie in the transition region between the stable isotopes near a closed neutron shell and a region of strong nuclear deformation. Ekström et al. /2/ have contributed important information on the more neutron-deficient isotopes by using the atomic-beam magnetic resonance method. An optical pumping experiment has been performed on ^{76}Rb at ISOLDE/CERN /2/. A rather comprehensive set of nuclear ground state properties in the region of light Rb isotopes has thus been obtained.

+ Institut für Physik der Universität Mainz, Germany

References

/1/ H. Schweickert, J. Dietrich, R. Neugart, E.W. Otten, Nucl. Phys. A 146 (1975) 187.

/2/ C. Ekström, S. Ingelman, G. Wannberg, M. Skarestad, Proc. 3rd Int. Conf. on Nuclei Far from Stability, Cagese, France, CERN 76-13 (1976) p. 193.

/3/ H. Fischer, P. Dabkiewicz, P. Freilinger, H.-J. Kluge, H. Kremmling, R. Neugart, E.-W. Otten, Z. Physik, to be published.

3.2 An Investigation of the Enhanced $4_1^+ \rightarrow 0^+$ Hexadecapole Transition in ^{140}Ce

A. Hanser, H. Klewe-Nebenius+, H. Rebel, J. Buschmann, and H.J. Gils

Previous experiments of different groups /1,2/ have shown that transitions between the first excited 4_1^+-state and the ground state of ^{140}Ce are strongly enhanced compared to the single-particle estimate for the transition probability. This fact indicates a strong hexadecapole motion of this nucleus

similar to that observed in various other spherical nuclei, as e.g. ^{60}Ni, $^{202,204}Pb$. However, the available experimental results for the L=4 enhancement G_4 in ^{140}Ce originating from the analysis of scattering experiments (G_4 = 7.8 s.p.u. from 45 MeV α scattering /1/, G_4 = 20 ± 4 s.p.u. from electron scattering /2/) do not agree quantitatively.

An alternate approach to investigate the enhanced hexadecapole transitions is to measure the intensity for the spontaneous γ-ray transition $4_1^+ \rightarrow 0^+$. This method has the advantage that it does not rely on complicated evaluation procedures and on particular nuclear models. Thus, one might expect from such a measurement a more reliable value for the enhancement of the $4_1^+ \rightarrow 0^+$ transition. The main difficulty with this type of measurement arises from the problem to detect the very weak cross-over γ-ray transition $4_1^+ \rightarrow 0^+$ in the presence of the much more intense γ rays from the competing cascade $4_1^+ \rightarrow 2_1^+ \rightarrow 0^+$.

The 4_1^+-state of ^{140}Ce at 2083 keV is strongly populated in the β^- decay of ^{140}La (see fig. 1). We succeeded in detecting the 2083 keV cross-over transition in the γ-ray spectrum from the decay of ^{140}La (see fig. 2) using a Ge(Li) spectrometer with Compton suppression and placing a 5 cm thick lead absorber between source and detector. This absorber strongly suppresses the γ rays from the $4_1^+ \rightarrow 2_1^+$ transition whose energy is only 487 keV. Thus, the chance summing up of γ rays from the cross-over cascade becomes negligible.

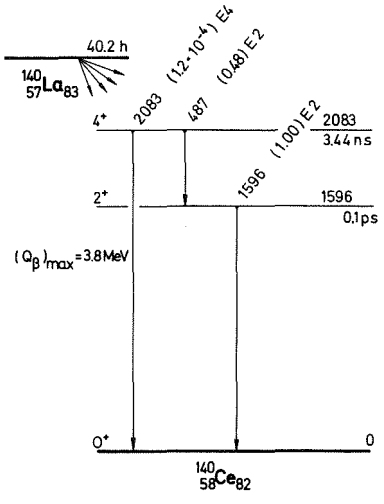

Fig. 1. Simplified decay scheme of ^{140}La.

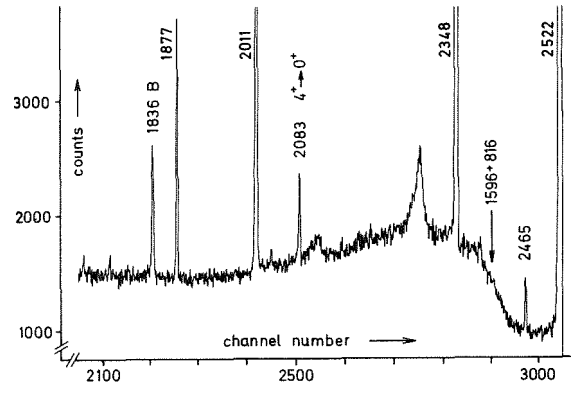

Fig. 2. Region of interest of one of the four measured γ-ray spectra from the ^{140}La decay.

A precise determination of the energy together with a check of the half-life assures that the observed 2083 keV peak can be unambiguously assigned to the $4_1^+ \rightarrow 0^+$ transition in ^{140}Ce. From the measured branching ratio $I_\gamma^{2083}/I_\gamma^{487} = (2.54 \pm 0.15) \times 10^{-4}$ and the known half-life of the 4_1^+-state ($T_{1/2} = 3.44 \pm 0.03$ ns) /3/, an enhancement $G_4 = 11.8 \pm 0.7$ s.p.u. is derived for the $4_1^+ \rightarrow 0^+$ transition.

In a second experiment, the strength of the $0^+ \rightarrow 4_1^+$ transition in ^{140}Ce has been determined from inelastic scattering of 104 MeV α particles. Because of the various impurities in the target, only data for scattering angles ranging from 18° to 27° could be evaluated. This angular range exhibits two distinct diffraction maxima (see fig. 3). The data from the scattering experiment were analyzed by means of a folding procedure for the optical potential using the method of coupled channels as described in ref. /4/. The matrix element β_{02} for the $0^+ \rightarrow 2_1^+$ transition required for the analysis was taken from ref. /3/. Although somewhat uncertain, this quantity does not significantly affect the evaluated $0^+ \rightarrow 4_1^+$ transition strength because for ^{140}Ce the double excitation of the 4_1^+-state is almost negligible. For the enhancement of the $0^+ \rightarrow 4_1^+$ transition a value $G_4 = 13 \pm 2$ s.p.u. was obtained in agreement with the result from the $4_1^+ \rightarrow 0^+$ transition measurement in the ^{140}La decay. This good agreement corroborates the folding model procedure used for extracting isoscalar transition rates from α scattering

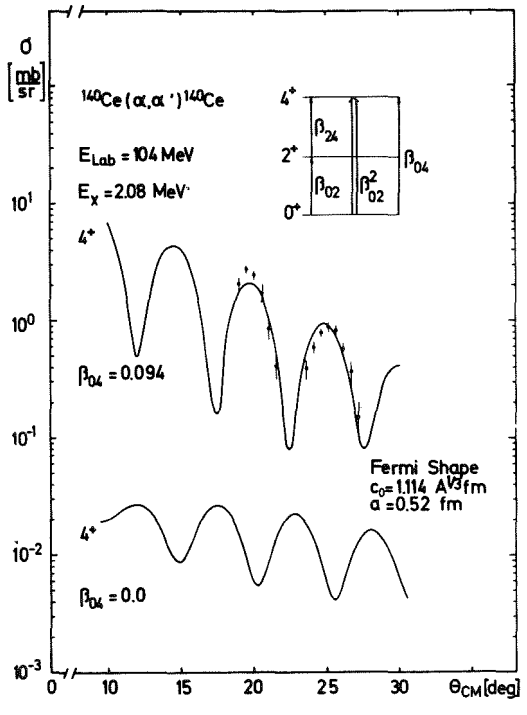

Fig. 3. ^{140}Ce(α,α')^{140}Ce: Measured differential cross sections for the α scattering from the 4_1^+-state and results from coupled channel calculations. To demonstrate the sensitivity of the experiment, the lower curve is calculated assuming a vanishing hexadecapole transition strength.

data. In the analysis of the previous 45 MeV α scattering data /1/, a more simple DWBA procedure was used. A reanalysis of the previous data based on a folded optical potential yields a value $G_4 = 14 \pm 2$ s.p.u.

+ Institut für Radiochemie

References

/1/ F.T. Baker, R. Tickle, Phys. Rev. C5 (1972) 182.
/2/ R. Pitthan, Z. Phys. 260 (1973) 283.
/3/ L.K. Peker et al., Nucl. Data Sheets 12 (1974) 343.
/4/ H. Rebel, Report KFK 2065 (1974).

3.3 Study of the Level Structures of ^{80}Br and ^{82}Br Using the Thermal Neutron Capture Reaction*

Do Huu Phuoc+, R. Chery+, H. Börner++,+++, W.F. Davidson++, J.A. Pinston++, R. Roussille++, K. Schreckenbach++, H.R. Koch+++, H. Seyfarth+++, and D. Heck

The level structures of the doubly odd nuclei ^{80}Br and ^{82}Br have been studied by means of the thermal neutron capture reactions ^{79}Br(n,γ)^{80}Br and ^{81}Br(n,γ)^{82}Br. Capture γ-ray spectra from isotopically separated targets have been measured in the approximate energy intervals $30 < E_\gamma(\text{keV}) < 1100$ with three bent crystal spectrometers installed at the Grenoble high-flux reactor. Measurements with Ge(Li) detectors operated in Compton-suppression and pair-mode covered the energy range $0.1 < E_\gamma\,(\text{MeV}) < 8$. Gamma-gamma coincidences have been taken with different Ge(Li) detectors at the research reactor FRJ-2 (Dido) at the Kernforschungsanlage Jülich. The conversion-electron spectra of ^{80}Br and ^{82}Br from thermal neutron capture have been measured with the beta spectrometer at the Grenoble high-flux reactor. Using all these data the level schemes of ^{80}Br and ^{82}Br are

proposed up to 1.5 MeV. Spin assignments for the excited states below 800 keV are proposed.

* Nucl. Phys. (in print)

+ Institut de Physique Nucléaire, Laboratoire associé à l'IN2P3, Université Claude Bernard, Lyon I, F-69621 Villeurbanne, France

++ Institut Laue-Langevin, 156 X Centre de Tri, F-38042 Grenoble Cédex, France

+++ Institut für Kernphysik, Kernforschungsanlage Jülich, D-5170 Jülich, Germany

4. THEORY

4.1 Validity of the Adiabatic Cranking Model When Applied to Fission*

E.F. Chaffin+ and F. Dickmann

The cranking model is applied to a two-center, asymmetric shell model plus a pairing interaction. The energy increase due to the enforced collective motion is determined up to fourth order in the collective velocity. For a motion across the second saddle of ^{236}U the higher order terms are so large that the validity of the adiabatic model as a first approximation to fission dynamics is questionable.

* Phys. Rev. Lett. 37 (1976) 1738.

+ Present address: U.S. Naval Nuclear Power School, U.S. Naval Training Center, Orlando, Florida 32813, USA.

4.2 How to Generate a Deformation Velocity in the Shell Model

F. Dickmann

The Hartree-Fock (HF) approximation to a system of interacting fermions provides the conceptual basis for single-particle models. By introducing suitable subsidiary conditions one can deal with collective degrees of freedom /1/.

We consider the constrained Hamiltonian

$$\hat{G} = \hat{H} - \lambda \hat{A} = \sum_{pqst} t_{ps}\, b_p^+ b_s + \frac{1}{4} \sum_{pqst} v_{pq,st}\, b_p^+ b_q^+ b_t b_s - \lambda \sum_{ps} a_{ps}\, b_p^+ b_s \qquad (1)$$

and ask for the normalized Slater determinant $|\psi\rangle$ which produces a stationary expectation value of the operator $\hat{G}$

$$\delta \langle \psi | \hat{G} | \psi \rangle = 0 \qquad (2)$$

and a prescribed expectation value of the operator $\hat{A}$

$$\alpha = \langle\psi| \hat{A} |\psi\rangle = \mathrm{Tr}\ (\rho a). \tag{3}$$

The single-particle density matrix occurring in eq. (3) has the elements

$$\rho_{sp} = \langle\psi| b_p^+ b_s |\psi\rangle \tag{4}$$

The constraining operator $\hat{A}$ is chosen so that its expectation value characterizes the nuclear shape.

In order to fulfill the H-F stationarity condition(2), the commutation relation

$$[\rho,h] = 0 \tag{5}$$

must hold. The single-particle Hamiltonian matrix has the elements

$$h_{ps} = t_{ps} + \sum_{tq} v_{pqst}\ \rho_{tq} - \lambda\ a_{ps} \tag{6}$$

Phenomenological deformed single-particle models aim at a good guess of the one-body Hamiltonian

$$\hat{H}_1 = \sum_{ps} h_{ps}\ b_p^+\ b_s \tag{7}$$

The matrices ρ and h can be simultaneously diagonalized because they commute (eq. (5)):

$$\rho_{sp} = \rho_s \delta_{sp} \quad \text{where} \quad \begin{array}{l} \rho_s = 1 \text{ for occupied states } s = i,j \\ \rho_s = 0 \text{ for vacant states } s = k,l \end{array}$$
$$h_{ps} = \varepsilon_s\ \delta_{ps}. \tag{8}$$

In order to find a Hermitian conjugate momentum operator $\hat{P}$ associated with the deformation operator $\hat{A}$ we first ask for a Hermitian operator

$$\hat{R} = \sum_{ps} r_{ps}\ b_p^+\ b_s$$

which generates an infinitesimal change $\delta\alpha$ of the deformation α.

$$\alpha + \delta\alpha = \langle\psi| e^{-i\delta\alpha\hat{R}} \hat{A} e^{i\delta\alpha\hat{R}} |\psi\rangle = \mathrm{Tr}\,(e^{i\delta\alpha r}\,\rho\, e^{-i\delta\alpha r}\, a)$$

$$= \alpha + \delta\alpha\ \mathrm{Tr}\,(|ir,\rho|\, a) + \sigma(\delta\alpha^2) \tag{9}$$

The imaginary unit is denoted by i. Differentiating both sides of eq. (9) with respect to $\delta\alpha$, we see that the matrix r must fulfill the equation

$$\mathrm{Tr}\,(\lceil ir,\rho\rceil a) = 1 \tag{10}$$

The H-F condition (5) must be valid also at the displaced deformation. Inserting the transformed density $e^{\delta\alpha ir}\,\rho e^{-\delta\alpha ir}$ into eq. (5) and differentiating with respect to $\delta\alpha$, we obtain

$$\lceil d\rho/d\alpha, h\rceil + \lceil\rho,\ dh/d\alpha\rceil = 0, \tag{11}$$

where

$$d\rho/d\alpha = \lceil ir,\rho\rceil$$

$$dh/d\alpha = \mathrm{Tr}(\upsilon\lceil ir,\rho\rceil) - a\, d\lambda/d\alpha$$

The trace of the two-body matrix υ with a one-body matrix a is a one-body matrix, defined as

$$\mathrm{Tr}(\upsilon a)_{ps} = \sum_{qt} \upsilon_{pq,st}\, a_{tq}$$

Equations (10) and (11) constitute a linear system of equations from which the particle-hole matrix-elements r_{kj} and the derivative of the Lagrange parameter $d\lambda/d\alpha$ can be determined. If we use a phenomenological single particle matrix h instead of the H-F term, we can easily solve the first eq. (11) for the matrix elements r_{kj}. Making use of equations (8) we obtain

$$r_{kj} = \frac{1}{i(\varepsilon_k - \varepsilon_j)}\ (dh/d\alpha)_{kj} \tag{12}$$

We now define the momentum operator $\hat{P}$ as

$$\hat{P} = - h \hat{R}$$

in analogy with ordinary space, where the momentum operator $\hat{P}_x$ generates a displacement of the expectation value of the operator $\hat{X}$.

Since only the particle-hole matrix elements of the momentum operator are fixed by the H-F condition (5) we are, in the absence of further constraints, free to choose the other matrix elements and require that the expectation value of the momentum operator with the "static" H-F wave vector is zero.

$$<\psi|\hat{P}|\psi>= 0 \qquad (13)$$

The momentum operator $\hat{P}$ can now be used as a constraining device to produce a Slater determinant which gives a finite expectation value of the collective momentum.

References

/1/ F.M.H. Villars, "Hartree-Fock Theory and Collective Motion" in Dynamic Structure of Nuclear States, ed. D.J. Rowe et al., Univ. Toronto Press (1972).

4.3 Rapid Change of Nuclear Structure During the Fission Process

E.F. Chaffin[+] and F. Dickmann

A standard method in the investigation of nuclear collective dynamics is to study the reaction of the nucleus upon an induced motion. Theoretically this is done by coupling a generating operator $\hat{P}_\alpha$ via a Lagrange parameter α to the model Hamiltonian $\hat{H}$. One thus obtains the modified Hamiltonian

$$\hat{H}' = \hat{H}(\alpha) - \dot{\alpha}\,\hat{P}_\alpha . \tag{1}$$

The generating operator

$$\hat{P}_\alpha = \frac{\hbar}{i}\frac{\partial}{\partial \alpha} \tag{2}$$

induces a change of the shape variable α with the collective velocity $\dot{\alpha}$.

We investigate the collective dynamics of fissionable nuclei at deformations close to the highest saddle point as shown in fig. 1 for the case of ^{236}U. In the five dimensional space depicted in the figure caption, we have so far studied the one dimensional motion along the scission line. It consists of an increase of the distance ℓ between the spheroid centres together with a constriction of the hyperboloidic neck.

Our static model Hamiltonian $\hat{H}(\alpha)$ is the sum of a Two-Center-Single Particle Model $\hat{H}_{TSCM}(\alpha)$ and a residual pairing interaction $\hat{H}_{pair}$

$$\hat{H}(\alpha) = \hat{H}_{TCSM}(\alpha) + \hat{H}_{pair} \tag{3}$$

In a more fundamental treatment one would start from a shape independent Hamiltonian with "realistic" two body forces and would apply a constrained Hartree-Bogoliubov method. We imagine the Hamiltonian $\hat{H}(\alpha)$ to have emerged

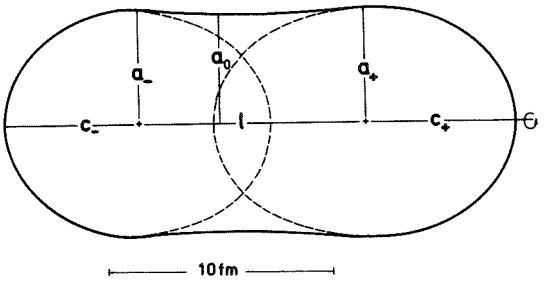

Fig. 1. The asymmetric saddle point shape for ^{236}U is characterized by the dimensionless quantities: $x_1 = \ell/2a_+=1$, $x_2=-c_0^2/a_0^2=0.05$, $x_3=(c_++c_-)/2a_+=1.25$, $x_4=a_+^2c_+/a_-^2c_-=1.2$, $x_5=(c_+-c_-)/2a_+=0.08$, where the quantities a and c are the principal axes of the two spheroids and the central hyperboloid. The one-dimensional motion across the second saddle is defined by the variations $\delta x_1=\alpha$, $\delta x_2=0.6\ \alpha$. The variables x_3, x_4, and x_5 , the center of mass position, and the volume of the nucleus are kept constant.

from such a treatment. In view of the success of Strutinsky's method for obtaining shell effects on the deformation energy we expect our simple model to be realistic enough to exhibit shell effects on the dynamics of fission.

In an attempt to determine the ground state wave function of the Hamiltonian $\hat{H}'$ (eq. (1)) it has been found /1/ that the term $\dot{\alpha}\hat{P}_\alpha$ cannot be treated as a small perturbation of the static Hamiltonian $\hat{H}(\alpha)$ (eq. (3)). The wave function changes drastically on imposing a collective kinetic energy of a few tenth of an MeV. This rapid change of the wave-function is analoguous to the backbending phenomenon in nuclear rotational motion. A component of the orbital angular momentum operator $\hat{L}_x$ which generates a rotation around the body fixed x-axis corresponds to our operator $\hat{P}_\alpha$, the rotational frequency ω corresponds to $\dot{\alpha}$. The backbending phenomenon implies a rapid change of the intrinsic nuclear wave function upon a small change of the angular momentum. The theoretical methods used in the treatment of backbending can also be applied to fission dynamics. Leaving aside projection techniques the constrained Hartree-Bogoliubov method for our simple model reduces to (i) a diagonalization of the single particle Hamiltonian

$$\hat{H}''(\alpha, \dot{\alpha}) = \hat{H}_{TCSM}(\alpha) - \dot{\alpha}\hat{P}_\alpha \tag{4}$$

which is feasible numerically also for large values of $\dot{\alpha}$ and (ii) a subsequent BCS calculation. The diagonalization of the Hamiltonian $\hat{H}''$ is done in the orthonormal basis of the eigenstates $|j(\alpha)>$ of the operator $\hat{H}_{TCSM}(\alpha)$. Matrix elements of $\hat{P}_\alpha$(eq. (2)) can be written in the form

$$<j(\alpha)|\hat{P}_\alpha|k(\alpha)> = <j(\alpha)|\frac{\frac{h}{i}\frac{\partial \hat{H}_{TCSM}}{\partial\alpha}}{\varepsilon_k - \varepsilon_j}|k(\alpha)> \quad (1 - \delta_{jk}) \tag{5}$$

where ε_k and ε_j are eigenvalues of $\hat{H}_{TCSM}(\alpha)$. The right hand side of the above equation shows that the eigenfunctions of $\hat{H}''$ will be very sensitive to $\dot{\alpha}$ if for a given deformation α the denominator in eq. (4) becomes small, provided the matrix element in the numerator is not zero due to selection rules. Since we consider axially symmetric nuclear shapes the projection Ω of the single particle angular momentum on the symmetry axis is a good quantum number. In a first calculation we have also adhered to a reflection-symmetric shape (symmetric saddle) and thus the parity π of the single particle state is a good quantum number.

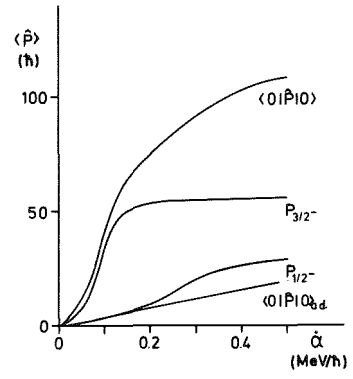

Fig. 2. The expectation value of the generating operator $\hat{P}_\alpha$ with the BCS ground state as a function of the collective velocity $\dot{\alpha}$ is denoted by $\langle O|\hat{P}|O\rangle$. The curves marked $P_{3/2}^-$ and $P_{1/2}^-$ give the contribution to $\langle O|\hat{P}|O\rangle$ from the states with $\Omega^\pi = 3/2^-$ and $1/2^-$. The lowest curve gives the result for $\langle O|\hat{P}_\alpha|O\rangle$ obtained from the adiabatic cranking theory.

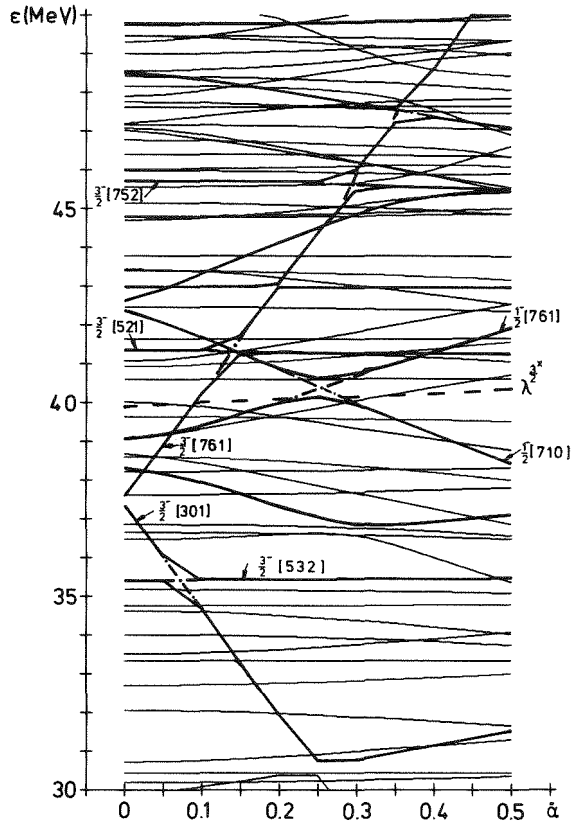

Fig. 3. Energy levels of the operator $\hat{H}''$ (eq. 4) as a function of $\dot{\alpha}$. The Fermi energy λ is plotted as a dashed line.

In figs. 2 and 3 numerical results for protons of ^{236}U and a pairing parameter $\Delta \gtrsim 1$ MeV are presented. Fig. 2 reveals the striking difference between the number for the expectation value of the generating operator $\hat{P}_\alpha$ obtained in this work and the adiabatic cranking model. The collective inertia $m = \langle O|\hat{P}_\alpha|O\rangle / \dot{\alpha}$ is much larger than for the cranking model. Most of this inertia comes from the contribution of the $\Omega^\pi = 3/2^-$ and $1/2^-$ states as shown separately in fig. 2. The explanation of this effect in terms of the single particle level structure can be extracted from fig. 3. At zero collective velocity, $\dot{\alpha} = 0$, two levels with the good quantum-numbers $\Omega^\pi = 3/2^-$ lie very close to each other about two MeV below the Fermi level. They repel each other strongly as the collective velocity increases. Simple algebra shows that this causes a strong increase of the expectation value $\langle O|\hat{P}_\alpha|O\rangle$

if the occupation probability of one of the levels changes as it crosses the Fermi surface. Fig. 3 also shows that there are two $\Omega^{\pi} = 1/2^{-}$ levels crossing the Fermi surface less steeply at a larger value of $\dot{\alpha}$. Thus the contribution of these states to the collective inertia is not so strong and sets in at a higher collective speed. The added contributions from these two groups of states account for the major part of the quantity $\langle 0|\hat{P}_{\alpha}|0\rangle$.

What implications do these results have for the theory of fission ? It has been demonstrated that collective dynamics is strongly influenced by the single particle structure of the deforming nucleus in the neighbourhood of the saddle point. These shell effects will only be reduced when the fissioning nucleus approaches scission because one fission fragment will no longer disturb the level structure of its partner beyond the scission point.

The effects that we have studied here are due to specific single particle states or rather quasi particle states. They will become smaller if the nucleus heats up between saddle and scission because the occupation probabilities of the states are smeared out at a finite temperature. None the less they will be important up to temperatures of more than 1 MeV as can be seen from fig. 3. The two levels that repel each other strongly lie two MeV below the Fermi energy at zero velocity. Thus the occupation probability of the lower one is not much effected by a low temperature. Perturbative methods like the linear response theory proposed for heavy ion reactions will thus only work if the excitation energy is sufficiently high.

+ Present address: U.S. Naval Nuclear Power School, U.S. Naval Training Center, Orlando, Florida 32813, USA.

References

/1/ E.F. Chaffin and F. Dickmann, Phys. Rev. Lett. 37 (1976) 1738.

5. LASER SPECTROSCOPY

5.1 Nuclear Radii and Magnetic Moments of ^{128,131}Ba from High-Resolution Laser Spectroscopy*

G. Nowicki, K. Bekk, S. Göring, H. Hanser, H. Rebel, and G. Schatz

Mass separated samples of the instable nuclides ^{128}Ba ($T_{1/2}$=2.4 d) and ^{131}Ba ($T_{1/2}$=11.5 d) have been investigated by means of Doppler free laser spectroscopy, using cw dye lasers and a well collimated atomic beam. From isotope shifts and hyperfine structure of the $^1S_o - {}^1P_1$ transition (λ = 553.6 nm) we obtained the differences of mean square charge radii $\delta \langle r^2 \rangle$ (^{131}Ba - ^{130}Ba) = -0.006 (3) fm^2 and $\delta \langle r^2 \rangle$ (^{130}Ba - ^{128}Ba) = 0.022 (3) fm^2 and the magnetic moment of ^{131}Ba μ = - 0.714 (6) μ_N.

*Phys. Rev. Lett. 39 (1977) 332.

5.2 Computerized Data Acquisition System for High-Resolution Laser Spectroscopy

K. Bekk and G. Nowicki

The experimental set-up for laser-spectroscopic measurements of instable atoms has been described in the last annual report /1,2/. The principle of the measurement is to observe the fluorescence intensity of an atomic beam as a function of the exciting laser frequency. The latter one is determined from the heterodyne frequency of this laser and a second laser providing the optical reference frequency. This second laser is locked to a known atomic transition. That means that the experimental information is given by the following two parameters: heterodyne frequency and related fluorescence intensity. In addition, some monitoring informations are needed for experiment control, e.g. single mode operation of both lasers, mode hopping of a laser, accurate locking of the reference laser, intensity of the laser and the atomic beam.

The data acquisition and experimental control is performed by a NOVA 2 computer which is interfaced to the experimental set-up by a single-crate Camac system. The hardware configuration of the computer and the Camac system is shown in fig. 1.

Both the heterodyne frequency and the respective frequency of the exciting laser which is locked to the adjusted heterodyne frequency are tuned by the computer via a digital-to-analog converter. The speed and the direction of the tuning is selected by means of switches. The fluorescence-light intensity corresponding to the actual laser frequency is measured by photon counting and read by the computer using an input register. Normalization of the fluorescence intensity to the laser intensity is achieved by integrating the current from a photodiode illuminated by the laser during each measurement cycle. In addition, the transmission maxima of two confocal Fabry-Pérot interferometers monitoring the single mode operation of the lasers and the presence of the heterodyne signal in

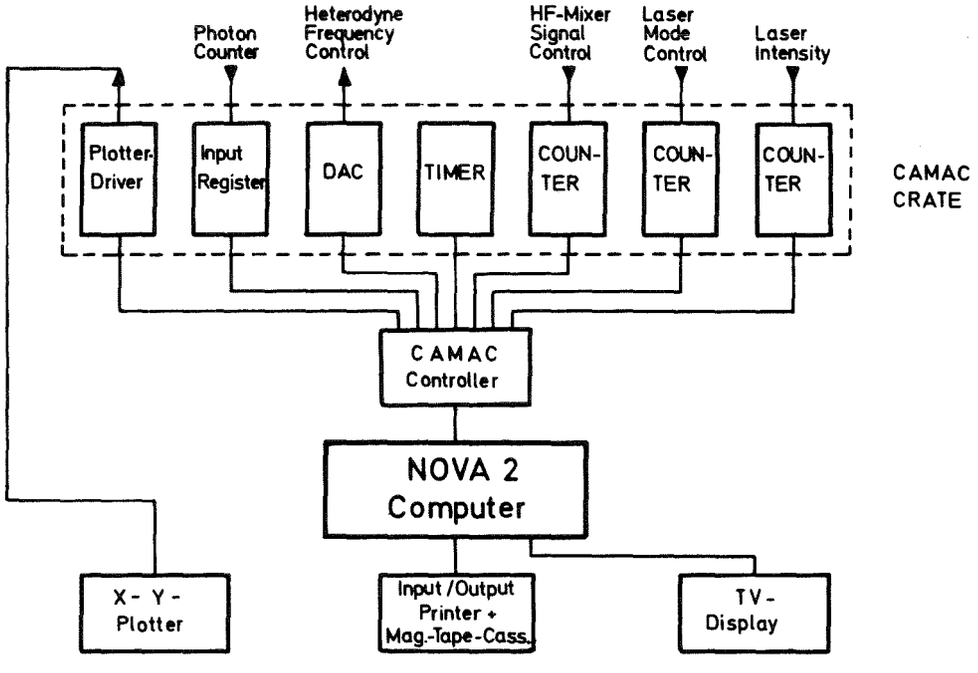

Fig. 1. Hardware configuration of the computer system for laser-spectroscopic experiments.

each scan of the RF-spectrum analyzer are counted and checked. A measurement cycle is only accepted when these two check measurements give correct results.

The synchronization of all measurement functions is performed by a timer having a 1 MHz clock. The atomic beam intensity is observed by collecting atoms cut off from the atomic beam on small aluminium sheets and measuring their radioactivity accumulated in a definite time interval.

The data are stored on a magnetic tape cassette and plotted on a X-Y plotter. The frequency scale can be calibrated by connecting the output of

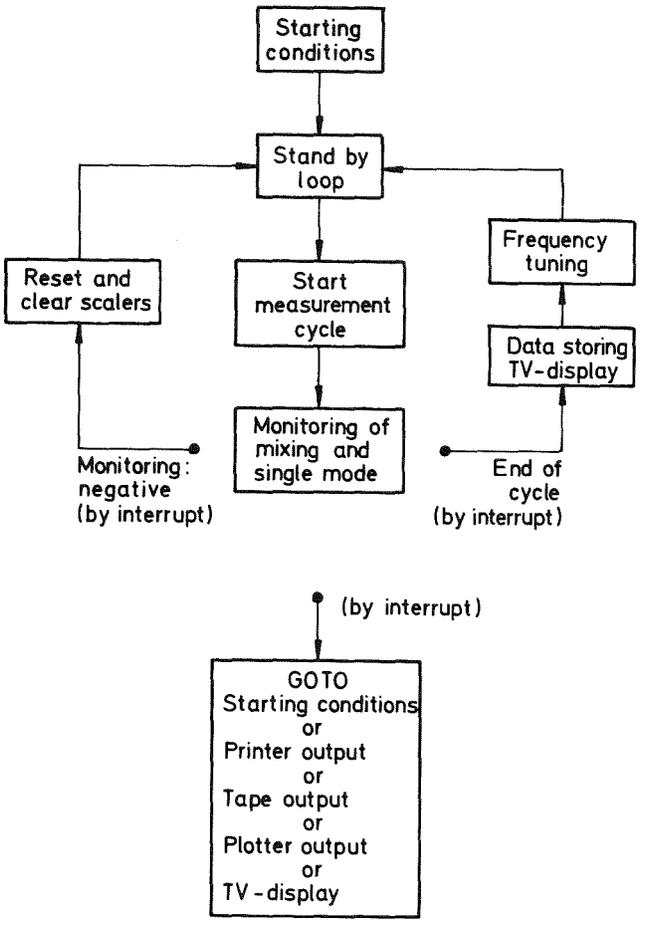

Fig. 2. Program flow chart for measurement control and data acquisition.

a frequency comb generator to the input of the RF-spectrum analyzer. The program flow chart shown in fig. 2 illustrates the interplay of the different components of the experimental set-up.

References

/1/ G. Nowicki, S. Göring, H. Rebel, G. Schatz, Report KFK 2379 (1976) p. 54.

/2/ B. Feurer, A. Hanser, Report KFK 2379 (1976) p. 56.

5.3 Sample Preparation for Laser Experiments on Instable Barium Isotopes

B. Feurer and A. Hanser

The laser experiments on instable barium isotopes at our laboratory aim at studying how the nuclear charge radii vary with the neutron number. Therefore all barium isotopes are of interest of which one can prepare sufficient sample quantities. Moreover, it is interesting to investigate the long-lived isomeres of the odd barium isotopes, because measurable differences in the nuclear radii of the isomeric and ground states are expected.

In the previous annual report the measuring device for the experiments has been described, and its high sensitivity has been pointed out /1,2/. The measurements carried out in the meantime showed that it is sufficient to bring one nanogram of the barium nuclides under investigation into the atomic beam oven of our experimental set-up. The contamination of the samples by other - stable or instable - barium isotopes should be as small as possible, and the barium has to be in the elementary form.

Two different procedures were employed in preparing the samples for the laser experiments:

1) Barium oxide with high enrichments of ^{130}Ba or ^{134}Ba is irradiated with the deuteron beam of the Karlsruhe Isochronous Cyclotron or with thermal neutrons. The deuteron irradiation primarily produces short-lived lanthanum isotopes. They convert to barium via ß decay. The instable barium isotope of interest is then separated by an electromagnetic mass separator. A high separation factor ($1 - 1.5 \times 10^4$) is necessary, since only a small fraction of the barium atoms in the target are converted by the nuclear reactions.

2) Cesium sulfate is irradiated with alpha particles or deuterons at the cyclotron. Alpha-particle irradiation leads to short-lived lanthanum isotopes which decay mainly to the ground states of the barium isobares. In contrast, deuteron irradiation leads to high-spin isomeres of the odd barium isotopes because of the high momentum transfer in the (d,xn) reaction. The produced barium is first parted chemically from the cesium target material. This is accomplished with an ion exchange column without using a carrier /3/. Then the barium is separated by an electromagnetic mass separator.

A surface ionization source which yields a good efficiency is used in the separation process. If high separation factors are needed as it is the case when separating instable barium isotopes from barium target material, then the efficiency of the mass separation amounts to 12 %. In this case the admixtures of neighbouring isotopes are reduced by a factor of 6000. When somewhat lower separation factors can be tolerated, then an efficiency of 25 % can be achieved. The mass separation process reduces the barium to the elementary form.

Samples of ^{131g}Ba ($T_{1/2}$ = 11.5 d), ^{128}Ba ($T_{1/2}$ = 2.4 d) and ^{133m}Ba ($T_{1/2}$ = 39 h) have already been produced in quantities sufficient for the laser experiments. ^{131g}Ba has been obtained by irradiating enriched ^{134}Ba with deuterons as well as by irradiating enriched ^{130}Ba with thermal neutrons.

The sample with the best properties was prepared by irradiation of 1.5 mg ^{130}BaO (enriched to 59 %) in the Karlsruhe Research Reactor FR2 for 7 days. The mass-separated sample contained 29 ng ^{131}Ba; it was contaminated by roughly the same quantity of stable barium isotopes, in particular ^{130}Ba. For the preparation of the ^{128}Ba sample, enriched ^{130}Ba (3 mg) was irradiated with 45 MeV deuterons for 3 days. This resulted in a sample with 6 ng ^{128}Ba; the contamination by stable barium isotopes was estimated to be three times this quantity. Samples for measurements on ^{133m}Ba were made from cesium sulfate (40 mg) which has been irradiated with 30 MeV deuterons. The samples contained ∿2 ng ^{133m}Ba and ∿2.5 ng ^{133g}Ba each.

For future experiments, samples containing ^{129m}Ba ($T_{1/2}$ = 2.1 h) and ^{129g}Ba ($T_{1/2}$ = 2.5 h) will be prepared by irradiating cesium sulfate with 52 MeV deuterons or with 104 MeV alpha particles. The expected ^{129}Ba quantities are very small. This has to be compensated by multiple sample preparation.

References

/1/ G. Nowicki et al., Report KFK 2379 (1976) p. 54.

/2/ B. Feurer, A. Hanser, Report KFK 2379 (1976) p. 56.

/3/ R. Shabana, H. Ruf, Report KFK 2460 (1977).

6. NUCLEAR FUEL AND ELEMENTAL ANALYSIS

6.1 Operational Experiences with a Portal Monitor for Fissile Material Detection

P. Matussek

The personnel portal monitor previously described /1/ has been installed at a nuclear facility at the Karlsruhe Nuclear Research Centre in 1976. This monitor which is built as a personnel lock (see fig. 1) shall detect special nuclear materials (SNM) possibly carried away by persons leaving the fissile material access area. The gamma radiation associated with all SNM is used to detect the presence of those materials in the personnel lock. A time period of 4 seconds is chosen for the personnel assay. The counts registered by the gamma detection system during this assay time are compared to continuously updated background counts which are measured in time intervals of 20 seconds as long as the lock is not occupied. The average count rate from the background radiation amounts approximately to 800 counts/sec. The alarm threshold was set at a level of 3σ above the last measured background count rate.

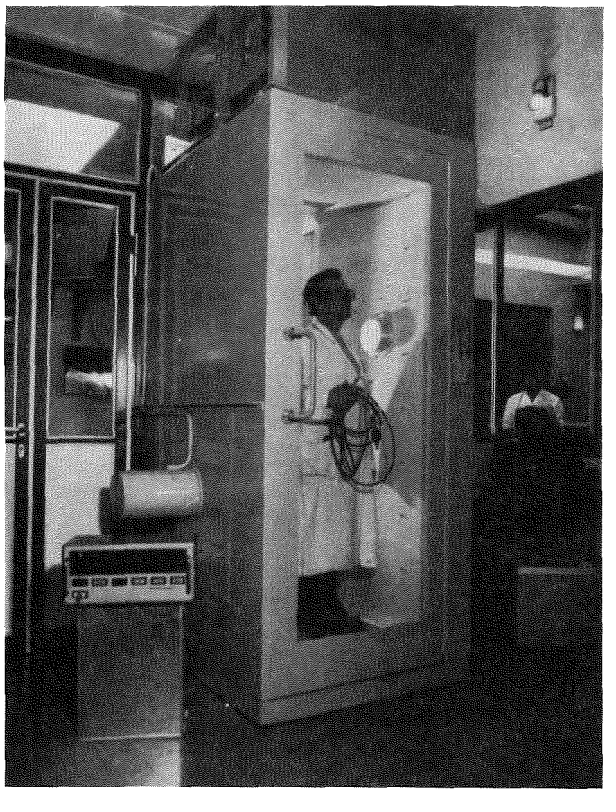

Fig. 1. View of the personnel monitor.

After the completion of initial adjustments and sensitivity measurements /1/, operational experiences with the doorway monitor have been gathered over a period of more than 6 months. In particular, we were interested in an analysis of the false alarm rate. The personnel monitor operates fully automated. Upon the detection of radioactive material an alarm is initiated and the doors of the monitor are locked. In this case the doors can be only opened by guards. We therefore asked the guards to carefully check with a hand-held gamma monitor all those persons who have caused an alarm and to make a short report on the results of these investigations as well as on all events indicating a faulty operation of the monitor. These reports form the basis for the information about the operational experiences.

Table 1. Summary of alarms from the personnel monitor observed during a period of six months of operation

Total number of passages	6052
Total number of alarms	214
Number of alarms caused by:	
Radioisotopes in wrist watches	107
Loose cable connection (caused 30 successive alarms)	30
Transport of radio isotopes and contaminated materials	13
Functional tests and demonstrations	12
Improperly noise-filtered electrical drilling machine used nearby (caused 10 successive alarms)	10
Strong gamma source near to the monitor	4
Use of the monitor within 20 sec after power failure preventing background updating	4
No report	5
True false alarms	29
Total	214

There are several causes which may result in a false alarm. First, counting statistics produces a false alarm rate of 0.15 % at the 3 σ level for the alarm threshold. Secondly, a sudden increase of the background radiation occuring either during a personnel assay or within a time interval of 20 seconds before entering the monitor can lead to a false alarm, because in both cases the stored background counts are not representative for the actual background. A third source which has been identified to be responsible for false alarms during the test period was radio noise from improperly noise-filtered electrical motors located near to the monitor.

Table 1 summarizes the alarms observed during the first 6 months of operation of the personnel monitor. The true false alarm rate turned out to be 0.5 %. This value compares well with the theoretical value of 0.15 % which has been calculated assuming a constant background radiation level. This assumption is certainly not fulfilled under the environmental conditions at the nuclear facility where the monitor is now successfully used.

References

/1/ P. Matussek, I. Michel-Piper, Report KFK 2321 (1976) 77.

6.2 Calibration Standards for ^{235}U Enrichment Measurements by Gamma-Ray Spectrometry

H. Eberle and P. Matussek

The ^{235}U enrichment in bulk uranium samples can be easily determined from an intensity measurement of the 185 keV γ rays emitted by the ^{235}U isotope. The enrichment analyses are usually performed in a well-defined geometry where a γ detector views part of the sample surface through a collimator. Most accurate analysis results are obtained when the instruments are calibrated by means of standards whose chemical and physical properties resemble the material to be assayed as closely as possible.

The Working Group on Techniques and Standards for Non-Destructive Analysis of the European Safeguards Research and Development Association (ESARDA) has initiated a programme to provide the users of the gamma-spectrometric enrichment analysis technique with recognized calibration standards. In a first step, standards for enrichment measurements on uranium oxide powders are in preparation. They will consist of carefully characterized uranium oxide powder sealed in cylindrical aluminium containers.

In the framework of this programme, calculations have been performed to determine the minimum required sample material quantities and sample sizes for different collimator geometries and uranium oxide densities. The sample dimensions were minimized with respect to infinite thickness geometry, i.e., the minimum sample dimensions were determined such that the samples should still emit 99.9 % of the 185 keV γ-ray intensity which would be observed from an infinitely thick sample. Only samples which meet this criterion assure the desired strict proportionality of the measured 185 keV γ-ray intensity with the ^{235}U enrichment. In table 1 the calculated minimum sample dimensions are listed for different cylindrical collimator geometries, assuming an uranium oxide density of 2.5 g/cm^3. For this density, uranium samples with a diameter of 7 cm and a height of 2 cm represent the required infinitely thick layer for all cylindrical collimators having diameters of $\leq$5 cm and lengths of $\geq$1 cm.

We also tried to calculate the 185 keV γ-ray intensity from basic nuclear data in order to estimate the degree of accuracy that can be achieved in cases where no standards are available. Assuming cylindrical collimators and neglecting multiple coherent scattering events within the sample, we derived a relatively simple analytical expression for the 185 keV γ-ray intensity at the exit of different collimators. The result of the calculations is shown in fig. 1 where for the case of UO_2 the calculated 185 keV photon intensity at the collimator exit per cm^2 of collimator area and sec and per % ^{235}U enrichment is plotted as a function of the ratio collimator diameter/collimator length. Experimental data points measured for three different collimator geometries with a Ge(Li) detector are shown for comparison. The experimental data points deviate systematically by about 20 % from the theoretical curve. This may be partly explained by the fact that in the calculations we did not correct

Table 1. Minimum sample dimensions required for infinite thickness geometry with respect to different collimator dimensions (ρ_u = 2.5 g/cm^3)

Collimator Diameter (cm)	Collimator Height (cm)	Minimum sample dimensions Diameter (cm)	Height (cm)	UO_2 Weight (g)
	1	4.9	1.6	76
	2	4.7	1.7	71
3	3	4.4	1.7	65
	4	4.1	1.8	59
	∞	3	2.0	35
	1	5.8	1.6	107
	2	5.7	1.7	106
4	3	5.5	1.7	102
	4	5.3	1.8	97
	∞	4	2.0	63
	1	6.7	1.6	143
	2	6.7	1.7	145
5	3	6.5	1.7	143
	4	6.4	1.8	140
	∞	5	2.0	98

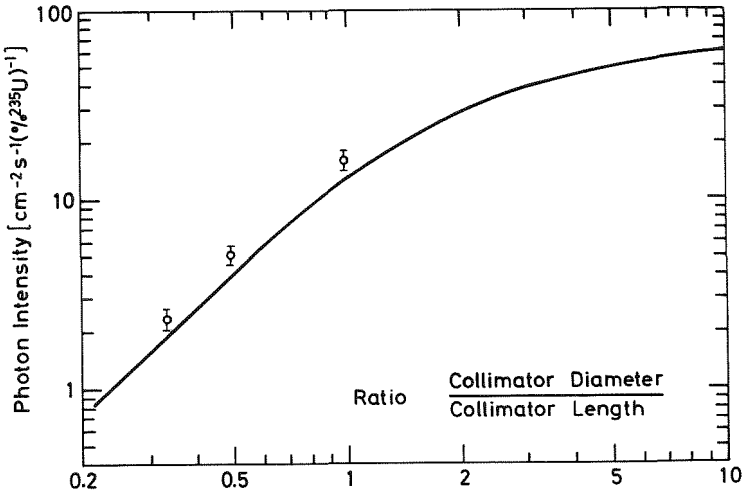

Fig. 1. Calculated 185 keV photon intensity at the collimator exit for different collimator geometries.

for coherent elastic scattering of the γ rays at the inner walls of the collimator. To a lesser extent, also the uncertainties of the nuclear data used, i.e. absorption and scattering cross sections and absolute γ-branching intensities, may contribute to the observed deviation between calculated and measured photon intensities.

6.3 Plutonium Fraction Measurements in Mixed U-Pu Fuel Materials

H. Eberle and H. Ottmar

An accurate determination of the plutonium fraction in mixed U-Pu fuel materials, preferably performed by a fast non-destructive analysis, is equally important both for material control measurements during the fuel fabrication process and for verification purposes in safeguards. In contrast to common non-destructive measurement methods which use isotopic gamma rays, we investigated the benefits of the X-ray fluorescence technique for this particular analysis problem. This method offers the advantage that it does not require any standards nor any *a priori* information about isotopic abundances, as it is the case in the isotopic gamma-ray analyses.

Uranium and plutonium K X rays were efficiently excited from various mixed U-Pu fuel materials using the 122.05 keV gamma rays from an 1 mCi

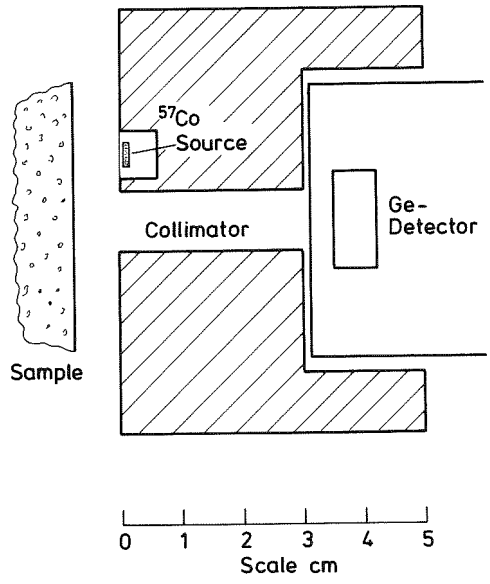

Fig. 1. Geometrical arrangement for the XRF analyses.

^{57}Co source. The geometry of the experimental set-up used for the analyses is shown in fig. 1. The measured fluorescence spectra must be corrected for X rays and gamma rays which arise from the natural decay of uranium and plutonium. Counts taken from the samples with the ^{57}Co source removed were used to correct for this interference.

As an example, fig. 2 displays the relevant spectra obtained from a mixed-oxide fuel pin with a plutonium enrichment of 7.3 %. A small volume Ge detector with an energy resolution of 550 eV at 122 keV was employed for the measurements.

The measured X-ray intensities from the net fluorescence spectrum, together with the necessary nuclear data, can then be taken to evaluate the Pu/U atom ratio from the relation

$$\frac{Pu}{U} = \frac{I_{Pu}}{I_U - \Delta I_{U,Pu}} \frac{(\sigma_K \omega_K f_K)_U}{(\sigma_K \omega_K f_K)_{Pu}} \frac{\varepsilon_U}{\varepsilon_{Pu}}$$

where

I = measured peak intensity of the uranium and plutonium K X rays used for the analysis (U K_{α_1}, U K_{α_2} or U $K_{\beta 1,3}$ and Pu K_{α_1})

$\Delta I_{U,Pu}$ = secondary fluorescence intensity of uranium K X rays induced by plutonium K_β X rays

$\sigma_K \omega_K f_K$ = K-shell photoelectric absorption cross section for the exciting energy (122.05 keV) times the probability ω_K that a K-shell vacancy will result in a K X-ray radiation of branching intensity f_K

ε = overall relative efficiency.

The overall relative efficiency in the energy region of interest was established using the known branching intensities of the uranium K_{α_1}, $K_{\alpha 2}$ and $K_{\beta 1,3}$ X rays. The correction for the enhancement of the uranium X rays induced by secondary fluorescence, $\Delta I_{U,Pu}$, can be calculated from basic nuclear data. The enhancement effect slightly depends on the geometry used, i.e. on the average inclination of the incident excitation radiation and the emitted fluorescence radiation with respect to the sample surface.

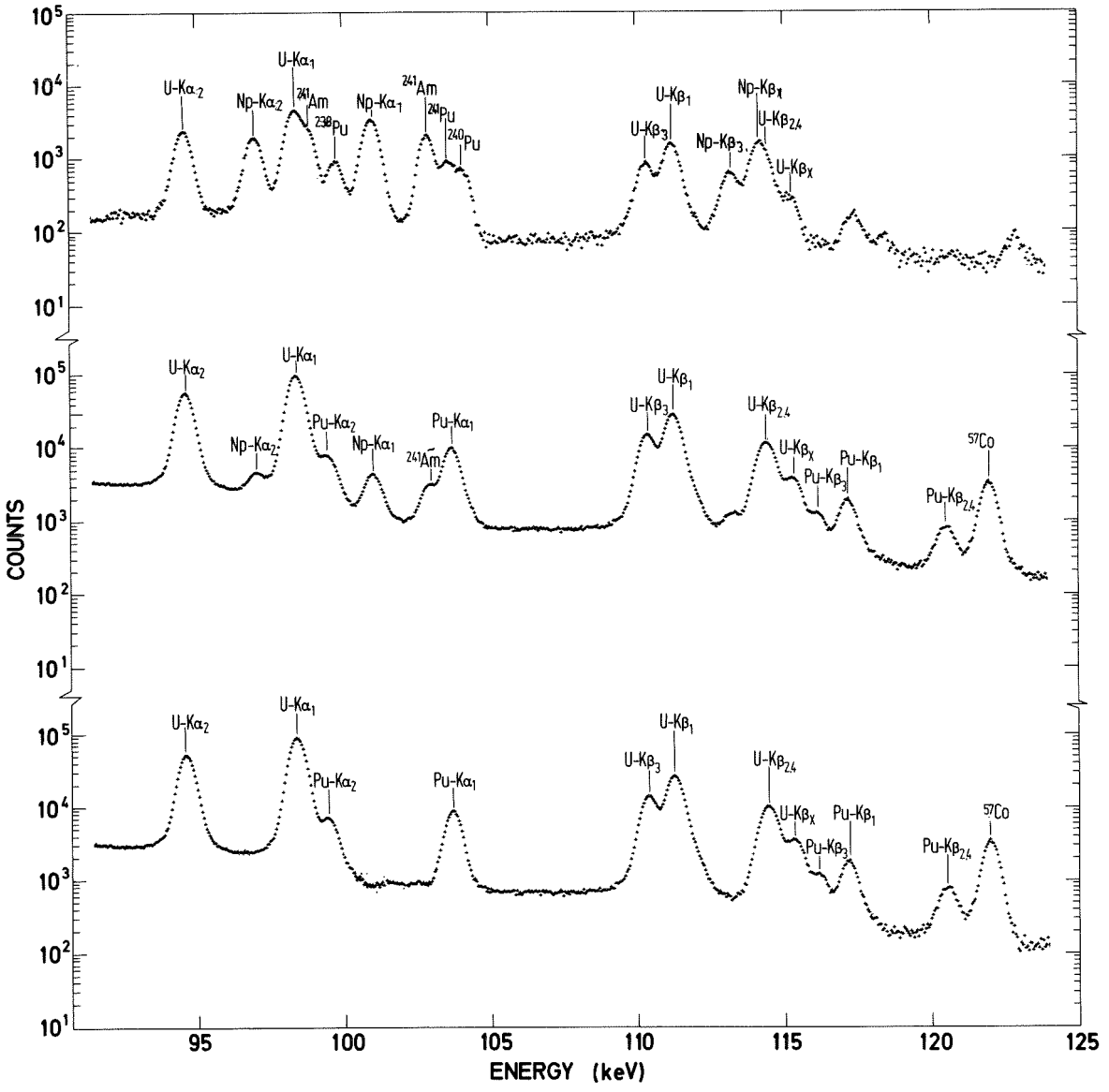

Fig. 2. Gamma spectra in the K X-ray region obtained from a mixed-oxide fuel pin (Pu/U = 0.078). Top to bottom: passive spectrum with ^{57}Co source removed, XRF spectrum superimposed on passive spectrum, net XRF spectrum after subtraction of passive spectrum.

Table 1 summarizes the results from the XRF analyses on various samples. The nuclear data necessary for the evaluation of the experimental results have been directly taken or interpolated from data given in ref. /1/. In the last column the applied percentage corrections for the enhancement effect are given. The liquid sample was nearly transparent for the X rays, thus no secondary fluorescence occured in this sample. Two observations can

Table 1. XRF analysis results for the Pu/U ratio

Sample	Pu/U Book Value	Pu/U XRF Analysis	(XRF-Book)/Book (%)	Enhancement Effect (%)
Rod	0.0239	0.0233	- 2.5	0.27
Rod	0.0251	0.0240	- 4.4	0.29
Platelet	0.0299	0.0284	- 5.0	0.34
Rod	0.0432	0.0418	- 3.2	0.48
Rod	0.0777	0.0737	- 5.1	0.86
Solution	0.315	0.289	- 8.6	0.
Platelet	0.363	0.327	- 9.9	3.5
Platelet	0.366	0.337	- 7.9	3.6
Platelet	0.404	0.384	- 5.0	3.8

be made from the results given in the table: i) there is a systematic bias between book values and XRF analysis results. The major component of this bias we attribute to uncertainties of the nuclear data used for the evaluation, ii) the bias seems to increase with increasing plutonium concentration, being in the order of 4 % for the lower plutonium enrichments and approximately 8 % for the higher plutonium enrichments. To resolve the discrepancies and to further study and evaluate the technique, additional measurements on samples better characterized than those used in the present investigations are in progress.

References

/1/ E. Storm, H. Israel, Nucl. Data Tables 7, No. 6 (1970).

6.4 Heavy Element Concentration Measurements Using Gamma-Ray Densitometry

P. Matussek, I. Michel-Piper, and H. Ottmar

Work has been started to evaluate non-destructive measurement techniques which allow to determine accurately the concentration of heavy elements like uranium and plutonium in solutions. Gamma-ray transmission measurements which make use of the total absorption cross section discontinuity at either the L- or K-absorption edge of these elements appear to be one of the most advantageous methods for this purpose /1,2/.

Consider the ratio of transmissions, $R = T(E_1)/T(E_2)$, of two gamma rays with energies E_1 and E_2 through a heavy element-bearing solution. This ratio is given by

$$R = \exp\ (-\Delta\mu_H\ \rho_H D)\ \exp\ (-\ \Delta\mu_M\ \rho_M D), \qquad (1)$$

where $\Delta\mu_H$, $\Delta\mu_M$ and ρ_H, ρ_M denote the differences between the mass attenuation coefficients at the transmission energies, E_1 and E_2, and the densities of the heavy element and the matrix material, respectively, and D the sample thickness. If the energies of the two transmission gamma rays closely bracket the absorption edge, then for low Z matrix materials like H_2O or HNO_3 the quantity $\Delta\mu_M$ becomes reasonably small, which, in turn, results in nearly constant values close to unity for the matrix dependent exponential term in (1). Hence, for a given sample thickness D, the transmission ratio R is almost uniquely determined by the change of the mass attenuation coef-

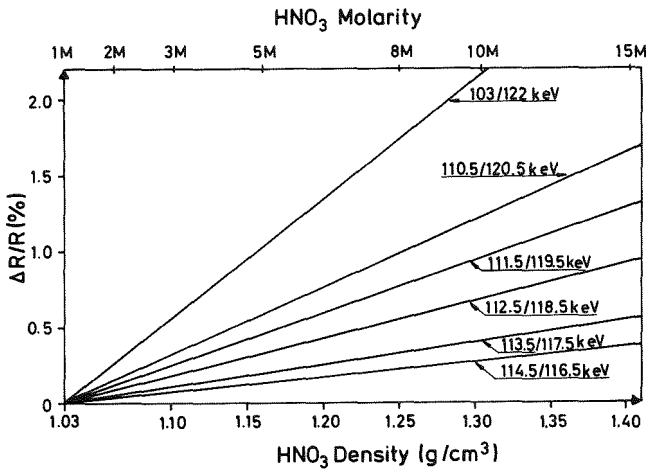

Fig. 1. Percentage change of the ratio of transmissions on either side of the uranium K-absorption edge (E_K = 115.6 keV) vs matrix density for different pairs of gamma-ray energies transmitted through an uranium nitrate solution.

ficient across the absorption edge, $\Delta\mu_H$, and the density ρ_H of the heavy element, respectively.

Fig. 1 illustrates the situation for the practical example of transmission measurements through an uranium nitrate solution using gamma rays on either side of the uranium K-absorption edge at E_K = 115.6 keV. The figure demonstrates the insensitivity of the ratio of transmissions to variations in the matrix density when transmission energies near the absorption edge are used. For example, a variation of 30 % in the matrix density corresponding to a change from 1 $MHNO_3$ to 10 $MHNO_3$ will change the transmission ratio of two gamma rays closely bracketing the absorption edge (114.5 keV and 116.5 keV) by only 0.25 %. In contrast, the uranium concentration determination will be noticeably affected by varying matrix densities in transmission measurements using the previously employed 103 and 122 keV gamma rays from the radioactive sources ^{153}Gd and ^{57}Co, respectively /3/.

To minimize the matrix effects, gamma-ray beams with a continuous energy distribution have been produced for transmission measurements at the K-absorption edges of uranium and plutonium. Fig. 2 shows a gamma-ray beam obtained from an X-ray generator. With this type of photon source relatively broad

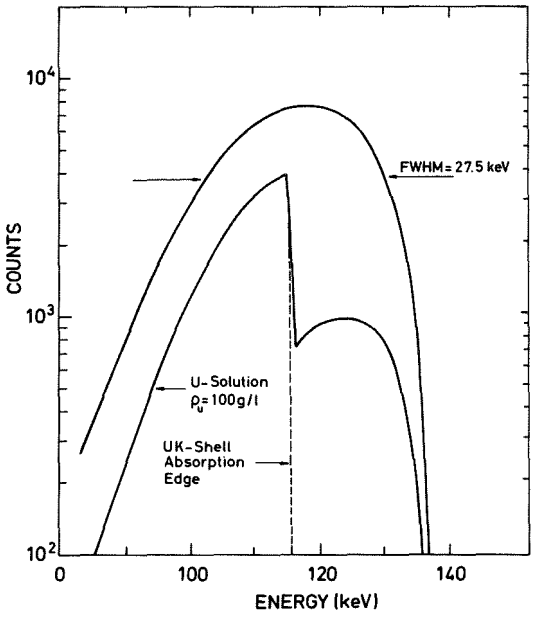

Fig. 2. Filtered X-ray beam from an X-ray generator before and after the transmission through a 5 cm thick uranium solution.

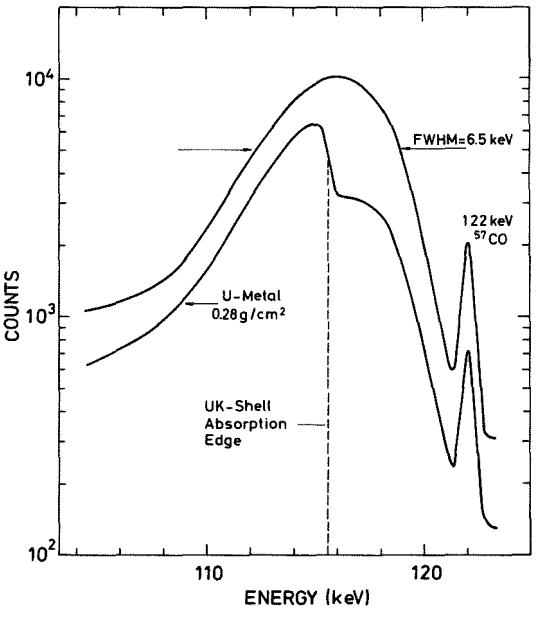

Fig. 3. Gamma-ray beam obtained from Compton scattering of the ^{57}Co, 122.1 keV, gamma rays before and after the transmission through an uranium metal foil.

gamma-ray energy distributions with an intensity maximum centered around the K-absorption edge energies can be obtained by appropriately filtering the X-ray beam. A half width of approximately 28 keV was achieved for the X-ray beam shown in fig. 1 by setting the high voltage at the generator at 140 kV and filtering the X-ray spectrum through 7 mm of copper and 2 mm of cadmium.

Compton scattering is an alternate method to produce a continuous gamma-ray beam. Fig. 2 shows a gamma-ray beam centered around the K-absorption edge of uranium as obtained from the inelastic scattering of the ^{57}Co, 122 keV, gamma rays on a low Z material. A relatively small half width can be achieved for the scattered beam, depending on the collimation geometry.

The most simple analysis procedure for the evaluation of the heavy element concentration from the measured transmission spectra is to determine the transmission ratio from counts in energy windows set on either side of the absorption edge. Another approach which better utilizes all the data offered by a continuous gamma beam consists of fitting the intensity ratios 'R(E)' of the transmitted and the original gamma beam as a function of the gamma energy E above or below the absorption to the expression

$$\ln R(E) = A_H E^{-m_H} + A_M E^{-m_M} ,$$

which uses the relation $\mu(E) = aE^{-m}$ for the mass attenuation coefficient. The parameters A_H and A_M determined from the fit are proportional to the heavy element and matrix material density, respectively, while the exponents m_H and m_M describing the energy dependence of the corresponding mass attenuation coefficients are assumed constant over the limited energy range of the gamma beam. The slopes m_H and m_M which are required as input data for the experimental fits are currently determined in the energy regions of interest both for uranium and plutonium , and for some typical matrix materials.

References

/1/ T.R. Canada, J.L. Parker, T.D. Reilly, Report LA-6040-PR (1975) p. 9.

/2/ T.R. Canada, W.B. Tippens, T.D. Reilly, J.L. Parker, Report LA-6675-PR (1976) p. 21.

/3/ O. Cristallini, E. Gantner, A. von Baeckmann, Report KFK 1703 (1972).

6.5 Assay of Plutonium in Process Wastes from Fuel Fabrication Plants*

M.R. Iyer+ and H. Ottmar

A gamma-spectrometric method for the assay of fissile plutonium in process wastes from fuel fabrication plants which are not mixed with fission products has been standardized. The method uses a multigroup analysis of gamma spectra measured with a NaI detector from waste samples. The attenuation in matrix materials is corrected by making transmission measurements using an external plutonium source. The method also provides an internal check on the presence of plutonium bearing materials with significant self-absorption. The results are compared with those obtained using higher resolution spectrometry with a Ge(Li) detector.

* Report KFK 2321 (1976).

+ Bhabha Atomic Research Centre, Bombay, India

6.6 An Assay System for Plutonium Contaminated Solid Wastes

M.R. Iyer+, P. Matussek, H. Ottmar, and S.J. Choithramani+

A plutonium waste monitor was installed at BARC, Bombay, India under the Indo German Collaboration Programme in March 1977. The work on the standardization of the measurement method was initiated in 1976 as a joint programme with participation from BARC. The method as developed has been published previously /1/ (see preceding contribution 6.5.). This is a passive gamma-spectrometric method for the assay of fissile plutonium in process wastes from fuel fabrication plants which are not mixed with fission products. It employs a multigroup analysis of gamma spectra measured with a NaI detector from waste samples. The procedure consists of setting up simultaneous equations using the counts in 3 energy groups after correction for Compton contribution from higher energies and solving for the ^{239}Pu and ^{241}Pu contents. The method can also check for the possibility of the presence of plutonium bearing materials with self-absorption.

The waste monitor now set up jointly by BARC and GfK employs in its present state a simpler procedure involving simple data reduction to give a display of the ^{239}Pu and ^{241}Pu content in standard waste containers. Counts from an energy window set on the 208 keV gamma line from ^{237}U can be taken to be proportional to the ^{241}Pu content, whereas the measurement of the ^{239}Pu content uses gamma rays from the energy interval 370 to 470 keV. Both peak count rates are corrected for Compton background by using adjacent background windows.

The block diagram of the set-up is shown in fig. 1. It basically consists of a 5" x 2" thick NaI detector coupled to a multichannel analyzer. A digital stabilizer compensates for signal gain variations by stabilizing on a reference peak. For this purpose we first tried to use the reference peak produced by a light-emitting diode in front of the photomultiplier, but we found the stability of this type of reference peak to be unsatisfactory. Therefore, we now use for stabilization the gamma line from a low-energy external gamma source (^{241}Am or ^{57}Co). Address pulses from the ADC of the multichannel analyzer pass on to a quad digital single channel analyzer which produces logic signal outputs whenever the ADC address falls within the selected window limits. These window limits for the four channels are digitally set by 3-digit thumbwheels. The output count rates c_1, c_2, c_3 and c_4 from the digital windows are given to a dual multiplying up-down scaler on which the multipliers can be set. The unit can carry out the operations

$$A\,c_1 - B\,c_2 \quad \text{and}$$
$$C\,c_3 - D\,c_4$$

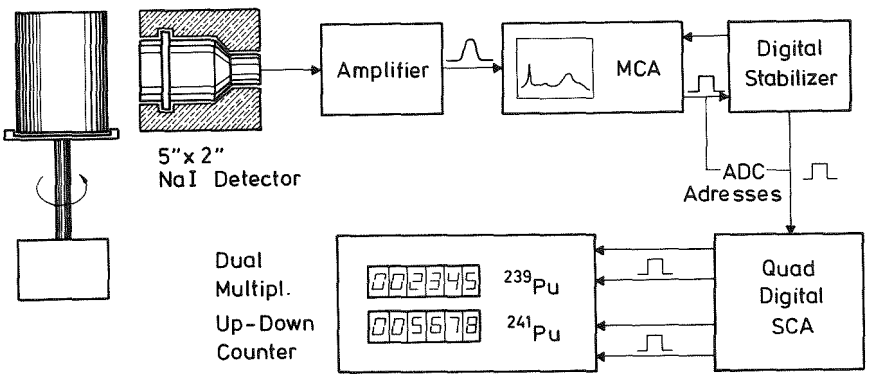

Fig. 1. Block diagram of the plutonium waste monitor .

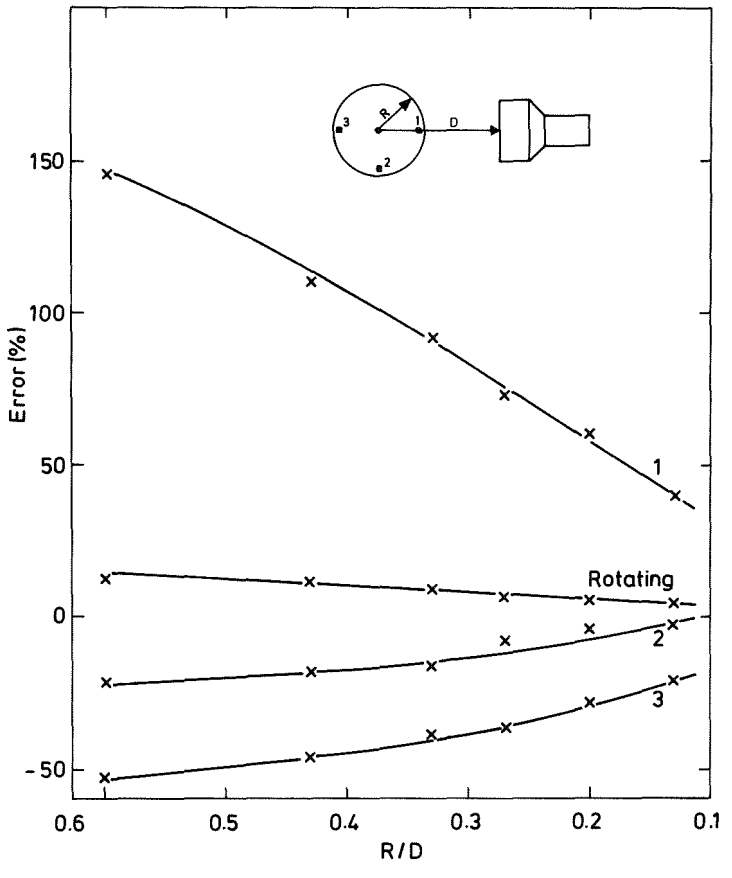

Fig. 2. Variation of count rates relative to centre position as a function of R/D for different peripheral sample locations in a non-rotating and rotating sample container.

and displays the ^{239}Pu and ^{241}Pu content on two numeric LED diplays. For calibration purposes also the individual count rates c_i can be displayed. The calibration constants A, B, C and D are obtained by using a set of six standards and adopting a linear regression method. The standards consist of several small sealed polyethylene packets containing known amounts of plutonium dispersed in representative matrix materials in standard waste containers (15 cm dia. and 21 cm height). The plutonium contents can be estimated within 5 to 10 % in the system with a sensitivity of 10-20 mg for ^{239}Pu and $\sim$0.1 mg for ^{241}Pu for a detector distance of 20 cm.

The effect of inhomogeneity of the sample material in the container was studied by locating a sealed packet of plutonium (0.5 g) at different locations in the container. The variation of the estimated Pu content for different locations of the material in the container relative to the response

from a centre position, as a function of R/D,is shown in fig. 2. By rotating the sample, the error is reduced considerably as can be seen from the figure. For example, we find that an error of about 90 % is brought down to 10 % for R/D = 0.33.

Work is in progress for the study of matrix absorption effects and their corrections by means of transmission measurements with an external plutonium source. The final version of the system will include a microprocessor performing the more elaborate data evaluation as suggested previously /1/.

+ Bhabha Atomic Research Centre, Bombay, India

References

/1/ M.R. Iyer, H. Ottmar, Report KFK 2321 (1976).

6.7 Measurements with the Sledlike Bottom Device MANKA 01 (Manganese Nodules Analysis System) Before and During the Deep Sea Test

H. Eberle

During the preparation for a deep sea test of the sledlike bottom device MANKA, extensive measurements were performed with the analysis system which was designed for in-situ elemental analysis of manganese nodules using neutron capture gamma-ray spectrometry. Part of the activities concentrated on the calibration of the analysing system so as to obtain immediately the results from the manganese nodules analyses in the in-situ test. For calibration purposes solutions of well-known chemical compositions were used and both (n,γ) spectra and neutron flux profiles as well as gamma transmission spectra were measured. The method of these measurements has been described in detail in ref. /1/. The basic calibration data required for the manganese nodules analyses could be determined from these experiments and were implemented into an automatic data evaluation program.

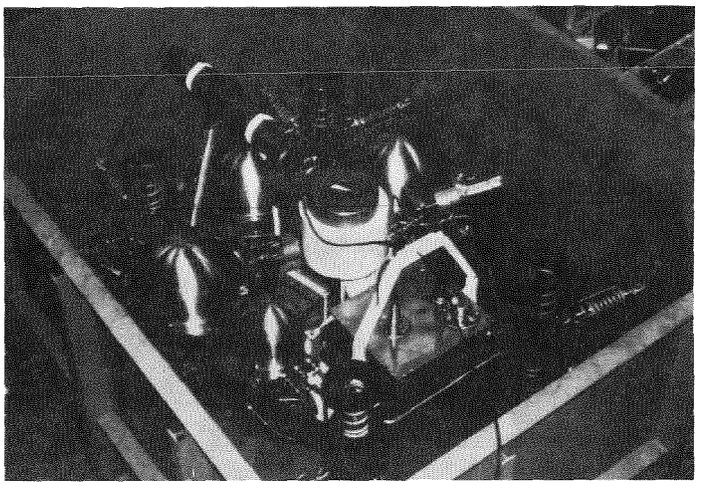

Fig. 1. The analysing system placed in a basin for test measurements in salt-water.

Upon the completion of the calibration measurements, test measurements under realistic conditions have been carried out with the complete system. For this purpose the system was installed in a basin which was subsequently filled with salt-water (fig. 1). The analysis results obtained from numerous measurements on mixtures of manganese nodules with salt water as well as on pure salt-water were satisfactory. The performance of the system also did not deteriorate during dynamic tests /2/ in which the analysing system in the salt-water basin was pulled over a jolting section on a flat-bed trailer. After all system components had operated without faults over a longer period of time, the whole equipment was shipped to Honolulu, Hawaii, in November 1977 for the deep sea test in the Pacific.

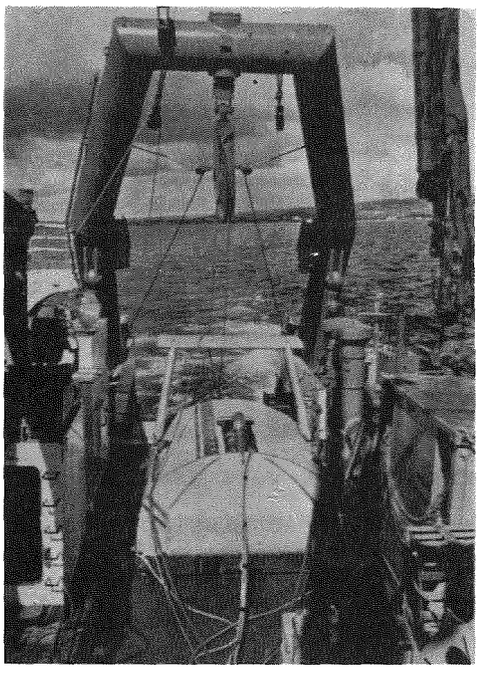

Fig. 2. MANKA aboard the RS 'Valdivia' prior to operation.

After the arrival in Honolulu all system components were examined again ashore for transport damage before they were installed on the research ship 'Valdivia' for use during the research expedition VA 14/8. Outside the 12 miles zone at 21.5°N and 157.5°W test measurements were performed in the open sea. Neutron capture gamma-ray spectra from sea-water were measured while the analysis system was towled at a depth of 25 m below sea-level. Fig. 2 shows MANKA aboard the RS 'Valdivia' prior to operation and fig. 3 shows a measured (n,γ) spectrum

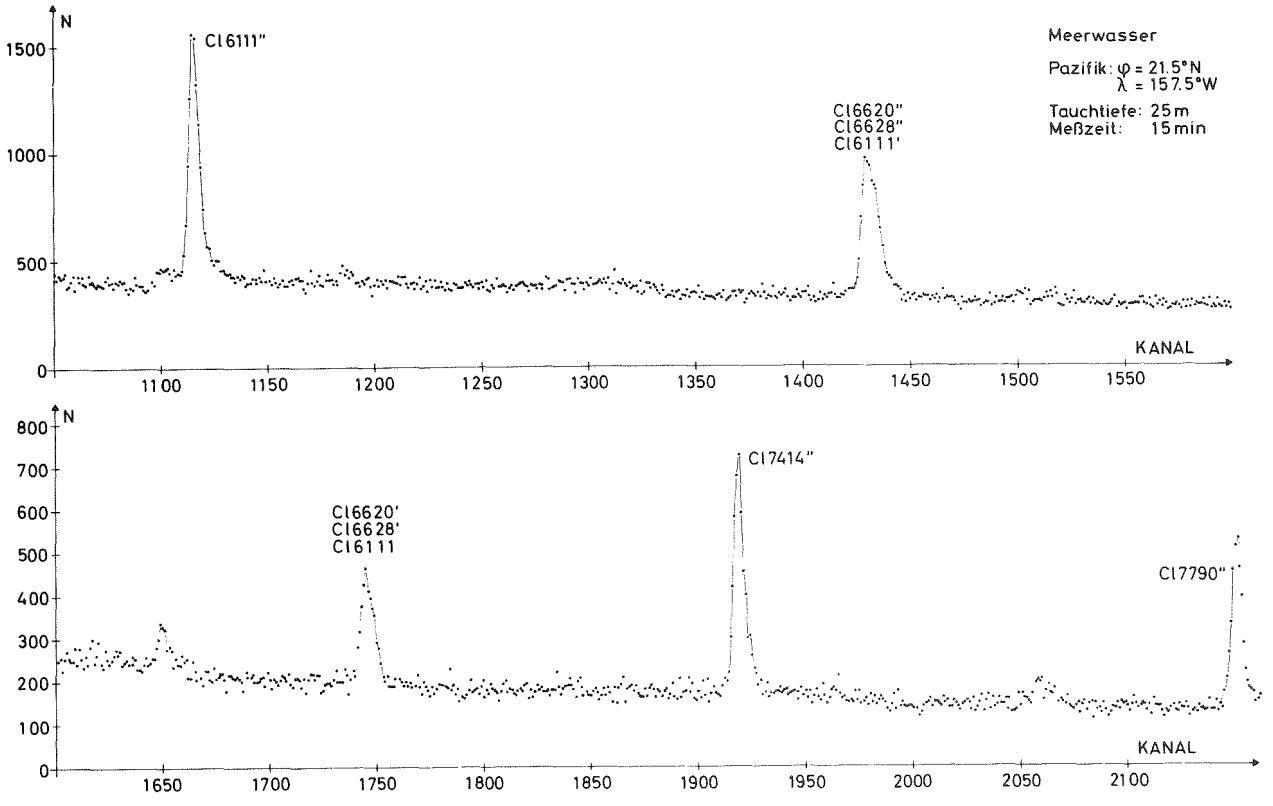

Fig. 3. Part of a (n,γ) spectrum from sea-water measured with MANKA in the Pacific at 21.5°N and 157.5°W at a water depth of 25 m (measuring time 15 min).

from sea-water.

When all test measurements had been successfully completed, the passage started to the deep sea test region situated southeast of Hawaii. There the sledlike bottom device was used again on December 27, 1976. While the sledlike bottom device was lowered, sea-water spectra were measured. The measurements started when 2000 m of the towing cable had been reeled off.

Because of a computer defect recognized before, which could not be repaired on board, only the storage of the raw data on magnetic tape but no final data evaluation was possible on the spot. When more than 5000 m of the towing cable had been reeled off and the analysis system had reached a position of approximately 3700 m below sea-level, a short-cirucit occurred in the cable, probably near the analysis system or within the system. Since no more data could be transmitted from the probe, it was decided to lift the probe on board. Immediately before taking the analysis system on board,

the towing cable tore off and the system got lost. More details and results may be found in the report entitled 'Manganese Nodules Analysis System-MANKA (Final Report)' which is presently being prepared.

References

/1/ H. Würz, H. Eberle, Report KFK 2160 (1975).

/2/ J. Lange, U. Tamm, Report KFK 2224 (1977).

7. TECHNICAL DEVELOPMENTS

7.1 CYCLOTRON

7.1.1 Operation Summary of the Karlsruhe Isochronous Cyclotron

F. Schulz and H. Schweickert

During the period of report the machine was in full operation (see table 1). The cyclotron beam was used for irradiations for 7660 hours, which amounts to 89.3 % of the total shift time. The available beam time increased by 409 hours as compared to the last year /1/. For approximately 17 % of the experimental time the axial injection system was used to study nuclear reactions with polarized 52 MeV deuterons (562 h) and 156 MeV $^{6}Li^{3+}$ ions (436 h).

Table 1. Operation of the cyclotron from July 76 to June 77

Cyclotron operational	with internal ion sources		with external ion sources		total	
for experiments	6112 h	86.4 %	1008 h	67.2 %	7120 h	83.0 %
for beam developments and testing new components	418 h	5.9 %	122 h	8.1 %	540 h	6.3 %
time of operation	6530 h	92.3 %	1130 h	75.3 %	7660 h	89.3 %
scheduled shut-down for maintenance, repair and installations	201 h	2.8 %	65 h	4.3 %	266 h	3.1 %
unscheduled shut-down	345 h	4.9 %	305 h	20.4 %	650 h	7.6 %
total shift time	7076 h	100 %	1500 h	100 %	8576 h	100 %

During typical beam time periods of five days a stable polarized deuteron beam has been achieved giving target currents of 30 nA in the large scattering chamber.

Again a considerable improvement could be achieved in the available $^{6}Li^{3+}$-beam intensity. The external Penning ion source delivers now up to 5 μA of $^{6}Li^{3+}$ into the external injection line.

The actual available intensities in the large scattering chamber are listed together with the numbers of the preceding years in table 2.

Table 2. $^{6}Li^{3+}$ intensities from 1975 to 1977

Year	Max. beam current (electrical) in scattering chamber	total charge for the experiments	experimental time
1975	1 nA	50 μCb	272 h
1976	15 nA	1.2 mCb	378 h
1977	80 nA	3.8 mCb	225 h

On the user's side (table 3) 43 % of our machine time is given to visitors from laboratories outside the Nuclear Research Center Karlsruhe. Our aims are in fact to accomodate every experiment for which the facilities of this laboratory are particularly appropriate, independent of questions of institutional affiliation. The use of the cyclotron for application oriented research projects amount to about 45 % of the total time available for experiments.

Table 3. User statistics for 1976

GfK - Karlsruhe users

Institut für Angewandte Kernphysik	2426 h	34,1 %
Labor für Isotopentechnik	498 h	7,0 %
Institut für Radiochemie	474 h	6,7 %
Institut für Experimentelle Kernphysik	458 h	6,4 %
Projekt Schneller Brüter	170 h	2,4 %
Institut für Heiße Chemie	8 h	0,1 %
Institut für Material- und Festkörperf.	6 h	0,1 %
	4040 h	56,8 %

External users

Max-Planck-Inst. für Kernphysik Heidelberg	575 h	8,1 %
Freie Universität Berlin	570 h	8,0 %
Technische Universität München	447 h	6,3 %
Universität Erlangen	291 h	4,1 %
Universität Saarbrücken	264 h	3,7 %
Kernforschungsanlage Jülich	166 h	2,3 %
Universität Hamburg	151 h	2,1 %
Universität Mainz	111 h	1,6 %
Deutsches Krebsforschungszentrum Heidelberg	110 h	1,5 %
Universität Konstanz	97 h	1,4 %
Universität Clermont	81 h	1,1 %
Universität Heidelberg	72 h	1,0 %
Nuklear-Med. Klinik München	64 h	0,9 %
Universität Ulm	32 h	0,5 %
Universität Gießen	17 h	0,2 %
Universität Bonn	16 h	0,2 %
Universität Stuttgart	11 h	0,1 %
Centre de Recherches Nucléaires Strasbourg	5 h	0,1 %
	3080 h	43,2 %
Grand total	7120 h	100 %
Nuclear reactions	2080 h	29,2 %
Solid State physics	1411 h	19,8 %
Nuclear spectroscopy	922 h	13,0 %
Nuclear medicine	693 h	9,7 %
Neutron physics	667 h	9,4 %
Engineering	548 h	7,7 %
Materials research	506 h	7,1 %
Nuclear chemistry	207 h	2,9 %
Astrophysics	86 h	1,2 %
	7120 h	100 %

References

/1/ F. Schulz, H. Schweickert, Report KFK 2298 (1976), p. 1.

7.1.2 Present Status of the New Correction Coils

V. Bechtold, L. Friedrich, and L. Wiss

After the decision in 1975 to build a new set of trim coils for the cyclotron, numerical calculations were done to investigate whether a suitable new configuration of trim coils is able to accelerate $^{3}He^{2+}$ and

H^+ ions in addition to the e/m = 1/2 particles. According to these calculations a prototype coil is now under construction /1/.

Currents up to 50 A for each coil are necessary to get the calculated field corrections. These high currents are producing a power density of 1 W/cm^2. To transport this power loss quickly to the cooling plates, a good thermal conductivity is necessary. The thermal conductivity depends on the distance and the medium between windings and cooling plate.

The power dissipated in the coil windings is transported through a thin insulation layer on the copper band, a thin glass silk (0.1 mm) instead of Kaptonfoil and a thin layer of epoxy resin with quartz to a copper plate on each side of the coil. These plates are cooled by water. Fig. 1 shows a top view of the prototype trim coil without the upper cooling plate.

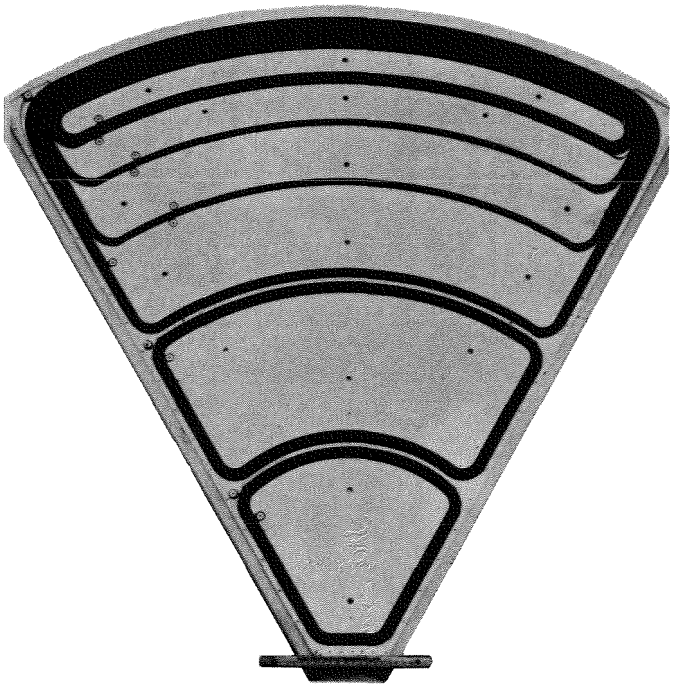

Fig. 1. Top view of the prototype coil with layout of the coil windings. The coil conductor for the six coils is a copper band wound tightly around aluminium forms. The overall thickness of the trim coil plate is 13.3 mm.

The distance between the windings and cooling plate is minimized by pressing the whole winding of the coils. The trim coil set is then completely filled with epoxy resin and the cooling plates are pasted on each side. This leads on one hand to a good mechanical stability of the coil, on the other hand to an improvement of the thermal conductivity between windings and plates by appropriate selection of the epoxy resin.

We tried two epoxy resins from Ciba[+), namely Araldit F and Araldit F doted with quarz powder. The measured thermal conductivity for both epoxy resins is

$$\lambda = 0.58 \cdot 10^{-3} \frac{\text{cal}}{\text{cm sec } ^{\circ}\text{C}} \quad \text{for Araldit F}$$

$$\lambda = 1.75 \cdot 10^{-3} \frac{\text{cal}}{\text{cm sec } ^{\circ}\text{C}} \quad \text{for Araldit F doted with quartz powder}$$

The thermal conductivity λ for the doted resin is a factor of 3 higher than for the resin without quartz. The processing of the epoxy resin at 70°C was done in vacuum to ensure a proper outgassing. The hardening was made at 90°C while simultaneously pressing the whole trim coil set. This is done in vacuum, too. The arrangement for this procedure is shown in fig. 2.

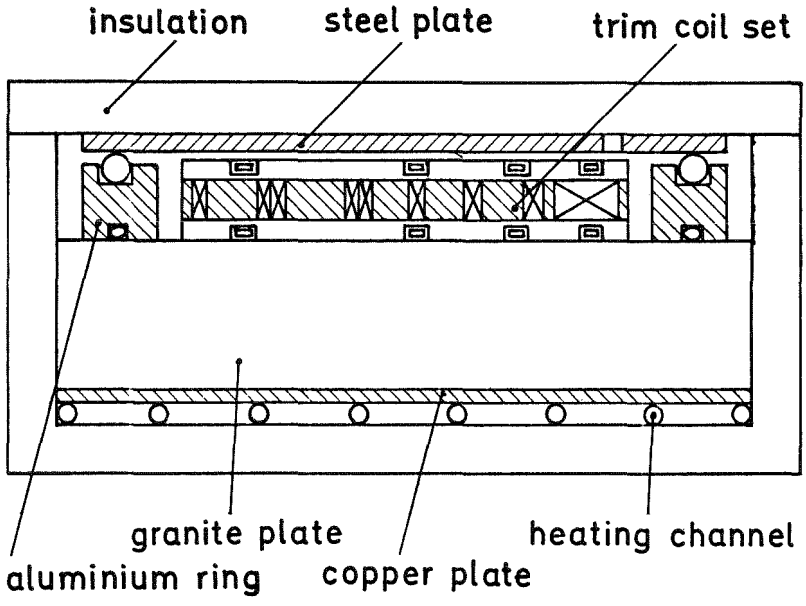

Fig. 2. The arrangement for pressing and outgassing the whole trim coil set during the hardening time of the epoxy resin by means of vacuum. The whole set-up can be heated to 90° C.

The basis is a granite plate (150 x 150 x 20 cm) which can be heated up to 100°C by means of heating channels at the bottom. The surface of the granite plate is manufactured with an accuracy of 1-5 µ and a parallelism of 1/10 mm. This surface quality will not change while heating up the plate to 100°C. A vacuum chamber is built up with an aluminium ring on the surface

+) Ciba Geigy, Wehr/Baden

of the plate. A steel plate will close this chamber. The whole trim coil set will be inserted into this chamber and can be heated. By properly dimensioning the height of the aluminium ring it is possible to press the trim coil set between the steel plate and the granit plate by evacuating the chamber. In this way the trim coil set is fixed during the hardening time of the epoxy resin.

At the end of 1977 a prototype of the trim coil will be ready for the test bench. If all experimental investigations and tests are satisfying, the new trim coils will be available at the end of 1978.

References

/1/ H.J. Gils, D. Heck, Report KFK 2379 (1976) p. 101.

7.1.3 New Results of the Computer Aided Cyclotron Operation

H. Heinzmann+, W. Kappel, J. Möllenbeck, W. Kneis, and H. Schweickert

The computer controlled diagnostic and data logging system /1,2/ has proved to be very suited for routine operation of the cyclotron. In the meantime the system has been increased enormously by adding a variety of new diagnostic programs. Besides the development of new programs reorganization, the improvement and modification of old programs took a great part of the work performed.

Time-of-flight measurements:

All programs using time-of-flight measurements like phase-width measurements, quality tests of the pulsing system and the measurement of the absolute energy have been improved considerably by including an electronic test into the measuring procedure. This always ensures information about reliability and state of the measuring hardware (fig. 1).

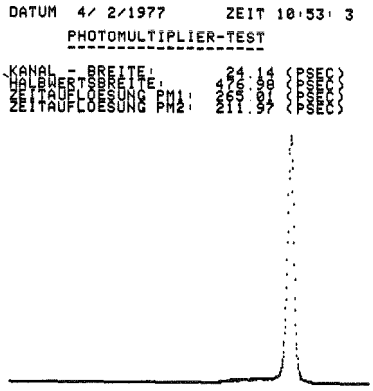

Fig. 1. Photomultiplier and electronic test for internal phase width showing that photomultiplier PM2 has a slightly better time resolution than PM1.

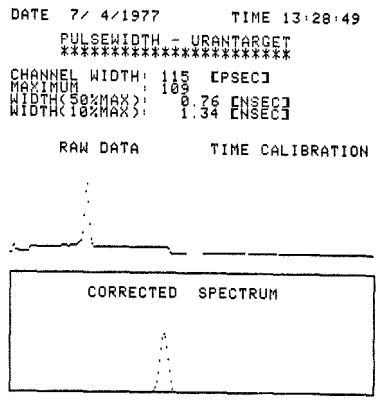

Fig. 2. Typical results of a phase width measurement on the uranium target with the 26 MeV proton beam.

Concerning the experiment with the neutron time-of-flight spectrometer it has been desirable to use the computer not only in the adjustment phase but also during the measuring period. For this a modified program now measures the phase width on the uranium target which is also used by the experiment (fig. 2). The program allows to survey the phase width to be within a limit of 5 % and to call for attention if the phase width is out of limits.

Status programs:

Since the status programs, status injection, cyclotron, external beam etc. and the monitor program all use the same measuring procedure, they were reorganized to use a common data base. Especially the file handling for loading and saving user data records has been completely rewritten. Now it is possible to have no boundaries in the number of users and in the number of data records a user can allocate to save his machine adjustments.

Furthermore, first results of Fortran tests are present. Fortran is interesting because programs are faster than in Basic especially if much computation is involved. The Fortran test has been performed with the program status cyclotron. The result is that in Fortran 15 parameters can be scanned in about 1.5 sec. In Basic this procedure takes 4 sec.

Control of correction coils:

The ajdusting of the currents for the correction coils /1/ has now been subdivided into three parts. The test program 'trimcoil test' enables to perform rapid and reliable tests of the power supplies and the output modules. The 'moduletest' mode checks each bit of the output modules and prints a detailed diagnostic if errors occur. The mode 'power supply test' checks if the power supplies follow the different adjustments issued by the output modules. A linearity test is made and a detailed record of the test for all power supplies is printed. The program 'adjustment of the correction coils' has been described in detail earlier /1/. It contains the possibility to adjust and monitor the isocronism correction, the amplitude and the angle of the first harmonic for the five radii. The 'status magnetic fields' has similar capabilities like the other status programs. It contains scanning of the actual correction coil settings as well as loading and saving these settings onto disk (fig. 3). The file handling for user data records is the same too with nearly unlimited number of users and number of data records for each user. In contrary to the normal status programs the loading of a user data record contains the adjustment of the actual currents to the loaded nominal values.

DATUM 8/ 7/1977 ZEIT 10:56:34

STATUS - MAGNETFELD

SAVED :JOD : 1 - 8/ 7/1977

	SOLL	IST
FREQUENZ	= 33.256	33.255
MAGNETFELD	= 9.013	9.013
NMR MAGNETFELD	= ******	******

SPULE	MODULANZEIGE SOLL	IST	STROM SOLL	IST
1	465	465	2.311	2.310
2	399	399	2.016	2.010
3	454	454	2.298	2.295
4	257	257	1.312	1.309
5	399	399	2.005	1.999
6	- 254	- 254	- 1.220	- 1.222
7	438	438	2.168	2.165
8	270	270	1.368	1.367
9	441	441	2.199	2.197
10	412	412	2.012	2.011
11	- 448	- 448	- 2.245	- 2.246
12	146	146	0.720	0.718
13	363	363	1.820	1.819
14	232	232	1.130	1.129
15	- 138	- 138	- 0.695	- 0.694
16	0	0	*******	*******
17	0	0	*******	*******
18	0	0	*******	*******

Fig. 3. Display picture of the program 'status magnetic field'. The actual values of the correction coil currents are saved to the record no. 1, from 8-7-77 of the user JOD.

+ Fachhochschule Karlsruhe

References

/1/ H.J. Gils, D. Heck, Report KFK 2379 (1976) p. 96.

/2/ F. Schulz, H. Schweickert, Report KFK 2298 (1976) p. 9.

7.1.4 A Time-of-Flight Device for Ultra-High Resolution Transmission Measurements

G. Schmalz, D. Erbe, G. Haushahn, K. Heidenreich, and F. Schulz

For the study of energy sharp T = 3/2 resonances in light T_z = 1/2 nuclei it was of interest to further improve the energy resolution of the Karlsruhe fast neutron time-of-flight spectrometer. Typical values for the widths of the lowest T = 3/2 resonances are of the order of 3-10 keV, which have to be resolved at laboratory energies E_n of about 10 MeV (compare also section 1.1.2 and 1.1.3 of this report). Thus an energy resolution of better than 4×10^{-4} was required for that energy range.

This high energy resolution could be achieved by optimizing the phase conditions of the accelerated beam in the centre of the cyclotron, and by using a neutron detector with a largely improved time characteristic.

To adjust the internal phase, a slit diaphragm was inserted in the south-east-valley position of the cyclotron. A slit width of 0.3 mm was used to select a small region of the totally accepted phase width. Further restriction of the accepted phase was provided by application of an additional radial beamstop used in the 3:1 beam reduction system. The new system was recently used in an experimental run for ultra-high resolution transmision measurements on ^{16}O and ^{12}C. During a four-week period the internal phase width (fig. 1) was continuously measured by the new computer-controlled beam diagnostic system.

Despite the severe masking of the internal beam, a large average beam intensity of 10 μA at a pulse repetition rate of 50 kc/s was obtained. Under final beam deflection condition for the spectrometer this value compared favourably with the previously achieved 20 μA at 100 kc/s. The internal phase width was proven to be smaller than 0.8 nsec, though the simultaneous deflection of about 40 microstructure pulses extending over a radial range of ∿5 cm contributed to this value.

This together with the time resolution of 0.5 nsec of the detector resulted in a total time uncertainty of the spectrometer which was definitely better than 1 nsec.

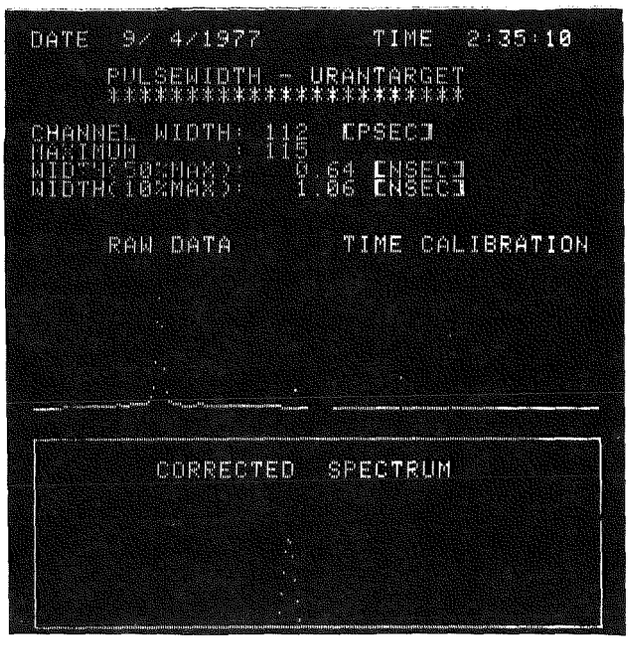

Fig. 1. TV-screen of the diagnostic computer after the measurement of the internal phase width on the uranium target.

7.1.5 Routine Production of ^{123}J at the Karlsruhe Isochronous Cyclotron

K.H. Assmus, K. Jäger, F. Michel[+], H. Münzel[+], R. Schütz, F. Schulz, and H. Schweickert

The production method for iodine-123, described in the Annual Report 1975 /1/, has been used routinely to prepare amounts of ^{123}J in excess of several 100 mCi per 2-5 hr run on a weekly basis for trials at selected hospitals in the southern part of Germany. A total of more than 1500 patients have been treated with ^{123}J produced in 35 separate runs. The essentials of irradiation parameters are shown in table 1. Our arrangement /1/ worked reasonably well as can be seen in a summary of production figures given in fig. 1.

Reaction:	$^{124}Te(p,2n)^{123}J$
	$E_p = 26$ MeV
Target:	96.5 % ^{124}Te
	Molten TeO_2 in platinum backing
	$\varnothing_t$ = 6mm; 150 mg/cm^2 → 5 MeV
Extraction:	dry destillation at 820 °C
Yields:	8-12 mCi/μAh a.c.s.
Impurity:	≤ 1,1 % ^{124}J a.c.s.
Production rate:	once in a week
	actual: 300-500 mCi/batch
	possible: 1000 mCi
Price:	actual: 12,50DM/mCi

Table 1. Production parameters for ^{123}J at Karlsruhe. The yields and the ^{124}J impurity are given after the chemical separation (a.c.s.). The calculation of costs includes machine time (740 DM/hour) and the manpower for the production process and further developments.

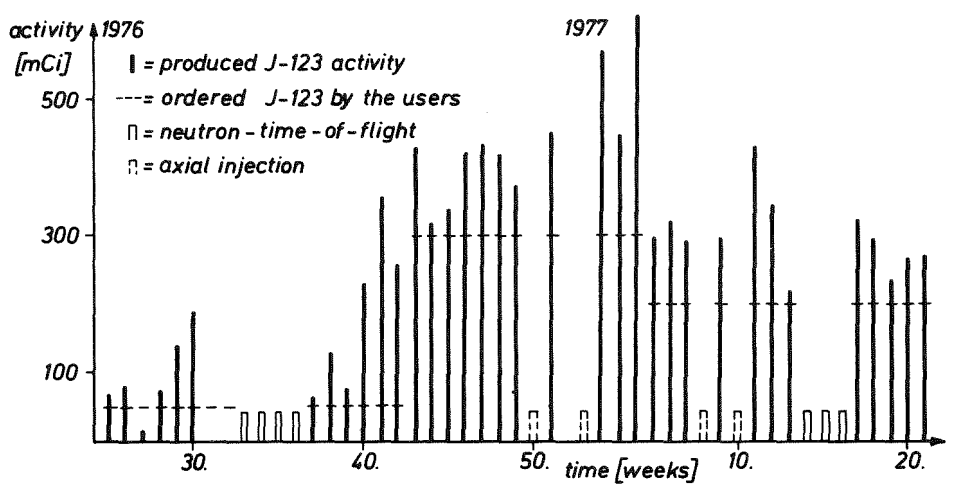

Fig. 1. Production figures of ^{123}J at Karlsruhe. At the moment a production is not possible when the cyclotron is modified for axial injection or for the neutron time-of-flight spectrometer.

Only in the following three cases in the middle of 1976 the produced quantities of ^{123}J have been smaller than the orders from the users:

(1) A simple operating error during the dry destillation process inside the glove box.

(2,3) The emission of ^{131}J for the whole research center is limited to 20 mCi/year and hence we got some problems with our health physics department. A special iodine filter (KJ-impregnated activated carbon SA 1565) was installed in the exhaust system of the glove box.

Now a weight factor of 5000 relative to ^{131}J has been calculated for ^{123}J. It is remarkable that during one and a half year production period not a single unscheduled shutdown of the cyclotron has occurred.

The radionuclide purity of the NaJ solution was analyzed using Si(Li) and Ge(Li) detectors, both immediately after chemical separation and at intervals over the next few weeks. The following relative activities normalized to the end of bombardement were found:

Iodine	$T_{1/2}$ (h)	Concentration (% of J-123)
120	1.35	$<7 \cdot 10^{-3}$
121	2.12	0.2
123	13.2	100
124	99.6	1.03
126	312.0	<0.02
128	0.42	4.1
130	12.4	<0.03

Since the beginning of 1977 a quality control certificate accompanies the batches to be sent to the hospitals. This certificate is produced by an automatic analysis of the γ spectrum using the cyclotron control computer.

+ Institut für Radiochemie

References

/1/ K.H. Assmus, F. Michel, H. Münzel, F. Schulz, R. Schütz, and H. Schweickert, Report KFK 2379, p. 86.

7.2 VAN DE GRAAFF ACCELERATOR

7.2.1 Technical Design of the Proton Microbeam at the Van de Graaff Accelerator

D. Heck

Proton-induced X rays or secondary particle emission will be exploited for microanalytical studies. For this purpose, a proton microbeam is presently being installed at the Van de Graaff accelerator. A view of the experimental set-up is shown in fig. 1. Protons coming from the accelerator pass the analyzing magnet without deflection; they are bent by 30° to the left in the heavy-ion magnet and cross the switching magnet undeflected. By means of two quadrupole doublets the beam is then focused onto the collimator (object) slits. A water-cooled precollimator cuts off a large

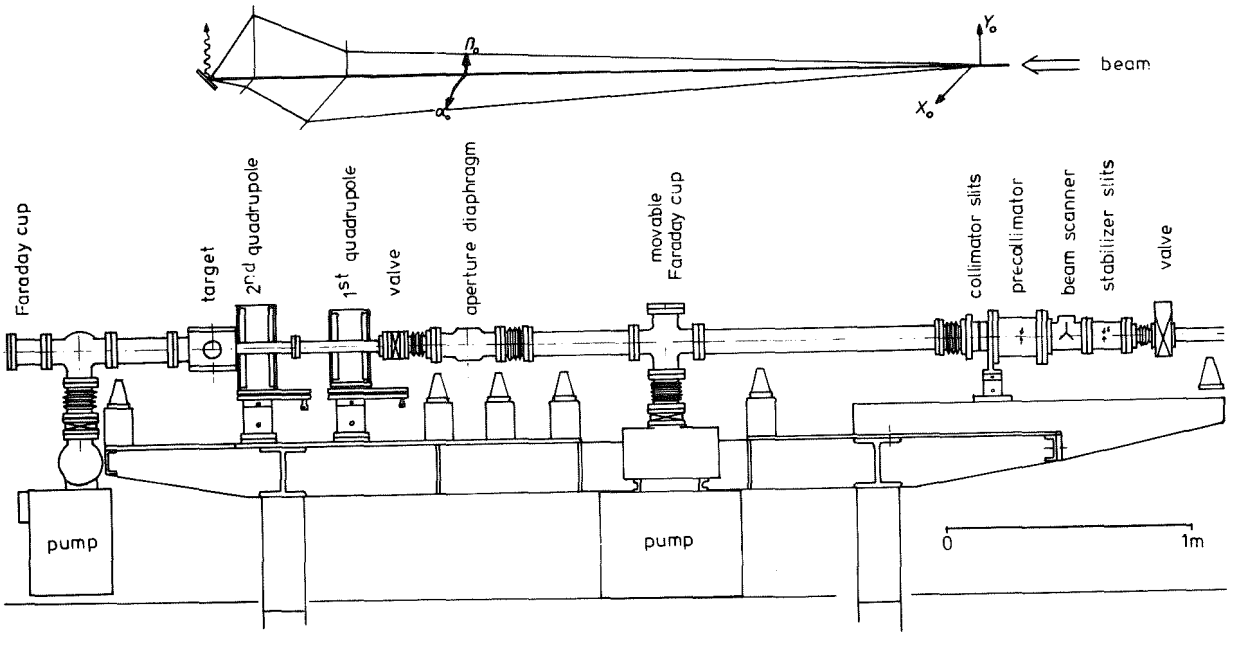

Fig. 1. Side view of the proton microbeam set-up. The beam enters from the right. A schematic beam tracing in the horizontal and vertical plane is given in the top of the figure.

fraction of the beam diameter in order to avoid a thermal overload of the collimator. The collimator slits are precisely polished edges and the width is adjustable by means of Piezo drives /1/.

The large distance of more than 4 m between the heavy-ion deflecting magnet and the stabilizing slits (see fig. 1) results in a high energy stability of the accelerator and minimizes chromatic aberrations of the quadrupole doublet which forms a reduced image (3 µm x 3 µm) of the collimator slits on the target /2/. To keep the aperture aberrations small enough, the divergence of the beam is limited by means of an aperture diaphragm having a variable diameter of 1 to 19 mm. Two Faraday cups monitor the beam intensity, where the one mounted before the aperture diaphragm is retractable. The magnetic quadrupoles are mechanically adjustable to meet the narrow tolerances required for minimal image aberrations /3/. The polarity of the quadrupoles is chosen such as to provide first focusing in the horizontal plane as shown schematically in the top of fig. 1.

The target is movable in three independent directions and can be observed during irradiation with a microscope which has a mirror objective (X 15) mounted inside the target chamber. Objectives of this type can easily be provided with a hole along the optical axis. With the proton beam oriented in the optical axis of the objective, the beam can be steered through this hole (diameter 3 mm).

Since the scattering of the protons on the residual gas molecules produces a halo around the focus spot /1/, the drift tube and the target chamber must be well evacuated. Therefore, all vacuum components are manufactured from stainless steel material and are provided with UHV knife-edge flanges and copper gaskets. An oil-free vacuum of better than 10^{-7} mbar is achieved with two turbomolecular pumps. These are connected to the vacuum system by means of soft bellows in order to prevent the transmission of vibrations. The whole microbeam set-up is built on a rigid steel table to suppress uncontrolled deformations and displacements to orders of the sub-micrometer range. Special care is taken to keep away vibrations from the microbeam set-up by laying the foundation of the steel table on the rigid cellar floor of the Van de Graaff building and using exclusively flexible and soft connections to the equipments placed on the metal grating floor.

References

/1/ R. Nobiling et al., Nucl. Instr. Meth. 130 (1975) 325.
/2/ D. Heck, Report KFK 2379 (1976) p. 108.
/3/ D. Heck, contribution 7.2.2.

7.2.2 Misalignment Tolerances for the Proton Microbeam at the Van de Graaff Accelerator

D. Heck

Together with the image aberrations inherent in magnetic quadrupole lenses, the precision of the adjustment of the quadrupoles essentially determines the minimal beam diameter attainable with proton microbeams. Therefore, the influence of the displacements along the individual degrees of freedom - three translational and three rotational - must be known to derive misalignment tolerances.

The formalism developed in ref. /1/ and implanted into the program IONBEAM /2/ has been used to calculate the behaviour of the beam diameter as a function of the magnitude of the misalignment. The beam system parameters /3/ used for the calculations are:

Distance from object slits to entrance of first quadrupole	250 cm
Length of the quadrupoles	10 cm
Distance from first to second quadrupole	29 cm
Distance from exit of second quadrupole to target	12.5 cm

With the acceptance parameters $x_o \leq 3.24$ µm, $y_o \leq 48$ µm, $\alpha_o \leq 1.26$ mrad, and $ß_o \leq 0.48$ mrad, the beam spot size amounts to 3 µm x 3 µm.

For pure parallel shifts of the quadrupoles the system behaves just as for misplacements of the collimator slits from the origin (x_o, α_o, y_o, $ß_o$) to the position (x_v, α_v, y_v, $ß_v$). The dominating image aberration terms which limit the tolerances for pure shifts are

$(x/x\alpha\alpha)\ (x_o + x_v)(\alpha_o + \alpha_v)^2$

$(x/x\beta\beta)\ (x_o + x_v)(\beta_o + \beta_v)^2$

$(x/\alpha y\beta)\ (\alpha_o + \alpha_v)(y_o + y_v)\ (\beta_o + \beta_v)$ for the x-direction

and $(y/x\alpha\beta)\ (x_o + x_v)\ (\alpha_o + \alpha_v)\ (\beta_o + \beta_v)$

$(y/\alpha\alpha y)\ (\alpha_o + \alpha_v)^2(y_o + y_v)$

$(y/y\beta\beta)\ (y_o + y_v)\ (\beta_o + \beta_v)^2$ for the y-direction.

If image aberrations of 1.3 μm are admitted, then the following tolerances must be met:

1st quadrupole:	horizontal shift	≤ 20 μm
	vertical shift	≤ 10 μm
2nd quadrupole:	horizontal shift	≤ 30 μm
	vertical shift	≤ 20 μm

If the quadrupoles are tilted or rotated, then the mirror symmetry with respect to the horizontal or vertical plane is destroyed and additional transport matrix elements must be taken into account. The dominant matrix elements are

		horizontal (x)	vertical (y)
tilt	α	(x/αα)	(y/βα)
tilt	β	(x/βα)	(y/ββ)
rotation	γ	(x/β)	(y/α)

The image aberrations including the contributions of these matrix elements are shown as a function of the tilt or rotation angles in fig. 1. Respecting the 1.3 μm image aberration limit, the following alignments must be attained: first quadrupole $\alpha \leq 15'$; $\beta \leq 30'$; second quadrupole $\alpha \leq 1^o$; $\beta \leq 1^o$. The rotation γ around the beam axis of the first quadrupole with respect to the second must not exceed 8".

To meet these specifications, special rigid supports have been built. The adjustments are performed with micrometer screws having sufficient sen-

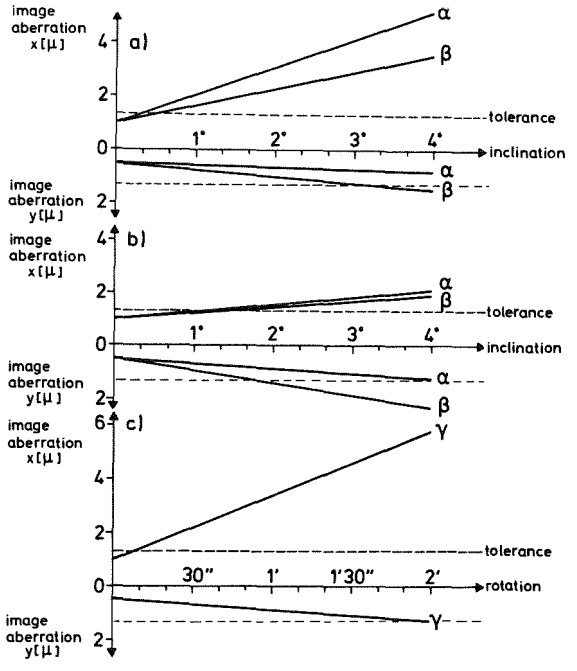

Fig. 1 Image aberrations as a function of tilt or rotation angle. The dashed lines represent the 1.3μm limit for the image aberrations. a) First quadrupole tilted in directions α and ß. b) Second quadrupole tilted in directions α and ß. c) First quadrupole rotated around beam axis by angle γ , with respect to second quadrupole.

sitivity such that at minimum one scale division corresponds to the tolerance movement.

References

/1/ D. Heck, Nucl. Instr. Meth. 143 (1977) 423.

/2/ D. Heck, E. Kasseckert, Report KFK 2379 (1976) p. 130.

/3/ D. Heck, Report KFK 2379 (1976) p. 108.

7.2.3 Ion Beam Optics of Misaligned Beam Transport Elements*

D. Heck

To study the influence of misaligned ion optical beam elements on the image aberrations, a theoretical approach has been developed which is suited to higher order (≥ 3) beam transport matrix theory.

For practical applications a set of subroutines based on this formalism has been implanted into the program IONBEAM, thus arbitrary beam element displacements and inclinations can be treated in the calculations.

* Nucl. Instr. Meth. 143 (1977) 423.

7.2.4 Routine Fabrication of Metallic Li Targets for Neutron Production at Van de Graaff Accelerators

D. Roller[+] and F. Käppeler

The ^{7}Li (p,n) reaction is most frequently used for neutron production at Van de Graaff accelerators. In order to achieve the highest possible neutron yield, the use of metallic Li targets is desirable. Because of its chemical instability, special techniques are necessary for the fabrication and storage of such metallic lithium layers. During the past years the following procedure was developed in our laboratory: metallic lithium grains of about 1 to 2 g are cleaned in methanol and then cooled down quickly in liquid nitrogen for storage. The lithium targets are thin metallic layers evaporated onto 0.3 mm thick tantalum or copper backings. The evaporation is carried out in a vacuum of better than 5×10^{-5} Torr. First, the lithium grains are melted slowly in a tantalum boat to get volatile impurities pumped away. Then a shutter above the boat is opened and the evaporation is carried out at a rather low speed. A symmetric frame with 6 positions 30 cm above the boat allows the simultaneous evaporation of 5 targets. At the sixth position an oscillator quartz is mounted. The quartz frequency changes with the evaporated layer thickness, so that the evaporation speed and the layer thickness can be controlled during evaporation. Fig. 1 gives the calibration curve for the conversion factor relating the frequency change to target thickness as a function of proton energy for a 5 MHz quartz. The best target quality is achieved for an evaporation rate of 10 - 15 Hz sec^{-1}. The target thickness is given in units von keV of the proton energy loss because this parameter is the quantity of interest for neutron experiments. A target

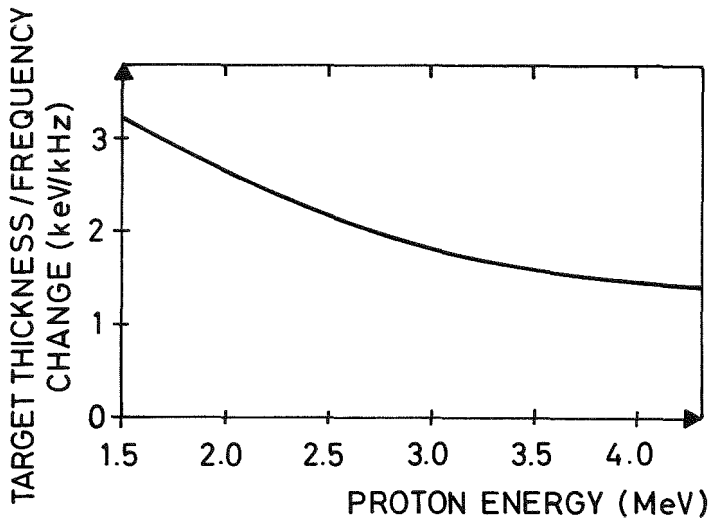

Fig. 1 Conversion factor C relating the frequency change of the oscillator quartz to the evaporated target thickness.

thickness of 1 keV corresponds to a thickness of the Li layer of about 8 μg cm^{-2}. At present, the size of our boat limits the maximum target thickness to 80 keV, but thicknesses up to 200 keV can be made by repeated evaporation. After a cooling time of at least 30 minutes, the vacuum chamber is floated with argon. In this way the metallic surface is protected for a few minutes against chemical reactions, so that the targets can be cooled down in liquid nitrogen for almost unlimited storage.

+ Van de Graaff operating group

7.2.5 Neutron Yield from the ^{7}Li (p,n) Reaction Near Threshold

F. Käppeler

Differential cross sections for the ^{7}Li (p,n) reaction have been reported by several authors (see for example refs. /1/ and /2/). However, no data for cross sections are given for proton energies below 1.920 MeV where two neutron energies appear for each proton energy due to the reaction kinematics. Because of this ambiguity, cross sections cannot be defined for the energy range from threshold to 1.920 MeV. The corresponding neutron energy interval ranges up to 120 keV. As background problems in time-of-flight experiments are critical for these rather low neutron energies, some information about the neutron yield would be very important for the planning of experiments.

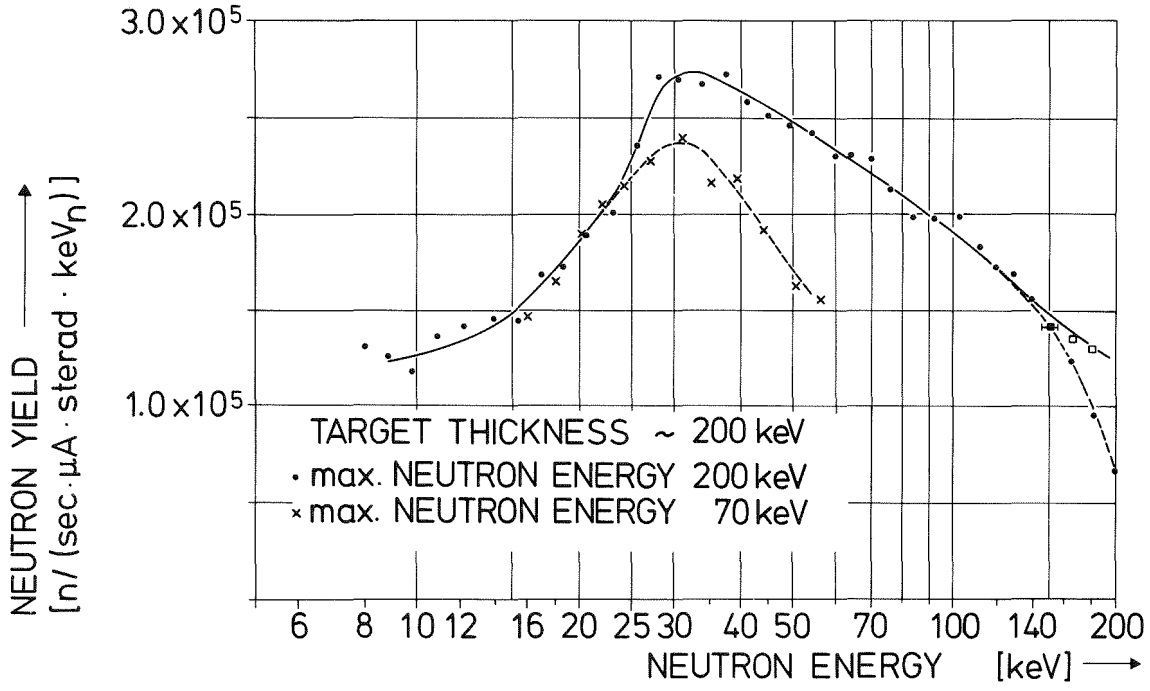

Fig. 1 Integral neutron yield in the forward direction ($\Theta = 0^{o}$) from thick metallic targets in the $^{7}Li(p,n)$ reaction.

For this reason, integral neutron yields per neutron energy interval from thick metallic Li targets have been determined for the forward direction (0^{o}) at our Van de Graaff accelerator. Relative yields were calculated from capture cross section measurements on ^{197}Au for neutron energies up to 200 keV. The normalization of this curve was performed in the interval from 144 to 157 keV by means of the cross section values of ref. /2/. The resulting neutron yield curves for two different proton energies are given in fig. 1 for a target thickness of 200 keV ($\sim$ 2 mg/cm^2). The solid curve gives the integral thick target yield. The deviations near the respective maximum energies are due to straggling effects of the protons which have been discussed by Palmer /3/.

References

/1/ J.H. Gibbons and H.W. Newson, "Fast Neutron Physics I", J.B. Marion and J.L. Fowler eds., Interscience Publishers Inc., New York (1960), p. 133.

/2/ H. Liskien and A. Paulsen, Atomic Data and Nuclear Data Tables, 15 (1975) 57.

/3/ D.W. Palmer, Nucl. Phys. 75 (1966) 529.

7.3 COMPUTERS

7.3.1 Data Acquisition and Analysis Program for the Experiment Computer Nova 2 at the Cyclotron

W. Karbstein, W. Kneis, and W. Segnitz

A data acquisition and analysis program has been developed for experiments at the Cyclotron. The program is written in BASIC running under the real-time operating system RDOS /1/. The hardware already described earlier /2/ is an extended Nova 2/10 with 96 K of memory, a dual disk, two tapes, one video and one live display, a Camac branch system and a special Laben multiparameter system for data acquisition. The memory of 96 K consists of 32 K internal memory usable for system, user programs and data and of 64 K of external memory usable only for data, data acquisition, TV-display buffer, intermediate data storage and spectrum areas.

The program is divided into two overlays: the initial and the runtime part. The first part comprises the definition of the experiment parameters. This is done by a question/answer play. It contains the mode selection of the three input channels for list or increment data acquisition, the word-length of one data word (16/32 bit), the length of the buffer for list mode and the spectrum length for the increment mode. Up to ten subspectra can be combined to form one total spectrum. The second part is started automatically using the experiment parameters defined in part one. It manages the handling of interrupts for the data acquisition like buffer-switch or spectrum overflow as well as the manual interrupts from the control keyboard. Via the control keyboard the experimentalist communicates with the program to guide the experiment, to display the interesting spectra or to make on-line calculations.

For the display of spectra a live display and a video display is present. While the live display can be used for all spectra, the video display is only used for spectrum parts because of its small resolution of 256 points. Peak handling is also done using the TV-display. For peak analysis the user selects the appropriate subspectrum and defines 4 bounds for linear background subtraction. The maximum, integral and FWHM are calculated according to the Gauß-Papier method. The spectrum part containing the peak

and the four bounds is shown on the TV-display.It is possible to define and store five peaks within each of the ten subspectra.

Commands available for the experimentalists

A) General management

'S' - start data acquisition
'U' - interrupt data acquisition
'F' - continue data acquisition after 'U'
'E' - stop data acquisition and terminate program execution

B) Display management

'G' - display total spectrum on the live display
'L' - delete total spectrum (only after 'G')
'nT' - display subspectrum nr. n on the live display
'nB' - choice the Z-scale for live display
(only for 32-bit data words;
n=1: bit 0-15 displayed
n=2: bit 8-23 displayed
n=3: bit 16-31 displayed)
'nP' - display of 256 channels on TV-display for peak integration
(only possible after nT)

C) Peak integration and analysis

'V' - move marker to the right
'R' - move marker to the left
'A' - stop marker
'H' - take over marker position as one of the four bounds.
'M' - repeat definition of the last four bounds.
'W' - repeat the last defined peak integration
'##' - delete subspectrum (only possible after T)

References

/1/ Data General, RDOS manual 093-000075-05 (1974).
/2/ W. Karbstein, Report KFK 2379 (1976) p. 122

7.3.2 An Interrupt Handler for Fortran IV

G. Ehret[+] and H. Sobiesiak[+]

The aim of the work presented in the following contributions was to provide the users of NOVA 2 FORTRAN IV with most of the convencience that has been implemented into Extended BASIC during the last years. In contribution 7.3.3 the general interface between FORTRAN IV and the assembly-language subroutines written for BASIC[*)] is described, while the following section deals with those procedures that are necessary to receive interrupts from user devices in a real-time environment.

The interrupt routines contained in the RDOSCALL.LB store the codes of the incoming interrupt into a table which has one entry for each device. In BASIC this table is scanned every time when a new statement is scanned. For FORTRAN this scan is done by the interrupt routine itself and if an interrupt code is found, this code is transferred to the FORTRAN level by the task call .IXMT.

To receive this interrupt message, one of the FORTRAN TASKS must use the CALL ITWAIT (KODE) which uses task call .REC to the location used by .IXMT the interrupt routine. From the FORTRAN level the interrupt code table may be also scanned by one of the following two calls:

```
CALL  CA103
CALL  SCHARF
```

Furthermore any of these three calls will force the multitasking modules from the FORTRAN-RDOSCALL.LB interface to be loaded. Thus, even if no user interrupts are to be serviced in a multitasking program, but modules from RDOSCALL.LB are used by more than one task, one of these three calls must be present at least as a dummy.

In the following there is a programming example for the use of the interrupt handler.

*) contained in the "RDOSCALL.LB"

```
C   TASK INTER SERVICES USER IT'S
    TASK INTER
C   ENABLE INTERRUPT FROM VARIOUS  DEVICES
C   1. SINGLE-BIT-CONTROL
    CALL CAL60 (0,-1,-1)
C   2. TV-LIGHTPEN
    CALL CA230 (1)
C   3. TELETYPE CONTROL-CHARACTERS
C   ASSUME $ TTI IS OPENED  ON FILE NO.  11
    CALL TTIT (11)
C   NOW WAIT FOR INTERRUPTS
1   CALL ITWAIT (ITCODE)
C   GET INTERRUPTING DEVICE
C   CODES FROM SINGLE-BIT: 600-750
C               LIGHTPEN   : 300
C               TELETYPE   : 300+ASCII -VALUE
    ID = ITCODE/100
    IF (ID .LT.1.OR.ID.GT.9) GOTO 1
C   BRANCH TO DEVICE SERVICE-ROUTINES
    GOTO (10,20,30,40,50,60,80,90) ID
    .
    .
    .
    .
C   LIGHTPEN AND TELETYPE
30  IF (ITCODE.EQ.300) GOTO 31
C   ONLY 'ESC' IS WANTED FROM TTI
    IF (ITCODE.EQ.327) CALL ESCSERVICE
C   SCAN IT-TABLE ONCE MORE
    CALL CA103
C   WAIT FOR NEXT IT
    GOTO 1
    .
    .
    .
```

7.3.3 An Interface Between FORTRAN IV and the RDOSCALL.LB Assembler Routines for Both Single and Multitasking FORTRAN IV

G. Ehret[+], H. Sobiesiak[+], and B. Volk[+]

RDOSCALL.LB is a library containing assembler routines for EXTENDED BASIC which are accessible via the EXT. BASIC 'CALL' statement. Most of these routines are used to drive user devices such as the TV-display, increment unit ,Camac etc.

These routines cannot be called directly from FORTRAN IV because the data linkage is different between BASIC and FORTRAN. Furthermore FORTRAN provides the use of integer or floating-point data while BASIC is restricted to only floating-point data.

Besides these two problems a third one arises when multitasking FORTRAN is used. Though the BASIC system is a multitasking program too, the execution of a call statement is only processed by one task. This was the reason why the routines of RDOSCALL.LB were not coded to be reentrant. Thus in a REAL-TIME FORTRAN environment the program might be destroyed when two or more tasks will reach one of the RDOSCALL.LB routines simultaneously.

As most of the users of NOVA 2 FORTRAN IV did programming in EXTENDED BASIC before, the FORTRAN entries to the RDOSCALL.LB are called via a pseudonumeric mnemonic.

The translation rules can be taken from the following table:

BASIC		FORTRAN	
CALL nx,	Arguments	CALL CALnx	(Argum.)
CALL nxx,	Arguments	CALL CAnxx	(Argum.)
CALL nxxx,	Arguments	CALL Cnxxx	(Argum.)

where each x stands for a digit in the range 0-9 and each n for a digit in the range 1-9.

To solve the three problems mentioned above the following steps were taken:

1. In their first release the RDOSCALL routines stored their return address in a page-zero variable. This has been eliminated and replaced by a call to a subroutine (.SADR) which is resolved differently in BASIC, Singletask FORTRAN and Multitask FORTRAN. Equivalent coding has been done for the return (.LADR).
2. To overcome the problems arising in a multitask environment, special groups of RDOSCALL routines are locked by the .REC/.XMT mechanism. Great care had to be taken to ensure that no routine is locked for all times. Using only the .REC/.XMT mechanism this would occur when a task is killed while it is executing in the locked part of a routine. This could be avoided using the kill processing formalism provided in RDOS 4.2 (not provided by the Fortran IV task scheduler).

   For this reason the routines described here require the use of the RDOS 4.2 RLDR.SV (RLDR REV 4.0). It has been tested that RLDR REV 4.0 runs under RDOS REV 3.03,too. To force the loading of the multitask module, one of the following two subroutines must be called from one of the FORTRAN routines:

   a) CALL CA103
   b) CALL ITWAIT (KEY)

   (both are mentioned in 7.3.2).
   If none of these have a reference in the FORTRAN programs,the singletask module will be loaded.

3. The FORTRAN-callable entries set up the stack frame for the RDOSCALL routines (variable length = 25 octal) store the argument address on this frame and establish a format-control information for each argument, whether it is Real, Integer or Double-precision Integer.

The interface between FORTRAN IV and RDOSCALL.LB is available in two libraries named FHCALL.LB and FSCALL.LB for FORTRAN IV with or without Hardware Floating-Point Processor.

+ IAK Computer Group

7.3.4 A Soubroutine Call for EXTENDED BASIC to Execute 'Keyboard-Only Commands' in a Running Program

H. Sobiesiak+

The programming language most frequently used on our NOVA 2 computers is an old schedule of DGC's EXTENDED BASIC (Rey 3.6). Newer releases (Rey 4.01-4.20) offer much more convenience than Rey 3.6 but they are too core-consuming for a lot of problems. A lot of the advantages of Rey 4.01 arise from the fact that the user has access to BASIC system resources in his program which could only be used as 'Keyboard Commands' in Rey 3.6.

The following two commands are examples that affect the printout format.

a) PAGE = nnn ↓ to set the length of a print-line

b) TAB = nnn ↓ to set the tabulator margins

Another example is the command to delete a number of lines from the program source text.

3000, 4000 ↓ delete all statements between line 3000 and 4000

To enable the users of Rey 3.6 to use such commands in their programs,an assembler routine has been written that changes the input sequence of the BASIC statement editor to request characters from a string constant or variable instead of requesting them from the keyboard input buffer. The routine has been entered as CALL 205 into the RDOSCALL.LB. The argument for this routine can be any legal BASIC command.

In the following some examples will be given

a) set line limit to 80 characters

```
10 CALL 205, 'PAGE = 80'
20 -------
```

b) erase the statements 1000 to 2000

```
10 CALL 205, '1000, 2000'
```

c) assume a string variable A$ contains the character representation for a number and this is to be converted into numeric representation.
Let A$ be '1234.5E6', than the following program will convert it.

```
10   DIM A$ (20), B$ (20)
      :
     : A$ is given a value here
      :
100  LET B$ = 'B =', A$
100  CALL 205, B$
```

The variable B now contains the numeric representation of the string of digits that has been in A$.

+ IAK Computer Group

7.3.5 A FORTRAN IV Program for Multiparameter Data Acquisition on a NOVA 2 Computer

A.A. Naqvi and H. Sobiesiak+

This program has been written to meet the requirements for data acquisition of a 4-parameter fission experiment being performed at the Van de Graaff laboratory. In this type of experiment the data are acquired and stored in list mode but in addition, control spectra have to be created on-line during the measurement.

As BASIC is too slow for this problem, the multiparameter acquisition program was written in FORTRAN IV using the multitask programming technique. The program is only partially core resident and has a number of overlay programs on disc.From the three DMA channels available for data acquisition the program uses the first two for list mode aquisition allowing up to four 16 bit words as input. The data are stored in 4 K buffer regions and are then transferred blockwise to magnetic tape. Thereafter the data are transmitted to the third DMA channel which is operated in increment mode for creating the control spectra.

From the available 40 K memory region 26 K have been allocated to the control spectra, 10 K have been reserved for the operational region and 4 K are used by the software display. In the operational region various mathematical operations can be performed on the spectra.

The program offers also the standard features for data analysis like acquisition control, markers, data storage on disc or magnetic tape etc. These functions are controlled by a single-bit handler.

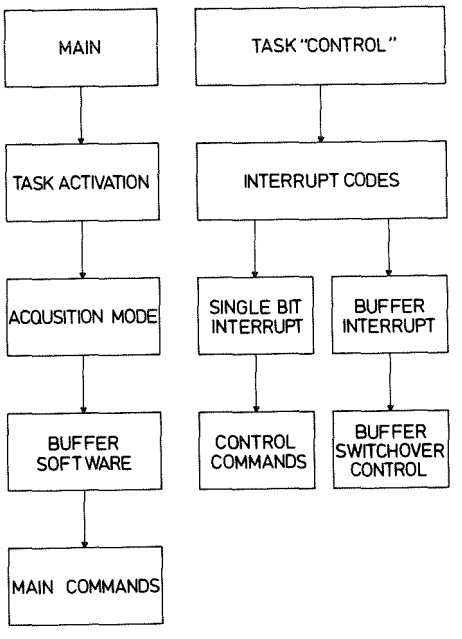

Fig. 1. The block diagram of the program organization.

The block diagram of fig. 1 shows the organization of the program. It consists of two tasks, the main program and the task "CONTROL". The task "CONTROL" is activated by the main program and is always waiting for interrupts. Whenever an interrupt is generated it is analyzed by the task "CONTROL" which then informs the main program about the nature of the interrupt. The main program contains two acuqisition modes (list or increment mode), different control commands and buffer software programs for data handling.

+ IAK Computer Group

7.4 ION SOURCES AND DETECTORS

7.4.1 Present Status of the Karlsruhe Polarized Ion Source C-LASKA

V. Bechtold, L. Friedrich, and P. Ziegler[+]

The Lambshift source C-LASKA producing polarized deuterons from charge exchange of metastables with iodine is in operation at the Karlsruhe Isochronous Cyclotron since the beginning of 1974. The source is installed in the basement of the experimental hall, separated from the cyclotron vault by 3 m of shielding. The distance between the axial injection system and the source is 11 m. Thus the magnetic strayfield of the cyclotron is eluded. In addition the source can be handled when the cyclotron is in operation. The source delivers 0.8 μA vector polarized deuterons with an emittance of 1.1 cm rad $eV^{1/2}$. Of this, 5 % could be extracted from the cyclotron.

Source current		Current in scattering chamber	
vector pol.	tensor pol.	vector pol.	tensor pol.
0.8 μA	0.6 μA	40 nA	30 nA

Two important improvements have been achieved in 1976:

1. To protect the bearings and the oil of the turbopumps from the very agressive iodine evaporated in the source, a low iodine pressure in the forevacuum has been maintained by liquid nitrogen traps. The consumption of the liquid nitrogen was high and every three hours a refilling of the traps led to an interruption of 10 minutes. These traps have been replaced by an iodine condensor which is cooled by alcohol at $-80^{o}C$. The source can now be operated continuously for more than 150 h.
2. The determination of vector and tensor analysing powers in scattering experiments with polarized deuterons necessitates besides a pure and a mixed polarized beam an effective method to flip the polarization.

The latter improvement has been achieved in the following way:
To get a transversely polarized beam, a transverse magnetic field is produced in the charge exchange cell (fig. 1). This field is compensated electrically

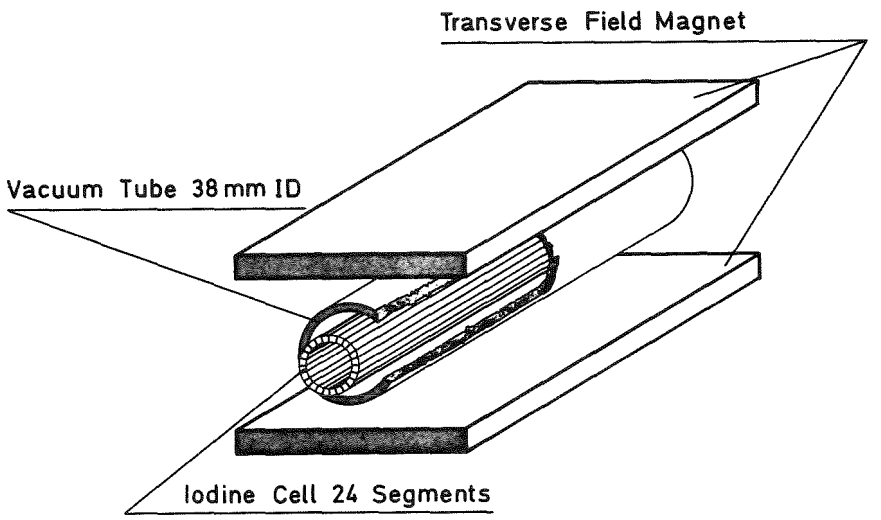

Fig. 1. The charge exchange cell with the transverse field magnet. The sliced iodine cell is able to compensate the transverse field.

to avoid quenching of the metastables and broadening of the beam. For this purpose the cell (18 mm diameter and 200 mm length) has been sliced into 24 segments which are operated at different potentials. The polarization of the metastable atoms is rotated to transverse direction by superimposing the outgoing field of the second quenching magnet and the strayfield of the iodine cell. Shaping of this field is achieved by an additional coil.

The polarization is flipped by simultaneously reversing the magnetic and electrical field. This results in small changes of the beam direction which have to be corrected carefully because the acceptance of the cyclotron depends very critically on the beam direction. The correction is done by compensating separately the magnetic field for both directions. In addition a transverse field magnet is applied at the exit of the cell which also can be excited separately for both directions. The magnet looks like the stator of an electric motor. Careful adjustment gives equal intensity for both directions. The measured vector polarization P_3 for spin "up" and "down" as a function of time is given in fig. 2. The direction of the polarization can be automatically controlled by the data acquisition system of the experiment.

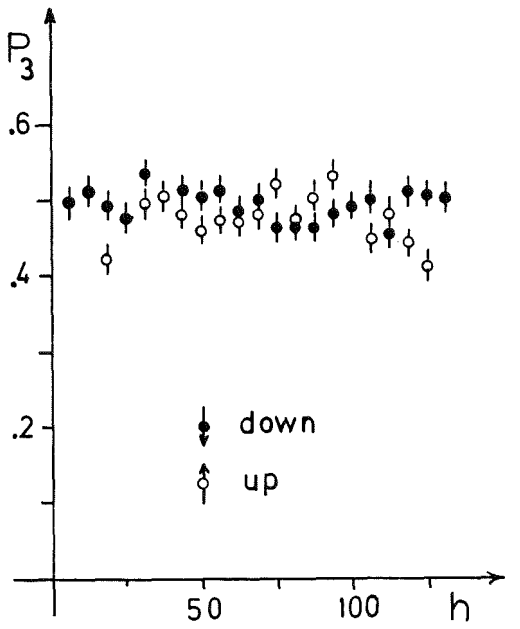

Fig. 2. The vector polarization P_3 measured during a period of 125 hours for "spin up" and "spin down".

+ Institut für Experimentelle Kernphysik der Universität Karlsruhe

7.4.2 Development of a Fast Spherical Avalanche Fission Detector with Good α Discrimination

M.A. Kazerouni and F. Käppeler

For the measurement of fission cross sections of highly α-active transuranium isotopes a detector with good α discrimination, very fast timing and long lifetime is required. As described in the preceding annual report /1/ a spherical avalanche detector was developed for this purpose. First tests of this detector with ^{252}Cf and ^{241}Am sources showed an excellent behaviour with respect to the above requirements. The α discrimination can be achieved by setting the gas pressure and counter voltage such that the weaker ionization of the α particles is quenched completely by the gas and only the fission fragments can be detected. Fig. 1 shows this behaviour for a gas pressure of 21 mbar. The dashed lines give the relation between pulse height and voltage for fission fragments and α particles (left scale). Important for the discrimination between the two groups is the pulse height ratio R which is given by the full line (right scale). As the voltage is decreased the α pulses are more efficiently quenched than those caused by fragments. In this way the ratio R can easily be set to 100 or even more. With an ^{241}Am source of 2×10^6 α sec^{-1} a discrimination factor of better than 10^{-10} was measured in a two-days run.

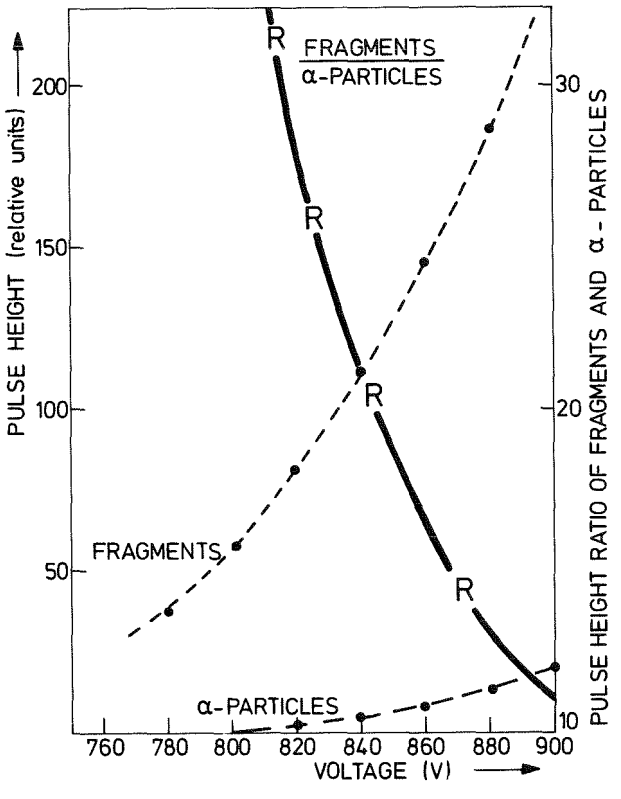

Fig. 1. Relative pulse heights of α particles and fission fragments as a function of the counter voltage (dashed lines). The solid line gives the pulse height ratio (right scale).

Furtheron, the efficiency and the time resolution were determined with a ^{252}Cf source. The time resolution was measured against the prompt fission γ rays which were detected by a fast plastic scintillator. A time resolution of $\lesssim$1 nsec was found for the avalanche detector. As the rise time is only about 3 nsec it is hoped that this value may be reduced with improved electronics. The efficiency was determined with a calibrated ^{252}Cf source to 97.5 ± 2.0 %. This high efficiency makes the detector also suitable for very accurate measurements.

The lifetime of the detector is also important because neutron cross section measurements are often run over several weeks. Even gas counters are not completely insensitive to the heavy bombardment of highly ionizing particles. By the time the counter gas is dissociated and loses its quenching properties. Therefore the detector is operated in a steady gas flow which is automatically controlled so that the pressure is kept constant within ± 0.1 mbar. In this way stable operation can be guaranteed over long periods. A first application of the detector is planned in a fission cross section measurement of ^{244}Cm.

References

/1/ M.A. Kazerouni and F. Käppeler, Report KFK 2379 (1976) p. 116.

8. SEMINARS

2.6.76 G. Buttermann, TU München
Klinische Ergebnisse nuklearmedizinischer Leber- und Nierendiagnostik unter Verwendung von ^{123}J-markierten Radiopharmaka

9.6.76 R. Beck, TU München
Elastische und inelastische α-Streuung an ^{6}Li im Rahmen der Zweizentren-Generatorkoordinatenmethode

16.6.76 P. Paul, SUNY Stony Brook und MPI Heidelberg
Elektrische Multipolresonanzen in Kernen

30.6.76 W. Glöckle, Universität Bochum
Das Wenig-Teilchen-Problem der Kernphysik

13.10.76 G. Baur, KFA Jülich
Deuteron-Aufbruch an schweren Kernen und Stripping zu ungebundenen Zuständen

29.10.76 A. Michaudon, Bruyères-le-Châtel
Neutron-Induced Fission

10.11.76 B. Zeitnitz, Universität Bochum
Neuere Entwicklungen auf dem Gebiet der Neutronen-Detektoren

1.12.76 F. Resmini, Universität Mailand
The Superconducting Cyclotron Project at the Milan University

8.12.76 R. de Swiniarski, Universität Grenoble
Recent Polarization Experiments at the Grenoble Cyclotron

12.1.77 L. Lassen, Universität Heidelberg
Aufbruch von Lithium im Feld schwerer Kerne

26.1.77 W. Rödel, Universität Heidelberg
Kernphysikalische Analyseverfahren in der Aerosolphysik

2.2.77 W. Wölfli, ETH Zürich
Hochempfindliche Spurenanalyse mit einer Protonenmikrosonde

7.2.77 Z. Majka, Universität Krakau
Antisymmetrization Effects and the Form-Factor of the Real Part of the α-Nucleus Potential

27.4.77	D.D. Clayton, Rice University, Houston Nuclear Clues to the Origin of the Solar System
3.5.77	H.D. Zeh, Universität Heidelberg Elementhäufigkeiten im Sonnensystem
11.5.77	S. Bjørnholm, NBI Kopenhagen Energy in Denmark 1990 - 2005, a Case Study
25.5.77	E. Löpfe, EIR Würenlingen Produktion von Radioisotopen für die Medizin am SIN-Injektor-Zyklotron
8.6.77	C. Rolfs, Universität Münster Kernreaktionen in der frühen Sternentwicklung
15.6.77	E. Hilf, TH Darmstadt Elemententstehung bei hohen Temperaturen und Dichten
28.6.77	R.A. Kenefick, Texas A&M University The Electron Beam Ion Source (EBIS)

9. PUBLICATIONS AND CONFERENCE CONTRIBUTIONS

9.1 PUBLICATIONS

Bechtold, V., Friedrich, L., Strassner, G.

Experimental Investigations of Charge Exchange Processes in Lambshift Sources with Argon and Krypton for Production of D-Ions.
Nuclear Instr. and Meth. 136 (1976) S. 361-62.

Eyrich, W., Hofmann, A., Scheib, U., Schneider, S., Vogler, F., Rebel, H.

Alpha-Gamma Angular Correlation Measurements as a Sensitive Method Determining the Sign of the Nuclear Quadrupole Deformation.
Physics Letters, 63B (1976) S. 406-8 (9858).

Hartrott, M. von, Hadijuana, J., Nishiyama, K., Quitmann, D., Riegel, D., Schweickert, H.

Nuclear Spin Relaxation of Xe in Liquid Te.
Zeitschrift für Physik A 278 (1976) S. 303-308.

Kropp, J., Klewe-Nebenius, H., Buschmann, J., Rebel, H., Faust, H., Gils, H.J., Rieder, J., Wisshak, K.

Excitation Functions of $^{191+193}Ir$, ^{197}Au (^{6}Li, xn+yp) Compound Nuclear Reactions at E_{Li} = 48-156 MeV.
KFK 2342 (August 1976); Zeitschrift für Physik A280 (1977) S. 61 - 72.

Cierjacks, S. (HRSG.)

Progress Report on Nuclear Data Research in der Federal Republic of Germany for the Period January 1 to December 31, 1976.
NEANDC(E)-182 U, Vol. 5 (July 1976), INDC(Ger) - 18/L + Special.

Böhnel, K., Iyer, M.R., Matussek, P., Michel-Piper, I., Ottmar, H.

Zerstörungsfreie Methoden.
in: Projekt Spaltstoffflußkontrolle, Jahresbericht 1975, KFK-2295 (Aug. 76) S. 2/1--/57.

Cierjacks, S., Erbe, D., Kari, K., Leugers, B., Schmalz, G., Schouky, I., Voss, F.

Messung von Wirkunsgquerschnitten.
in: Projekt Schneller Brüter, 2. Vierteljahresbericht 1976, KFK 1276/2 (November 1976) S. 121/1-5.

Cierjacks, S., Erbe, D., Kari, K., Leugers, B., Schmalz, G., Schouky, I., Voss, F.

Kerndatenmessungen am Zyklotron.
in: Projekt Schneller Brüter, 4. Vierteljahresbericht 1976, KFK 12-76/4 (Apr. 77)S. 121/1-5.

Schulz, F., Schweickert, H.

Operation of the Karlsruhe Isochronous Cyclotron in 1975.
KFK-2298 (Juni 1976).

Chaffin, E.F., Dickmann, F.

Validity of the Adiabatic Cranking Model When Applied to Fission.
Physical Rev. Lett., 37 (1976) No. 26 S, 1738-40.

Gils, H.J., Rebel, H., Buschmann, J., Klewe-Nebenius, H., Nowicki, G., Nowatzke, W.

Nuclear Matter Sizes and Isoscalar Octupole Transition Rates of $^{204,206,208}Pb$ from 104 Mev α-Particle Scattering.
Zeitschrift für Physik A 279 (1976) S. 55-68.

Gils, H.J., Rebel, H., Knüpfer, W.

Experimental Studies of Neutron Collectivities by α-Particle Scattering and Some Implications for Giant-Resonance Excitations.
Nuovo Cimento, 36A (1976) S. 258-70.

Pinston, J.A., Roussille, R., Boerner, H., Davidson, W.F., Jeuch, P., Koch, H.R., Schreckenbach, K., Heck, D.

Rotational States in ^{151}Nd Populated Through Thermal Neutron Capture.
Nuclear Physics A 270 (1976) S. 61-73.

Beer, H., Ly Di Hong, Käppeler, F.

The Total Neutron Cross Section of ^{58}Fe in the Energy Range 7 to 325 keV.
KFK-2337 (August 76).

Iyer, M.R., Ottmar, H.

Assay of Plutonium in Process Wastes from Fuel Fabrication Plants.
KFK-2321 (September 1976).

Beer, H., Ernst, A., Käppeler, F., Roller, D., Rupp, G., Schreiber, H., Wisshak, K.

Wirkungsquerschnittsmessungen
in: Projekt Schneller Brüter, 3. Vierteljahresbericht 1976, KFK-1276/3 (Dezember 1976) S. 121/1-4.

Eyrich, W., Hofmann, A., Scheib, U., Schneider, S., Vogler, F., Rebel, H.

Alpha-Gamma Angular Correlations in the Reaction ^{24}Mg $(\alpha,\alpha_1\gamma)$ at E_α = 104 MeV.
KFK-2455 (Mai 1977).

Beer, H., Ernst, A., Käppeler, F., Kazerouni, A., Roller, D., Rupp, G., Schreiber, H., Wisshak, K.

Wirkungsquerschnittsmessungen
in: Projekt Schneller Brüter, 1. Vierteljahresbericht 1977, KFK-1277/1 (Juni 77) S. 212/12-17.

9.2 CONFERENCE CONTRIBUTIONS

Internat. Conf. on the Interactions of Neutrons with Nuclei, Lowell, Mass. July 6-9, 1976

Beer, H., Käppeler, F.
Intermediate Structure in the Capture-to-Fission Ratio of ^{235}U.

Beer, H., Rohr, G.
Investigation of (63,65) Cu Total Cross Sections in the Energy Range 30-150 keV.

Beer, H., Käppeler, F.
Valency Transitions in ^{56}Fe and (58,60) Ni.

Cierjacks, S.
Neutron Installations and Facilities.

Koch, H.R., Boerner, H., Davidson, W.F., Heck, D., Pinston, J.A., Roussille, R., Assche, P.H.M. van
(n,γ)-Measurements at the Grenoble HFR.

Müller, R., Goennenwein, F., Käppeler, F., Naqvi, A., Ernst, A.
4-Parameter (E,v)-Measurement on correlated Fragments from Fission Induced by 550 keV Neutrons.

Pinston, J.A., Roussille, R., Boehner, H., Davidson, W.F., Heck, D., Koch, H.R., Schreckenbach, K.
Nuclear Structure Study of $^{147,149,151}Nd$.

Scheer, K.E., Schmidt, K.A., Hoever, K.H.
Neutron Sources for External Medical Irradiation.

Internat. Conf. on Particles and Radiation Therapy, Berkeley, Calif., September 15-17, 1976

Schmidt, K.A., Reinhold, G.
The Haefely-GfK Fast Neutron generator.

Conf. on Microanalytical Techniques, Liverpool, Sept. 22-24, 1976

Heck, D.
Ion Optical Calculation of Focusing a 4 MeV Ion Beam to Micron Diameters.

15th Winter Meeting on Nuclear Physics, Bormio, January 17-21,1977

Dickmann, F., Chaffin, E.F.
Fission Dynamics

Gils, H.J., Buschmann, J., Faust, H., Klewe-Nebenius, H., Kropp, J., Rebel, H.
Nuclear Reactions Induced by ^{6}Li-Ions at E_{Li} = 156 MeV.

1st Technical Meeting on the Nuclear Transmutation of Actinides, Ispra, 15-18, 1977

Käppeler, F., Wisshak, K.

Experimental Techniques for Neutron Cross Section Measurements of Short-Lived Actinide Isotopes with a Van-de-Graaff-Accelerator.

Spring Meeting on Atomic Physics of the German Physical Society, Mainz, February 28-March 4, 1977

Nowicki, G., Bekk, K., Göring, S., Hanser, H., Schatz, G.

Hochauflösende Laserspektroskopie an leichten Barium-Isotopen.

Spring Meeting on Nuclear Physics of the German Physical Society, Konstanz, March 21-25, 1977

Aniol, R., Latzel, G., Paetz, H., Gen. Schieck, Bechtold, V., Friedrich, L.

Erzeugung polarisierter Protonen mit der Lambshiftquelle LASCO am Kölner Tandem.

Bechtold, V., Friedrich, L.,Haushahn, G., Möllenbeck, J., Schulz, F., Schweickert, H., Wiss, L.

Erweiterung des Teilchenangebots am Karlsruher Isochronzyklotron.

Bechtold, V., Friedrich, L., Breuer, H., Doll, P., Knöpfle, K.T., Mairle, G., Sessler, A., Wagner, G.J.

Struktur der Unterschalen von ^{16}O, ^{28}Si und ^{40}Ca aus Protonen Pick-up Messungen mit polarisierten Deuteronen.

Beer, H., Käppeler, F.

Intermediäre Strukturen im Verhältnis Spalt-zu-Einfangquerschnitt von ^{235}U.

Börner, H.G., Koch, H.R., Seyfarth, H., Schult, O.W.B., Heck, D., Mampe, W., Schreckenbach, K., Pinston, J.A.

Excited Levels in ^{235}U from Neutron Capture Gamma-Ray Measurements.

Buschmann, J., Gils, H.J., Rebel, H., Zagromski, S., Faust, H., Klewe-Nebenius, H., Kropp, J.

Kernreaktionen mit 156 MeV-^{6}Li-Ionen.

Chaffin, E.F., Dickmann, F.

Dynamik von Deformationsfreiheitsgraden.

Do, H.P., Chery, R., Boerner, W.F., Davidson, W.F., Pinston, J.A., Roussille, R., Schreckenbach, K., Koch, H.R., Seyfarth, H., Heck, D.

Level Structure of ^{80}Br and ^{82}Br from Thermal Neutron Capture Reactions.

Eyrich, W., Hofmann, A., Scheib, U., Schneider, S., Vogler, F., Rebel, H.

$(\alpha,\alpha'\gamma)$-Winkelkorrelationen an ^{28}Si bei E_α = 104 MeV.

Faust, H., Buschmann, J., Klewe-Nebenius, H., Rebel, H., Rieder, J., Wisshak, K.

Messung von Konversionselektronen-Winkelverteilungen in der In-Beam-Spektroskopie.

Gupta, S.K., Cierjacks, S., Schouky, I.

Untersuchungen von isobaren Analogzuständen in der Neutronenstreuung von ^{28}Si und Bestimmung von Isospinunreinheiten.

Hanser, A., Gils, H.J., Rebel, H., Faust, H., Klewe-Nebenius, H.

Direkte Beobachtung des stark beschleunigten $4_1^+ \rightarrow 0_1^+$ Überganges in ^{140}Ce und Vergleich mit inelastischer α-Streuung.

Käppeler, F., Kazerouni, M.A.

Ein schneller Gaszähler mit optimaler Diskriminierung zwischen α-Untergrund und Spaltfragmenten.

Käppeler, F., Wisshak, K., Hage, W., Hettinger, H.,

Messung des Querschnittes für neutroneninduzierte Spaltung von ^{241}Am im Bereich der Spaltschwelle.

Kappel, W.R., Kneis, W., Möllenbeck, J., Schweickert, H.

Status des rechnerunterstützten Zyklotronbetriebs am Karlsruher Isochronzyklotron.

Kari, K., Cierjacks, S.

Präzisionsmessungen der Spaltquerschnittsverhältnisse von $^{239}Pu/^{235}U$ und $^{240}Pu/^{235}U$.

Latzel, G., Paetz, H. Gen. Schieck, Bechtold, V., Friedrich, L.

Streuung polarisierter Protonen an ^{207}Pb im Bereich stark überlappender Analogresonanzen.

Schatz G., Bekk, K., Goering, S., Hanser, A., Nowicki, G., Rebel, H.

Hochauflösende Laserspektroskopie an leichten Barium-Isotopen.

Conf. on Nuclear Physics, Guildford, March 23-25, 1977

Eyrich, W., Hofmann, A., Scheib, U., Schneider, S., Vogler, F., Rebel, H.

The Sign of Nuclear Deformations from $(\alpha,\alpha'\gamma)$ Angular Correlations at E_α = 104 MeV.

Nowicki, G., Bekk, K., Goering, S., Hanser, A., Rebel, H., Schatz, G.

Nuclear Sizes of Light Barium Isotopes from Optical Isotopic Shifts Measured by High Resolution Laser Spectroscopy.

Internat. Specialists Symposium on Neutron Standards and Applications, Gaithersburg, Md., March 28-31, 1977

Cierjacks, S.

^{237}Np and ^{235}U as Possible Standards for the MeV Region.

APS Spring Meeting, Washington, D.C., April 25-28, 1977

Chaffin, E.F., Dickmann, F.

Dynamics of the Deformation in Fission

14^{th} European Cyclotron Progress Meeting, Uppsala, June 1-3, 1977

Assmus, K.H., Schulz, F., Schütz, R., Schweickert, H., Michel, F., Münzel, H.

Routine Production of iodine-123 at Karlsruhe.

Kappel, W.R., Kneis, W., Möllenbeck, J., Schweickert, H.

Status Report on the Computer Aided Cyclotron Operation in Karlsruhe.

9.3 LECTURES AND SEMINARS

Cierjacks, S.

Neutron Induced Fission of ^{235}U, ^{238}U and ^{239}Pu.
Vortrag vor der Nuclear Physics und der Neutron Physics Division des Oak Ridge National Laboratory, July 2, 1976.

Cierjacks, S.

Neutronenstreuung an leichten Kernen.
Vortrag im Institut für Strahlen- und Kernphysik der Universität Bonn, 25. Nov. 1976.

Gils, H.J.

Is the Nuclear Surface Neutron Rich ?
Vortrag im Institut für Atomic Physics, Bukarest, (Dez. 15, 1976).

Gils, H.J.

Gibt es Unterschiede in den kollektiven Eigenschaften von Protonen und Neutronen in schweren Kernen ?
Physikalisches Institut, Univ. Erlangen, 27. Juni 1977.

Nowicki, G.

Hochauflösende Laserspektroskopie an radioaktiven Barium-Isotopen.
Vortrag im Physikalischen Institut der Universität Mainz, 11. Mai 1977.

Rebel, H.

Alpha Particle Scattering Studies of Neutron Collectivities in Pb Nuclei.
11. Internat. School of Nuclear Physics, Predeal, Romania, August 26 - September 4, 76.

Rebel, H.

Ist die Kernoberfläche neutronenreich ?
Kolloquiumsvortrag beim Physikalischen Staatsinstitut in Hamburg, 22. November 1976.

Rebel, H.

Alpha Scattering and the Neutron Halo in Pb Nuclei.
Kolloquiumsvortrag, Eidgenössische Technische Hochschule, Zürich, 18. Januar 1977.

Schatz, G.

Laserspektroskopie an wenigen Atomen und die Kernradien der leichten Barium-Isotopen.
Kolloquiumsvortrag, Universität Erlangen 13. Juni 1977.

Voss, F.

Messung von γ-Produktionsquerschnitten am Karlsruher Neutronenflugzeitspektrometer.
Seminarvortrag bei der Physikalisch-Technischen Bundesanstalt, Braunschweig, 22. Sept. 1976.

10. PERSONNEL

Head of the Teilinstitut Kernphysik: Prof. Dr. G. Schatz

Scientific and technical staff:

Bechtold, G., Mrs.	Feurer, B.	Nowicki, G., Dr.
Beer, H., Dr.	Gils, H.J., Dr.	Ottmar, H., Dr.
Buschmann, J., Dr.	Göring, S.,Dipl.-Phys.	Rebel,H.G.,Dr.,Priv.-Doz.
Chaffin, E.F., Dr.	Hanser, A., Dr.	Rupp, G.
Cierjacks, S., Dr.	Heck, D., Dr.	Schmalz, G.,Dipl.-Ing.
Dickmann, F., Dr.	Käppeler, F., Dr.	Schmidt, K.A.,Dipl.-Phys.
Dohrmann, H., Ing.	Leugers, B.,Dipl.-Phys.	Voß, F., Dr.
Erbe, D.	Matussek, P.,Dipl.-Phys.	Wisshak, K., Dr.
Eberle, H., Ing.	Michel-Piper,I.,Mrs.,Ing.	Zagromski, S., Ing.

Guests and research students:

Bekk, K.,Dipl.-Phys.	Kazerouni,M.A.,Dipl.-Phys.	Neumann, B.,Dipl.-Phys.
Hensley,F.,Dipl.-Phys.	Ly Di Hong, Miss	Schouky, I.,Dipl.-Phys.
Kari, K.,Dipl.-Ing.	Naqvi, S.A.A.,Dipl.-Phys.	Sobiesiak,H.,Dipl.-Phys.

Secretarial staff: Mrs. H.M. Friederich, Mrs. E. Maaß

Head of the Cyclotron Laboratory: Dr. H. Schweickert

Scientific and technical staff of the Cyclotron Laboratory:

Assmus, K.H.	Günther, O.	Kneis, W.,Dipl.-Phys.
Bauer, G.	Haushahn, G.,Dipl.-Phys.	Kögel, B.
Bechtold, V., Dr.	Heidenreich, K.	Kuhn, H.
Biber, J.	Hirth, W.	Mangold, D.
Depta, A.	Jäger, K., Miss	Möllenbeck, J., Ing.
Ehret, H.-P.	Kappel, W.-R., Ing.	Radtke, G., Ing.
Erdel, E.	Karbstein, W.- Dipl.-Ing.	Rämer, Ch., Miss, Ing.
Franz, J.	Kauther, P.	Röhrl, E.
Friedrich, L., Dr.	Kessel, M.	

Schimpf, P.	Seidel, H.	Volk, B.
Schulz, F., Ing.	Seitz, J.	Wiss, L.
Segnitz, W.	Seufert, H.	

Workshops of the Cyclotron Laboratory:

Ernst, R.	Langenbein, R.	Schönstein, E.
Hauer, W.	Maier, W.	Schütz, R.
Fehling, H.	Möck, W.	Steigleder, C.
Illinger, P.	Ripp, H.	
Klinger, G.	Schlenker, G.	

Secretarial staff: Mrs. E. Kirste